Master's thesis

NTNU
Norwegian University of Science and Technology
Faculty of Information Technology and Electrical Engineering
Department of Electric Power Engineering

Kristian Husmo Lyngved

Investigating thermal management solutions in a modular high voltage machine for offshore wind applications

Master's thesis in Energy and the Environment
Supervisor: Pål Keim Olsen
June 2021

NTNU
Norwegian University of Science and Technology

Kristian Husmo Lyngved

Investigating thermal management solutions in a modular high voltage machine for offshore wind applications

Master's thesis in Energy and the Environment
Supervisor: Pål Keim Olsen
June 2021

Norwegian University of Science and Technology
Faculty of Information Technology and Electrical Engineering
Department of Electric Power Engineering

NTNU
Norwegian University of
Science and Technology

Norwegian University of Science and Technology

Department of Electric Power Engineering

TET4905 - Electrical energy, Master's thesis

Investigating thermal management solutions in a modular high voltage machine for offshore wind applications

Spring 2021

Kristian Husmo Lyngved

NTNU

Abstract

The energy market of the world is in continuous development. For energy transmission, high voltage is now being used more frequently for long transmission distances. Especially between countries, both onshore and offshore. Where HVDC has been more used for longer distances in the recent years. However, most of the energy production finds place on AC. Leading to costly conversion steps between the generation and the transmission. So what if energy could be generated directly at HVDC? This is the goal for the ModHVDC project lead by NTNU.

In the ModHVDC project, a new type of generator is developed. Called the Modular HVDC generator. The ModHVDC generator has a new modular design that can deliver energy directly on HVDC and thereby cutting the costs of the conversion steps. This is done while keeping the machine as a high power density machine with a high efficiency. During the past years, the ModHVDC project has been worked on by several students at NTNU. In addition, other universities and representatives from the energy industry have joined the project.

The ModHVDC machine is a high voltage machine with high power density. This in itself indicates that the machine may generate significant heat. In addition, the ModHVDC concept introduces an insulation layer around the stator that may be seen as a large thermal resistance. The main goal for this Master's thesis is therefore to make a thermal model of the ModHVDC machine, both analytically and as a numerical FEM model, that can be used to investigate different cooling methods. In doing so, answering the question "Is the ModHVDC concept possible to realize, with regard to thermal management?".

From the results, it was found that no single cooling method yielded sufficient cooling for the machine. However, by combining different cooling techniques, suitable solutions were found. This means that the concept is indeed possible to realize, with regard to thermal management. The most efficient cooling solution was a combination of forced air through the air gap, combined with a concentric duct between the stator surface and the machine frame. This cooling solution was also taken one step further, when waved cooling fins were made on the stator surface. Leading to a max temperature of $125°C$ in the machine.

The results also show a good coherence between the analytical thermal equivalent circuit and the numerical FEM model. With a maximum difference of only $2.58°C$ for the most complex cooling solution. Verifying the methods used.

A recommendation for further work is to make a complete 3D model of the machine. In doing so, CFD simulations can be done. When utilizing CFD simulations, more reliable heat transfer coefficients can be found and a more realistic design may be done. A complete 3D model is also needed for the complete design of the thermal management system.

Sammendrag

Verdens energimarked blir kontinuerlig utviklet. Når det gjelder selve energioverføringen, brukes det mer og mer høyspenning for lange transmisjonslinjer. Spesielt mellom forskjellige land, både til havs og på fastlandet. For de lengste overføringsetappene har HVDC blitt mest brukt i de senere årene. Samtidig blir energien produsert på AC, i de fleste tilfeller. Dette fører til dyre konverteringer mellom energiproduksjonen og transmisjonen. Derfor kan spørsmållet "Hva om energiproduksjonen kunne skje direkte på HVDC?" stilles. Det er dette som er hovedmålet til ModHVDC prosjektet som blir ledet av NTNU.

ModHVDC prosjektet går ut på å designe en ny type generator, som blir kalt en Modulær HVDC generator. Generatoren har et nytt segmentert design, som gjør at den kan levere direkte på HVDC. Dette kutter kostnadene ved konvertering, samtidig som maskinen beholder status som en effektiv maskin med høy effekttetthet. I de siste årene har mange studenter jobbet med ModHVDC prosjektet, samtidig som flere universiteter og representanter fra energisektoren har blitt med på utviklingen.

ModHVDC maskinen er en høyspenntmaskin med en høy effekttetthet. Det vil si at det også blir generert mye varme i maskinen. I tillegg innfører konseptet en isolerende kappe rundt statoren i maskinen. Denne kappen blir sett på som en stor termisk motstand. Hovedoppgaven i denne Masteroppgaven er derfor å lage en termisk modell av maskinen. Både analytisk og numerisk ved bruk av FEM modeller. Disse modellene skal kunne brukes til å teste forskjellige kjølemetoder for maskinen og samtidig svare på spørsmålet "Er ModHVDC konseptet mulig å realisere, med tanke på termiske begrensninger?".

Resultatene viser at det ikke ble funnet èn kjølemetode som ga god nok kjøling til maskinen. Derfor ble løsningen å kombinere flere metoder. Ved å kombinere flere metoder ble det funnet flere løsninger som gir akseptabel kjøling. Det betyr at ModHVDC konseptet er fullt mulig å realisere, med tanke på termiske begrensninger. Den beste kjølemetoden viste seg å være en kombinasjon av kjøling i luftgapet og en konsentrisk sylinder mellom statoren og rammen til maskinen. Denne metoden ble videreutviklet ved å lage bølgete kjøleribber på statoroverflaten. Dette førte til at den høyeste temperaturen i maskinen ble $125°C$.

Det ble også observert veldig god sammenheng mellom de analytiske modellene og de numeriske FEM modellene. Den største forskjellen mellom modellene ble $2.58°C$, for den mest komplekse kjølemetoden. Dette indikerer at metodene som blir brukt, fungerer bra.

En anbefaling for videre utvikling, er å lage en komplett 3D modell av maskinen. Gjør man det, kan man kjøre CFD simuleringer. CFD simuleringer vil gi mer nøyaktige varmeoverføringskoeffesienter og et mer realistisk design kan dermed bli laget. En komplett 3D modell trengs også for å kunne designe et fullstendig kjølesystem for maskinen.

Preface

This report is made as the Master's thesis and final work for the author in the study program of Energy and Environment at NTNU in Trondheim. The Master's thesis amounts for 30 credits and is a part of the course TET4905. The thesis has been written in the spring of 2021 and is a continuation of the author's specialisation project from the fall of 2020.

Gratitude and acknowledgement is given to my supervisor Pål Keim Olsen for giving valuable inputs and guidance throughout this thesis. Also, Professor Erling Næss is shown gratitude for giving inputs and discussions on several topics of thermal management. Especially on the topic of convective transfer coefficients.

This Master's thesis can hopefully be used as a reference and as a starting point, when further developing a complete thermal management system for the ModHVDC machine.

It is recommended that the readers familiarize themselves with basic knowledge in electrical machines and heat transfer, before reading the thesis. This is because not all basic concepts are described in detail in the thesis.

Trondheim, JUN 13th 2021

Kristian Husmo Lyngved

Disclaimer

The content in this Master's thesis is the author's own work, which is a continuation of a specialization project done in a preliminary course at NTNU in the Autumn of 2020.

In the specialization project, relevant literature studies were conducted and some simplified, yet useful preliminary models were created. As the specialization project is a direct prelude to this Master's thesis, reuse of literature, some mathematical formulas/models and figures from the specialization project finds place in this thesis. Where reuse of content takes place, the reference to the specialization project, [1], is cited.

This Master's thesis and the specialization project are both parts of the ModHVDC project at NTNU. Because of this, the introduction to the project and the explanation of the ModHVDC machine concept is also reuse of content. The reference to the specialization course, [1], is therefore found throughout the introduction chapter. Especially in section 1.1, which introduces the ModHVDC project and in section 1.2 where the ModHVDC concept is introduced. Additionally, the approach for both this Master's thesis and for the specialization project have been the same (Section 1.5).

In addition, appendix B, which describes the reference machine and material properties used for both the preceding specialization project and this Master's thesis, is attached as a direct copy from the preceding specialization course. This appendix describes the reference machine and the material properties in a complete and informative way, therefore only small changes or additional information is found in this appendix, compared to the same appendix in the specialization course.

Nomenclature

β	Coefficient of thermal expansion [1/K]
ρ	Density [kg/m^3]
θ	Angle [rad]
c	Fluid velocity [m/s]
c_p	Specific heat capacity [$J/(kg \cdot K)$]
N_{seg}	Number of segments [-]
P	Losses [W]
Q_s	Number of slots [-]
t_{ins}	Insulation thickness [m]
A	Area [m^2]
b or W	Width [m]
D	Diameter [m]
d or H	Height [m]
g	Constant of gravity acceleration [m/s^2]
h	Convective heat transfer coefficient [W/m^2K]
k	Thermal conductivity [$W/(m \cdot K)$]
L	Length or thickness [m]
N	Nusselt number [-]
R	Thermal resistance
r	Radius [m]
T	Temperature [K or $°C$]

Abbreviations

ModHVDC	Modular High Voltage Direct Current
FEM	Finite Element Method
FEA	Finite Element Analysis
LCOE	Levelized Cost Of Energy or Levelized Cost Of Electricity
CFD	Computational Fluid Dynamics
PMSM	Permanent Magnet Synchronous Motor

Contents

List of Figures

List of Tables

Chapter 1

Introduction

The energy market is in continuous development around the world. For more efficient transmission of energy, high voltage is used for longer and longer distances between countries both on land and offshore. Transmission lines can be found using HVAC or HVDC, where HVDC have been more frequently used for longer transmission lines in the recent years. Especially in offshore applications. A reason for this, is because HVDC can be used in interconnections between countries that uses different frequencies, like for example 50Hz and 60Hz. In addition, long HVAC lines experiences large charging currents each period, due to the capacitance of the lines. In HVDC lines, the charging current only finds place while ramping up or down the voltage. [2]

However, the energy is mostly generated on AC. Leading to costly conversions steps between the energy production and the transmission. A question that arises is therefore "What if energy could be generated directly at HVDC?", thereby cutting the cost of the conversion steps. This is the goal for the ModHVDC project. [1]

The ModHVDC project introduces a new type of generator, that can deliver energy directly on HVDC. Cutting the cost of conversion, while keeping the generator as a high power density machine with a high efficiency. [1]

The project has been going for some years and several students have taken part in the development of the ModHVDC concept. A suggested machine design have been developed by Solveig Samseth Strand in the Master's thesis cited here [3]. The design is used as a reference machine for this thesis and a description can be found in appendix B. [1]

The thermal design is crucial for an efficient and cost saving electrical machine. For all high voltage machines, the insulation may become thick. Thick insulation means a large thermal barrier, which may lead to high temperatures in the machine. A solution could be to reduce the power density of the machine, but this is not desirable for offshore wind applications. Hence, high voltage machines are dependent on a good thermal management system. Because of this, the thermal management of the ModHVDC machine is the focus in this Master's thesis. [1]

1.1 A modular high voltage direct current generator

The modular high voltage direct current generator, or the ModHVDC machine is a concept developed in the ModHVDC project at NTNU. The concept originates from Pål Keim Olsen who is the leader for the project. Other universities and participants from the energy industry from several countries have joined in on the project in recent the years. [1, 4]

Today, the main goal for the project is to develop a fully functional ModHVDC generator with all necessary equipment for offshore wind applications. That being said, the ModHVDC machine can potentially replace any rotating electrical machine in the future. Being used both as a generator or as a motor, the machine can be implemented by both consumers and by producers. Figure 1.1.1 illustrates a future, where the ModHVDC machine has reached a generalized use both on land and offshore. [1, 4]

Figure 1.1.1: *A future where the ModHVDC machine has reached a generalized use both on land and offshore. Figure taken from [4]. [1]*

1.2 ModHVDC concept

The stator of the ModHVDC machine is built as a modular stator. This in itself is not a new concept, as modular stators do exist in the market today. However, in the ModHVDC machine, each of the modules are connected to a DC-potential at the DC side of the converters. This is the concept that makes the ModHVDC machine special. The connection to the DC-potential separates the AC and DC voltages in the machine, leading to an ideal voltage distribution. The modular design thereby leads to an increase in power density, compared to conventional machines. Figure 1.2.1 shows the ModHVDC concept topology with four modules. [1, 4]

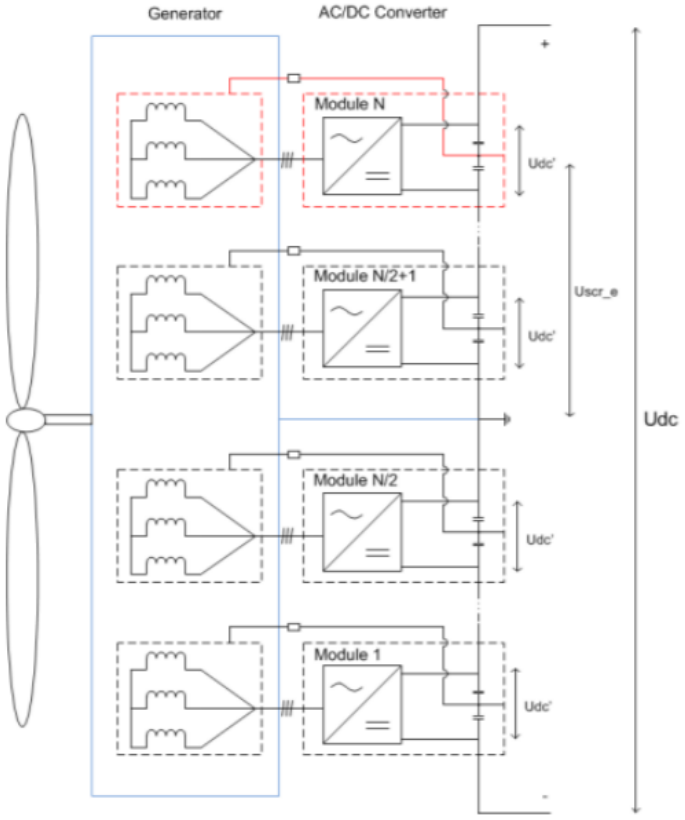

Figure 1.2.1: *The ModHVDC concept topology with four modules. Figure taken from [3].*

The resulting voltage distribution for the ModHVDC machine is shown in table 1.2.1. Additionally, a comparison to a conventional machine without segmentation is displayed. From the table it can be seen that the voltage potential is reduced to $\frac{V_{DC}}{N_{seg}}$, N_{seg} being the number of modules in the ModHVDC machine. The decrease in potential also leads to a decrease in the phase-to-ground AC component and the phase-to-phase line voltages. Since the voltages are decreasing for the modular design, the insulation needed in the slot is reduced. Although, insulation is needed around the stator that need to withstand the DC field. [1, 4, 5]

Table 1.2.1: *Voltage distribution for a the ModHVDC machine and for a non-segmented machine. Table remade from [5]. [1]*

Description	Voltages	Modular machine (ModHVDC)	Non-segmented machine
The rated system DC voltage	System voltage	V_{DC}	V_{DC}
The phase-to-phase voltage	$V_{ph-ph_{max}}$	V_{DC}/N_{seg}	V_{DC}
The phase-to-segment voltage	$V_{ph-seg_{max}}$	$V_{DC}/N_{seg} \cdot \frac{1}{2}$	$V_{DC}/2$
The segment-to-earth voltage	$V_{seg-earth_{max}}$	$(V_{DC}-V_{DC}/N_{seg}) \cdot \frac{1}{2}$	0
The segment-to-segment voltage	$V_{seg-seg_{max}}$	$V_{DC}/N_{seg} \cdot 2$	0

The insulation needed around the stator is shown in figure 1.2.2, indicated by the blue lines. The figure shows a design with four modules, where insulation can be seen around the stator surface, between each module and on the inner surface of the stator. As mentioned earlier, the insulation is needed since the modules are floating on HVDC. However, the windings are still on AC potential, as in conventional machines. To reduce the voltage potential between the winding in the slot and each module, both are kept at the same voltage potential as the windings. [1, 4]

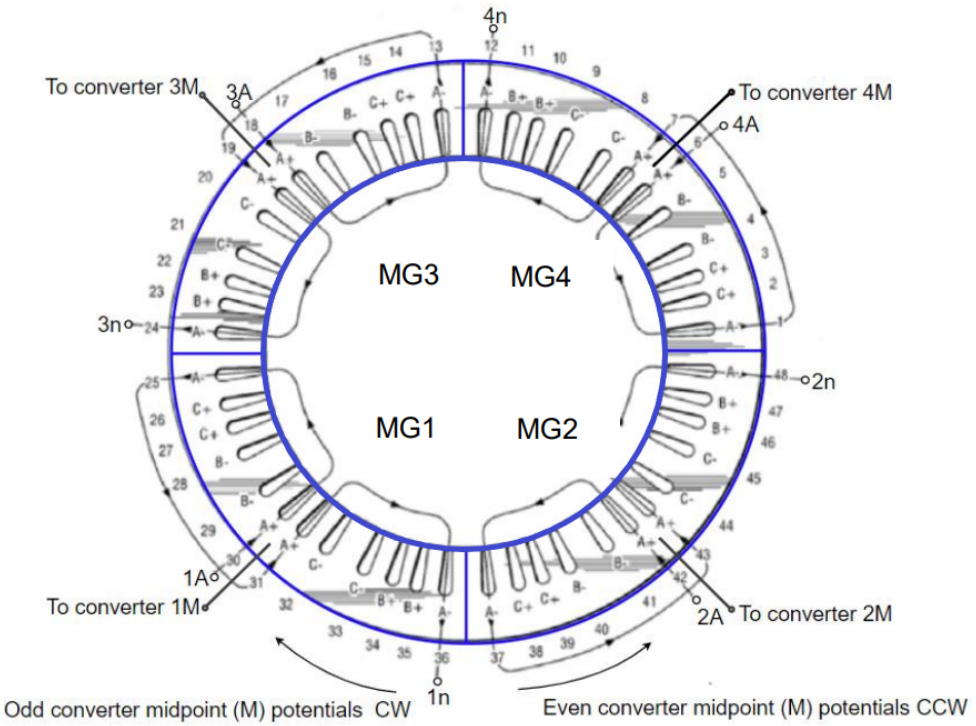

Figure 1.2.2: *Illustration of ModHVDC stator with the needed insulation for the concept. The figure is adapted from [6]. [1]*

However, the insulation around the inner surface of the stator may not be needed in reality [2]. Nevertheless, this insulation is included in this Master's thesis as a "worst case" scenario, as the insulation stands for a large thermal resistance.

1.2.1 Challenges & benefits

The main challenge of the ModHVDC machine for this Master's thesis, is the thermal management. The new insulation around the stator modules introduces large thermal resistances, which makes it harder for heat to flow out of the machine. This may lead to very high temperatures. A simple solution to this challenge could be to reduce the generated heat, by reducing the current density in the machine. However, this is not a feasible solution when it comes to offshore wind applications. This is because a less compact and larger machine would be needed for the same power output. [1, 2, 4]

When the challenges are overcome, the benefits by using the ModHVDC machine can be fully utilized. One of the most prominent benefits, is that the insulation in the slot can be reduced by up to 90%. This means that a large thermal resistance is almost removed, leading to a lighter and smaller machine. As mentioned earlier, the conversion steps are no longer necessary and no DC load breakers will be needed. These benefits have economical benefits tied to them and may even realize a reduction of over 10% in LCOE, for offshore wind farms as a system. [1, 4]

1.3 Problem formulation

For all high voltage machines with high power density, cooling becomes important for a fully functional machine with high efficiency. In addition, the insulation around the stator in the ModHVDC machine contributes to a large thermal barrier. A question that has arisen is therefore whether the concept is possible to realize or not, due to thermal management of the machine.

The goal for this thesis is therefore to make a thermal model of the ModHVDC machine, that can be used to investigate different cooling solutions. In doing so, answering the question "Is the ModHVDC concept possible to realize, with regard to thermal management?". Further, hopefully come up with a recommendation for development of a complete thermal management system for the ModHVDC machine.

1.4 Assumptions, limitations and simplifications

In this Master's thesis some assumptions, limitations and simplifications have been made. One of the most notable limitations is that the modelling in this thesis is done in a two dimensional perspective (2D-modelling) only. The effect of this 2D limitation, is that the heat flow in the axial direction is neglected. [1]

The 2D limitation also implies that the cooling methods that are investigated and implemented in the models, are not complete cooling systems. The models are rather methods used to investigate if a cooling method is applicable to the ModHVDC machine. This means that no heat exchanges, external fans, flow paths and so on, are modelled or investigated.

A key assumption in this thesis, is that all heat transferred out of the modelled section or to the cooling fluid, is also transferred out of the machine. However, heating of the cooling fluid is in some cases implemented by the correlations used in the thesis.

The thesis is limited to concentrate on the thermal aspect of the ModHVDC machine. This means that the effect that the cooling methods may have on the electromagnetic design of the ModHVDC machine, is not investigated.

A simplification when modelling the rotor, is that the rotor is stationary in the models. A discussion on the effects this may have, is done in chapter 5.

The thermal effects from radiation are neglected in all parts of this thesis. In addition to the effects of thermal expansion in materials or machine parts. [1]

Another limitation, is that only stationary models are made. This means that transients or time dependent temperatures are not investigated in this thesis.

1.5 Approach

In this Master's thesis, simulation have been the main approach for solving the thermal models made. Two types of thermal models are made in this thesis. One analytical thermal equivalent circuit model and one numerical FEM model. The analytically made thermal equivalent circuit, is made using MATLAB and Simulink. Where the complete circuit is simulated using Simulink. The numerical FEM model is made in the software COMSOL Multiphysics, using build in heat transfer modules. [1]

1.6 Thesis outline

This Master's thesis is outlined using six chapters. First, the reader is introduced to a literature study, where different aspects of thermal management are studied. Then, a modelling chapter is used to explain how all the models in the thesis are made. When the reader have been familiarized with all the models and what they are used for, the results are presented in chapter 4. The thesis is closed with a discussion, followed up by conclusions and suggestions for further work. All main results and models are displayed within the chapters. However, the appendixes also offer additional information or elaborations that are referred to when useful.

Chapter 2 presents a literature study on thermal modelling of electrical machines. The chapter starts with investigating the convection effects in the air gap, before going into thermal modelling of machine parts. Then, a study on contact resistance and different cooling methods and techniques is done. Additional focus have been given on how to determine the convective heat transfer coefficients, as it is one of the most important aspects of thermal management.

Chapter 3 is the modelling chapter. In this chapter, an explanation on how all machine parts are made as a FEM model and as an analytical thermal equivalent circuit is done. The chapter starts by showing different convection coefficients for the air gap and the frame-to-ambient, before a base thermal equivalent circuit is made. Then the same base model is made as a FEM model in the software COMSOL. A description of different convection coefficients for several cooling solutions is then presented, before closing with the implementation of different cooling solutions in the base models.

Chapter 4 presents the results from the Master's thesis. The chapter starts with a comparison of different methods used for modelling the stator slot with windings. Then, a comparison between the base models is done to see the coherence between the analytical method and the numerical FEM method. The rest of the chapter presents the resulting temperatures for different cooling solutions.

Chapter 5 discusses and evaluates the methods and results from the thesis. First, the cooling methods and the implementation of these are discussed. Then, a discussion on optimization and the impact on the electromagnetic design is done, before a short discussion on further investigations of different cooling methods. The chapter continues with an evaluation of the two methods used to model the slot with windings, before a discussion on the differences between the FEM model and the analytical thermal equivalent circuit. The chapter closes with an evaluation of assumptions, limitations and simplifications used in this Master's thesis.

Chapter 6 is the last chapter in this Master's thesis. In this chapter, conclusions are drawn based on the results and discussions within the thesis. The chapter is concluded with suggestions for further work.

Chapter 2

Literature study

In this chapter, a literature study on thermal physics and thermal modelling of electrical machines is conducted. The most focus has been given to the convection coefficient for different situations, as this is an important parameter when making thermal models. First, a study on the convection in the rotor-stator air gap is conducted, before the convection effects to the ambient. Then, thermal equivalent models for electrical machine parts are investigated. The last section in the chapter is dedicated to different cooling methods and techniques.

2.1 Convection in the air gap

Convection in the air gap of electrical machines can be very complex to model. This is because the convection is dependent on the structure of the machine and the flow of the fluid inside the air gap. There exist many correlations that can be used to determine the heat transfer in the air gap. These depend on the rotational speed of the machine, if there is air flowing through the machine in the axial direction (or flow just due to rotation), the geometry and so on. The main problem is to determine the heat transfer coefficient, h_{ag}, which on the base form can be written as equation 2.1.1. In the equation, Nu is the Nusselt number, k_{air} is the thermal conductivity of the air and D_h is the hydraulic diameter of the air gap. The equation illustrates that the correlation used to determine the Nusselt number becomes the deciding factor for the heat transfer coefficient and therefore the heat transfer in the air gap. [7]

$$h_{ag} = Nu \cdot \frac{k_{air}}{D_h} \tag{2.1.1}$$

In this literature study, mainly three different approaches to determine the heat transfer in the air gap has been found. The first is to only consider the axial fluid flow in the air gap, the second is to consider only the flow due to rotation of the inner cylinder, which is the rotor. While the last approach considers both the axial flow and the flow due to rotation of the rotor.

It is generally agreed that heat transfer in the air gap can be complex and varies a lot depending on the design of the machine and the needed thermal management system. Usually, the correlations used have been verified to some extent experimentally, but it is often recommended that a full Computational Fluid Dynamics (CFD) simulation is done. This is because CFD makes it easier to decide a more correct heat transfer coefficient for each individual machine. However, the correlations have proved to give adequate results, if the correlations are carefully chosen based on dimensionless numbers and the geometry of the machine. [7–21]

2.1.1 Airflow in the axial direction

In [7], a thermal model of a synchronous generator is made using lumped parameter thermal modelling. In the modelling process, the axial air flow is considered. However, the air flow due to rotation seem to be ignored. [7] mentions two correlations often used in the literature to determine the heat transfer coefficient in the air gap, using an analogy of airflow along smooth pipes. These correlations are illustrated as equation 2.1.2 and 2.1.3. Equation 2.1.2 is mentioned to be the correlation used in earlier works, while equation 2.1.3 is used in modern literature. Equation 2.1.3 can also be found in the book "Introduction to heat transfer"[9]. When calculating the heat transfer coefficient, [7] uses the average of these two correlations. In the correlations, P_r is the Prandtl number, R_e is the Reynolds number and f_c is a friction coefficient.

$$Nu = 0.023 \cdot P_r^{1/3} \cdot R_e^{0.8} \tag{2.1.2}$$

$$Nu = \frac{\frac{f_c}{8} \cdot (R_e - 1000) \cdot P_r}{1 + 12.7\sqrt{\frac{f_c}{8}} \cdot (P_r^{2/3} - 1)} \tag{2.1.3}$$

The friction coefficient can be found from equation 2.1.4, which is the friction equation for smooth pipes. While the Reynolds number can be calculated from equation 2.1.5. In the equation, ρ is the density, μ is the dynamic viscosity of the fluid in the air gap and v is the axial velocity of the fluid. The Prandtl number can be given a value of 0.7 for gasses, which is done in both [7] and [10]. [7]

$$f_c = \frac{1}{(1.82 \cdot log_{10} \cdot R_e - 1.64)^2} \tag{2.1.4}$$

$$R_e = \frac{\rho \cdot v \cdot D_h}{\mu} \tag{2.1.5}$$

2.1.2 Airflow due to rotation only

Often in low-speed electrical machines, the airflow in the axial direction is neglected. [8] claims that forced cooling through the air gap is not often used due to the cost of the external fan that is needed to force the air through. Because of this, the heat flow in the air gap is considered only in the radial direction, meaning the heat transfer from the rotor surface to the stator surface. [8]

When calculating the heat flow over the air gap, the Taylor number is often used. The Taylor number can be calculated from equation 2.1.6. In the equation, r_m is the average radius of the stator plus rotor and δ is the air gap length. This formulation of the Taylor number can be found in [8, 11, 12].

$$T_a = \frac{\rho^2 \cdot \omega^2 \cdot r_m \cdot \delta^3}{\mu^2} \tag{2.1.6}$$

Although [8], [11] and [12] agree on the definition of the Taylor number, they do not agree on the determination of the Nusselt number. [8] uses a modified Taylor number, $T_{a,mod} = T_a/F_g$, where F_g is a geometric factor. From the results, [8] uses the correlation shown as equation 2.1.7 to decide the Nusselt number. In [8], a complex formula for the calculation of F_g is used. However, [14] claims that the factor differs depending on the author and that it can be set to $F_g = 1$ for narrow gaps.

$$\begin{aligned} T_{a,mod} \leq 1700 &\rightarrow N_{nu} = 2 \\ 1700 < T_{a,mod} \leq 10^4 &\rightarrow N_{nu} = 0.128 \cdot {T_{a,mod}}^{0.367} \\ 10^4 < T_{a,mod} < 10^7 &\rightarrow N_{nu} = 0.409 \cdot {T_{a,mod}}^{0.241} \end{aligned} \tag{2.1.7}$$

[11] on the other hand, first calculates a critical Taylor number. This critical Taylor number is shown as equation 2.1.8. The factor F_g is the same geometrical factor as previously mentioned. [11] then uses equation 2.1.9 to calculate the Nusselt number. Stating that this correlation could be used for Taylor numbers in the range $0 < T_a < 10^8$.

$$T_{a_c} = 1697 \cdot F_g \tag{2.1.8}$$

$$N_u = 0.42 \cdot (T_a \cdot P_r)^{0.25} \tag{2.1.9}$$

[12], which is an article that reviews heat transfer between concentric rotating cylinders, refers to the flow in these types of systems (like the flow in the air gap) as a Taylor-Couette flow. In this article, both of the correlations described above are mentioned. The different correlations in

this article are based on several parameters. Among these are the radial cylindrical gap aspect ratio, $\eta = R_1/R_2$, the axial cylindrical gap aspect ratio, $\Gamma = L/R_2 - R_1$, the cylindrical gap thickness, $e = R_2 - R_1$ and a critical Taylor number, T_{a_c}. In the article, a list of different correlations and when they are valid is made. A selection from this list, is remade as table 2.1.1 in this thesis. The correlations are based on heat transfer in smooth and open cylinder gaps. The author of [12] makes clear that the correlations in the table have been modified to fit the definitions used in [12]. For more in depth information on each of the correlation, the article in [12] could be reviewed.

Table 2.1.1: *Table showing different correlations used for the calculation of the Nusselt number and when the correlation is valid. $A = 0.4614ln(3.3361\eta)$. The table is adapted from [12].*

η	e/R_1	Γ	T_a	T_{a_c}	**Correlations**	**Source**
0.807	0.238	172	$0 - 3.3 \cdot 10^5$	1994	Equation 2.1.7	Becker and Kaye [22]
0.75−0.938	0.07−0.33	2.25−11.25	$10^8 - 10^{12}$	-	$N_u = 0.092(T_a \cdot P_r)^{1/3}$	Tachibana and Fukui [23]
0.522−0.971	0.13−0.92	220−7000	$0{-}10^8$	1730-3000	Equation 2.1.9	Tachibana et al. [24]
0.8−0.948	0.054−0.246	32−147	$8000{-}4 \cdot 10^6$	1770-1994	$N_u = 0.35 \cdot T_a^{0.25}$	Bjorklund and kays [25]
-	-	-	$5000{-}2 \cdot 10^5$	-	$N_u = 0.44 \cdot T_a^{0.25} \cdot P_r^{0.3}$	Aoki et al. [26]
0.437−0.656	0.26−0.64	31.4−77.2	$4000{-}4 \cdot 10^5$	-	$N_u = 0.069 \cdot \eta^{-2.9084} \cdot (R_1\omega e/v)^A$	Ball et al. [27]
0.895	0.12	17	$7962{-}2 \cdot 10^8$	-	$N_u = 8.854(R_1\omega e/v)^{0.262} \cdot P_r^{0.4}$	Tzeng [28]

The method of using the Taylor number and the Nusselt number to find the heat transfer coefficient can be found in the above mentioned literature, in addition to [10, 15, 16, 18–21] and more. Where the difference is the choice of which correlation to apply.

[29] ,[30], [31] and [17] uses a correlation that is not found in table 2.1.1. Instead, a correlation modified by Gazley[32] is used. The Taylor number for this correlation is calculated as shown in equation 2.1.10. While the correlation for the Nusselt number is shown as equation 2.1.11. In equation 2.1.10, l_g is the thickness of the air gap and R_r is the outer radius of the rotor. [1]

$$T_a = R_e \cdot \sqrt{\frac{l_g}{R_r}} \tag{2.1.10}$$

$$\begin{aligned} T_a \leq 41 &\rightarrow N_{nu} = 2 \\ 41 < T_a \leq 100 &\rightarrow N_{nu} = 0.212 \cdot T_a^{0.63} \cdot P_r^{0.27} \\ T_a > 100 &\rightarrow N_{nu} = 0.386 \cdot T_a^{0.5} \cdot P_r^{0.27} \end{aligned} \tag{2.1.11}$$

2.1.3 Airflow in axial direction and due to rotation

When both axial forced airflow and rotation exists between two cylinders, there are four types of flow that can occur, according to [33]. The flow structure depends on the Reynolds number in the axial direction and the Taylor number due to rotation. The Reynolds number decides if the flow is laminar or turbulent, while the Taylor number describes if vortices called Taylor vortices, finds place in the gap between the cylinders. The four flow types can be characterized as laminar flow only, turbulent flow only, laminar flow with Taylor vortices and turbulent flow with vortices. [33]

The heat transfer is very dependent on the flow regime within the gap and the correlations used may change for different flow regimes. [33]

In [8], equation 2.1.12 is used to determine the Nusselt number for airflow caused by the rotating rotor and due to forced cooling in the form of axial fluid flow through the air gap. However, it is noted that this correlation is most often used for high-speed electrical machines and has only been verified for this use[8]. In the equation, L_δ is the length of the air gap in the axial direction. The rest of the parameters have been previously described, but the velocity used for the Reynolds number is calculated in a slightly different way. Equation 2.1.13 is used to calculate the helictical velocity of the fluid in the air gap, which is the combined velocity from the forced axial air flow and the rotating air flow due to the rotating rotor. In the equation, ω is the angular velocity of the rotating rotor, R is defined as the outer radi of the rotor and v_{axial} is the axial velocity of the fluid in the air gap. While equation 2.1.14 is used to calculate the hydraulic diameter. This method has also been used by [13] and the authors of [8], refers to the book [14] for the correlations used. [8]

$$N_u = 0.0214(R_e^{0.8} - 100) \cdot P_r^{0.4} \left(1 + \frac{D_h}{L_\delta}^{0.66}\right) \tag{2.1.12}$$

$$v_{comb} = \sqrt{\left(\frac{\omega \cdot R}{2}\right)^2 + v_{axial}^2} \tag{2.1.13}$$

$$D_h = \delta \cdot \sqrt{\frac{8}{3}} \tag{2.1.14}$$

A review on thermal modelling and fluid flow modelling in electrical machines is done in detail in [33]. Especially the heat transfer in the air gap with both axial and radial (rotational) flow has been investigated. The author of [33] summarized different correlations used for the calculation of the Nusselt number in a table, which is adapted for this thesis and shown as table 2.1.2. The table displays the validity, approach, source and the radius ratio used for the different correlations. However, it is stated that these correlations must be used with great care. This is because the fluid dynamic and heat transfer in gaps such as the air gap is very complex.

Because of this, the correlations should be used only if the radius ratio, the Reynolds number and the Taylor number is similar to the validity conditions listed in the table. In addition, these correlations are mostly used if there is air in the air gap and not for other fluids. [33]

Most of the parameters in table 2.1.2 have been introduced before, but some need to be clarified. V_e is the equivalent fluid speed in the air gap. In the table, s is the gap size, U is the fluid velocity in the axial direction, V_T is the rotational speed of the rotor, N_{u0} is the Nusselt number calculated from equation 2.1.3 and T_{a_c} is the critical Taylor number. The critical Taylor number is defined as shown in equation 2.1.15. In the equation, the factor 48.4 comes from the fact that Simmers and Coney had a radius ratio of 48.4 in the experiments. For more information on the background of the correlations it is recommended to read the work in [33]. [33]

$$T_{a_c} = \sqrt{166.75 \cdot R_e^{0.913}} + 48.4 \tag{2.1.15}$$

Table 2.1.2: *A Table displaying different heat transfer correlations used for air gap convection with both axial and radial fluid flow. The table is adapted from [33].*

η	**Validity**	**Approach**	**Correlations**	**Source**
0.904	$600< T_a < 5500$, $2 \cdot 10^3 < R_{e_e} < 1.5 \cdot 10^4$	Experimental	$1.3 \cdot 10^3 < R_e < 2 \cdot 10^4$ $N_u = 0.03 R_{e_e}^{0.8}, R_{e_e} = \frac{\rho D_h V_e}{\mu}, V_e = eq.2.1.13$	Gazley et al. [32]
0.75−0.937	$380< R_e < 4220$, $71 < T_a < 3415$	Experimental	$N_u = N_{u_{rot}} + N_{u_{axial}}$, $N_{u_{rot}} = 0.092(T_a^2 P_r)^{1/3}$ $N_{u_{axial}} = 0.015(1 + 4.6\frac{s}{L})(\frac{r_i}{r_o})^{0.46} R_e^{0.8} P_r^{1/3}$	Tachibana and Fukui [23]
0.57	$1.5 \cdot 10^4 < R_e < 6.5 \cdot 10^5$, $7 \cdot 10^4 < T_a < 9.3 \cdot 10^4$	Numerical, Experimental	$N_u = N_{u_0} \left(1 + (\frac{2sV_T}{\pi r_i U})^2\right)^{0.8714}$	Kuzay and Scott [34]
0.8 and 0.955	$400< R_e < 1200$, $100 < T_a < 1414$, $65 < L/D_h < 288$	Analysis, Experimental	$N_u = \frac{A P_r R_e^{0.5} T_a^{0.735}}{B\left(\frac{A}{1-\eta}\right)^{0.5}\left(\frac{\eta}{1-\eta}\right)^{0.25} T_{a_c}^{1.235}}$, $A = \frac{1+\eta^2+(1-\eta^2)/ln(\eta)}{2+(1-\eta^2)ln(\eta)}$ $B = P_r + ln(1 + P_r \cdot exp(C - P_r))$, $C = \frac{2}{3}\left(\frac{1-\eta}{\eta}\right)^{0.25}\left(\frac{\eta A}{(1-\eta)^2}\right)^{0.5} R_e^{-0.5} T_a^{0.265} T_{a_c}^{0.235} - 1$	Simmers and Coney [35]
0.87	$1.7 \cdot 10^5 < R_e < 3.7 \cdot 10^5$, $8 \cdot 10^3 < T_a < 1.6 \cdot 10^5$	Experimental	$N_u = N_{u_0}\left(1 + 0.068(\frac{V_T}{2U})^2\right)$	Childs and Turner [36]

It is important to note that the author of [33] uses equation 2.1.16 to calculate the Taylor number, yielding a different answer than 2.1.10. In the equation, r_m is the radius corresponding to the middle of the air gap and s is the gap thickness. Because of this, equation 2.1.16 should be used when utilizing the correlations shown in table 2.1.2. In addition the hydraulic diameter used, is equal to $D_h = 2 \cdot \delta$. [33]

$$T_a = \frac{\rho \cdot \omega \cdot r_m^{0.5} \cdot s^{1.5}}{\mu} \tag{2.1.16}$$

2.2 Convection to ambient

The convection to ambient for electrical machines, can be calculated on the same basis as the convection in the air gap. This means that the basis formula for the heat transfer coefficient is still equation 2.1.1. However, the correlations used to determine the heat transfer coefficient are not the same. In addition, the correlations used is dependent on the geometry of the outer surface and on the positioning of the machine. This means that it is important to know if the machine is placed vertically, horizontally or somewhere in between. [37]

At all surfaces there is either natural convection, forced convection or both. Natural convection takes place where no external force is moving the fluid over the surface, while forced convection happens when there is such an external force like a fan or a pump. According to [37], the correlation shown as equation 2.2.1 can be used for natural convection for a horizontal cylinder. In the equation, G_r is the Grashof number. If the product of the Prandtl number and the Grashof number ranges $10^4 < G_r P_r < 10^9$, it indicates that the flow is laminar. If the product ranges $10^9 < G_r P_r < 10^{12}$, the flow is turbulent. This correlation is used in [38] and [37] among others. [37, 38]

$$\begin{aligned} 10^4 < G_r P_r < 10^9 \rightarrow & N_{nu} = 0.525(G_r \cdot P_r)^{0.25} \\ 10^9 < G_r P_r < 10^{12} \rightarrow & N_{nu} = 0.129 \cdot (G_r \cdot P_r)^{0.33} \end{aligned} \tag{2.2.1}$$

The Grashof number can be calculated as shown in equation 2.2.2, according to [37]. In the equation, β is a coefficient of thermal expansion for the fluid, g is the gravitational constant, ΔT is the difference in temperature between the frame and the ambient. β can be calculated by $\beta = 1/T_k$, where T_k is the absolute temperature (kelvin) of the fluid. This is done in many text books, including [39]. Calculating β for atmospheric pressure and a temperature of about $20°C$, yields $\beta \approx 3.6 \cdot 10^{-3}$. This is also the value used in [40]. [1, 37, 39, 40]

$$G_r = \frac{\beta \cdot g \cdot \Delta T \cdot \rho^2 \cdot L^3}{\mu^2} \tag{2.2.2}$$

For forced convection over a horizontal cylinder, equation 2.2.3 can be used. One important note for this equation, is that the forced fluid flow is in the axial direction. This means that the hydraulic diameter when deciding the heat transfer coefficient in equation 2.1.1 becomes $D_h = L_{ec}$, where L_{ec} is the length of the external frame. This formulation for forced convection over a horizontal cylinder can also be found in books such as [9]. [37]

$$\begin{aligned} R_e < 5 \cdot 10^5 \rightarrow & N_{nu} = 0.664 \cdot R_e^{0.5} \cdot P_r^{0.33} \\ R_e > 5 \cdot 10^5 \rightarrow & N_{nu} = (0.037 \cdot R_e^{0.8} - 871) \cdot P_r^{0.33} \end{aligned} \tag{2.2.3}$$

[41] Uses a DC test to determine the natural convection as a thermal resistance. From the test the heat transfer coefficient is not directly found, however the thermal resistance between the frame and the ambient is found. The thermal resistance can be calculated by measuring the temperature of the surface and the ambient temperature and then utilizing equation 2.2.4. In the equation, T_c is the external temperature of the machine frame during the DC test, T_{amb} is the ambient air temperature around the machine and P_{loss} is the power losses of the machine. [41]

$$R_{amb} = \frac{T_c - T_{amb}}{P_{loss}} \tag{2.2.4}$$

A very simple and completely different method of calculating the thermal resistance between the frame and the ambient for natural convection, is found in [42]. In this article, it is stated that the thermal resistance for natural convection can be calculated by using equation 2.2.5. This thermal resistance includes the natural convection phenomena in addition to radiation heat transfer, according to the author(s). From [42], it becomes clear that the heat transfer coefficient for radiation effects is dependent on the temperature difference between the surfaces. In the equation, A is the total area of the machine frame. One thing to note, is that this method is stated for a totally enclosed electric machine with no fan. [42]

$$R_{amb} = 0.167 \cdot A^{1.039} \tag{2.2.5}$$

2.3 Thermal equivalent models of electrical machine parts

Depending on the desired accuracy and the geometry of the electrical machine, thermal models can be made with several different approaches. Different methods and equations can be found throughout the literature for the same machine parts, but there are also many similarities. Electrical machines are often treated as cylinders due to their cylindrical geometry, in which case the equation for thermal resistance in hollow cylinders can be used. This equation is displayed as equation 2.3.1[43]. [1]

$$R_{cond,cyl} = \frac{ln(r_2/r_1)}{2\pi \cdot L \cdot k} \tag{2.3.1}$$

When modelling smaller sections of electrical machines, the hollow cylinder equation is modified by an angle, θ, as [19] points out. The hollow cylinder equation for conduction is modified as equation 2.3.2 and the equation for convection on a cylindrical surface can be modified to equation 2.3.3. [1, 19, 43]

$$R_{cyl-seg_{cond}} = \frac{2\pi}{\theta} \cdot \frac{ln(\frac{r_o}{r_i})}{2\pi \cdot L \cdot k} \tag{2.3.2}$$

$$R_{cyl-seg_{conv}} = \frac{2\pi}{\theta} \cdot \frac{1}{2\pi r \cdot L \cdot h} \tag{2.3.3}$$

2.3.1 Stator yoke thermal resistance

In the literature it is generally agreed that the heat flow in the axial direction for the stator yoke and teeth can be neglected, due to the insulation between the stator sheets. Hence, only the thermal resistance in the radial direction need to be defined for the thermal models. The stator can be seen as a hollow cylinder and the thermal resistance can thereby be calculated by the equation for thermal resistance in hollow cylinders, equation 2.3.1. However, [44] points out that the whole length of the stator cannot be used, as a small part of the length is the insulating material. The length is therefore adjusted according to equation 2.3.4, where k_f is the iron space factor/stacking factor of the stator sheets and l_s is the length of the stator. Modelling the stator as a hollow cylinder is done in [31, 44, 45] among others. [1]

$$l_u = k_f \cdot l_s \tag{2.3.4}$$

According to [46–48], the stacking factor of electrical steel with a thickness of around 5mm is $k_f = 0.95$. [47] and [48] are product catalogues from two different manufacturers of electrical steel, while [46] uses rules of thumbs to decide the factor.

2.3.2 Stator teeth thermal resistance

For the thermal resistance of the stator teeth, both [31] and [45] uses the hollow cylinder equation modified with the factor, p_{st}, to account for the slots in the stator. This modified equation can be seen as equation 2.3.5. In the equation, p_{st} is a factor that weights the volume of the stator teeth with the total volume of the stator slots and teeth. Equation 2.3.6 can be used to determine p_{st}. [1]

$$R_{st} = \frac{2\pi}{\theta_s} \cdot \frac{ln(\frac{r_o}{r_i})}{2\pi \cdot L \cdot k \cdot p_{st}} \tag{2.3.5}$$

$$p_{st} = \frac{V_{teeth}}{V_{teeth} + V_{slots}} \tag{2.3.6}$$

2.3.3 Thermal modelling of stator slot with windings

The reviewed literature clearly indicates that modelling of the stator slot with windings is a complex area. Especially since this is one of the most important areas, when it comes to thermal modelling of electrical machines. As the windings usually stand for the largest share of losses in electrical machine. Several methods have been found in the literature and the some of the most relevant methods are described in this section. [1]

The first method, is called composite thermal conductivity by [29]. The composite thermal conductivity method can be seen utilized in [31, 42, 45] in addition to [29]. [29] explains that in this method, an equivalent thermal conductivity is calculated based on the material properties, residual air quantities, impregnation properties and so on of the slot with windings. The equivalent thermal conductivity, $k_{cu,ir}$, can be calculated by using equation 2.3.7, according to [42]. Knowing $k_{cu,ir}$, the thermal resistance of the stator slot with windings included can be calculated by equation 2.3.8. In the equation, t_{eq} is the equivalent thickness made out of the insulating material and air. [1, 29]

$$k_{cu,ir} = 0.2749 \cdot [(1 - k_f)A_{slot} \cdot L_{core}]^{-0.4471} \tag{2.3.7}$$

$$R_{cu,ir} = \frac{t_{eq}}{k_{cu,ir} \cdot A_{slot}} \tag{2.3.8}$$

A second method to make a thermal model of the stator slot with windings, is by simplifying the slot with the windings to complete rectangles. This is done in [19, 44, 49, 50]. This way of modelling the stator slot and windings enables the heat flow to be modelled in two directions, by making a so called "H-equivalent". The two directions being the radial direction and the tangential direction. Figure 2.3.1 illustrates the simplification made in [49]. In the model, two types of thermal resistances can be seen for each direction. The thermal resistance consisting of an equivalent air layer and the slot insulation, is denoted R_{ix} and R_{iy} for the two different directions, respectively. R_{xo} and R_{yo} is the thermal resistances of the equivalent slot material in the two respective directions. [1, 49]

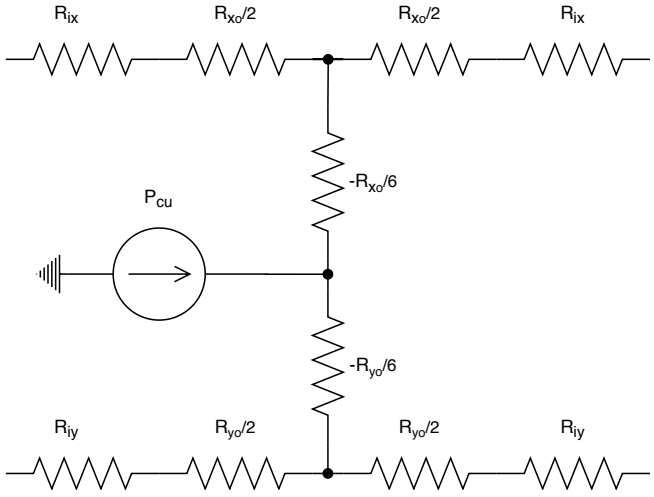

Figure 2.3.1: *Thermal equivalent circuit of stator slot with windings. The figure is remade from [49]. [1]*

The thermal resistances R_{ix} and R_{iy} can be calculated from equation 2.3.9 and equation 2.3.10, respectively. In the equations, d_i is the equivalent thickness of the slot insulation, d_a is the equivalent thickness of the air pockets in the slot, k_{ins} is the thermal conductivity of the insulation and k_a is the thermal conductivity of the air layers. While R_{xo} and R_{yo} can be calculated from equation 2.3.11 and equation 2.3.12, respectively. In these equations, k_{slot} is the thermal conductivity coefficient of the slot material, b is the width and h is the height. [1, 49]

$$R_{ix} = \frac{d_i}{h \cdot k_{ins}} + \frac{d_a}{h \cdot k_a} \tag{2.3.9}$$

$$R_{iy} = \frac{d_i}{b \cdot k_i} + \frac{d_a}{b \cdot k_a} \tag{2.3.10}$$

$$R_{xo} = \frac{b}{h \cdot k_{slot}} \tag{2.3.11}$$

$$R_{yo} = \frac{h}{b \cdot k_{slot}} \tag{2.3.12}$$

The equivalent air thickness, d_a, can be very complex to predict. [49] have proposed some solutions for d_a based on small induction machines. However, the author of [49] urges the readers to be careful when applying the numbers presented to other machines. The value of $d_a = 0.30mm$ is found utilized in [44], where a thermal model of a 50kW PMSM is made, using the work from [49] as a reference. [1]

According to [19], the equivalent thermal conductivity coefficient, k_{slot}, can be hard to predict. [19] claims that a DC-test would be necessary to accurately know its real value, while at the same time referring to [29], where three methods to predict the value have been mentioned. Among these is the composite thermal conductivity method that has been mentioned earlier. [19] continues without using equation 2.3.7 and instead uses the work presented in [49]. In [49], a relation between the equivalent thermal conductivity of the slot and the fill factor of the stator slot is suggested. The relation was plotted in [49] and the graph is displayed in appendix A as figure A.0.1.

Further, [19] explains that the total thermal resistance of the slot can be calculated as shown in equation 2.3.13. In the equation, Q_s is the number of stator slots and l is the length between the two nodes. R_x is calculated by equation 2.3.14 and R_y can be calculated form equation 2.3.15. [1, 19, 49]

$$R_{slot} = \frac{R_x \cdot R_y}{Q_s \cdot l(R_x + R_y)} \cdot \left(1 - \frac{R_{x0} \cdot R_{y0}}{720 \cdot R_x \cdot R_y}\right) \tag{2.3.13}$$

$$R_x = \frac{1}{2}(R_{ix} + \frac{R_{xo}}{6}) \tag{2.3.14}$$

$$R_y = \frac{1}{2}(R_{iy} + \frac{R_{yo}}{6}) \tag{2.3.15}$$

Finally, the total thermal resistance of the slot must be scaled when used to calculate the total thermal resistance between the slot node and adjacent nodes. This is done as shown in equation 2.3.16. In the equation, Φ_{slot} is the circumference of the slot and $\Phi_{slot,node}$ is the total length of the surface connecting the adjacent node with the slot. [19]

$$R_{slot,node} = R_{slot}\frac{\Phi_{slot}}{\Phi_{slot,node}} \tag{2.3.16}$$

The two methods mentioned above have some drawbacks. The first being that the models are not able to show the temperature distribution within the slot and windings. An other important drawback for the equivalent winding models, is that the average and maximum temperature becomes much higher than what they would be in reality, according to [51]. The author of [51] also highlight that because of this, equivalent winding models may not be applicable to high torque-density PM machines. Instead, a layered winding model is suggested. These models are

more complex than the equivalent winding models, but have been suggested in [29, 51–54] as they give a better temperature distribution than other models. Figure 2.3.2 represents a layered slot model for an arbitrary squared slot. It can be seen that the figure illustrates a four layer model, due to the four layers of copper in the slot. Note that the layers are not to scale.

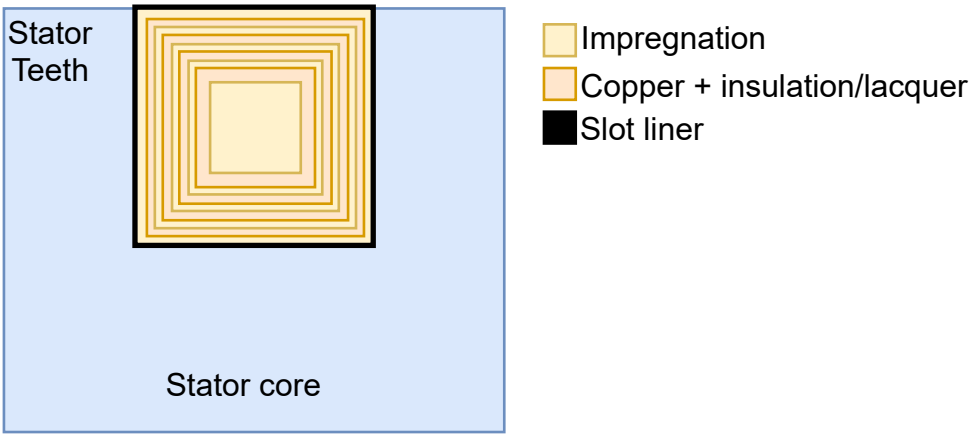

Figure 2.3.2: *Example of a layered slot model with four layers.[29, 51–54]*

In these layered models, the thermal resistances representing slot impregnation, liner, copper and wire insulation are placed in series from the slot wall to the middle of the slot. This is done in order to have conductors of about the same temperature in the same layer. In [29, 52–54], the first layer is the slot liner around the circumference of the stator slot. Determining the thermal resistance in each layer is easy, as they can be calculated by the equation for thermal resistance due to conduction, equation A.0.1 in appendix A. However, determining the air pockets in the insulation and the layer thickness can be more complex. To determine the air pockets in the impregnation, [29] and [52] mentions a factor called the impregnation goodness. If The impregnation goodness is 90%, it means that there is 10% air pockets in the impregnation. The thermal resistance of the impregnation is then equal to 0.9 times the thermal resistance of the impregnation plus 0.1 times the thermal resistance of motionless air. [29, 51–54]

[54] show an iterative approach to determine the layered model parameters, while [52] and [53] only mentions that these are decided by a programming software. [51] on the other hand, gives a set of equations that can be used to determine the layered model. For the calculations, [51] treats each wire as a square wire and calculates the area of all wires inside one slot as shown by equation 2.3.17. In the equation, N_t is the number of wires in each conductor, N_s is the total number of conductors in each individual slot and d is the diameter of the windings including the insulation lacquer. [51]

$$A_1 = N_t \cdot N_s \cdot d^2 \tag{2.3.17}$$

Using the slot fill factor, [51] calculates an effective area of the wires, by using equation 2.3.18. In the equation, F_{ss} is the stator slot fill factor. Around the square wires, there is also epoxy

resin. The total area of the square wire plus the resin can be calculated from equation 2.3.19, giving the area for each of the squares in the slot. All parameters in the equation have been described earlier. [51]

$$A_2 = \frac{A_1}{F_{ss}} \tag{2.3.18}$$

$$A_3 = \frac{A_2}{N_t \cdot N_s} \tag{2.3.19}$$

Knowing the area of the squared components in the slot, A_3, the average space between the wires can be calculated from equation 2.3.20. If a parallel arrangement of wires is assumed from the slot wall to the centre of the slot, the perimeter of the layers can be calculated from equation 2.3.21. In the equation, L_a is the slot perimeter and i denotes the number of layers in the slot. [51]

$$\delta = \sqrt{A_3} - d \tag{2.3.20}$$

$$L_i = L_a - 4 \cdot i \cdot (d + \delta) \tag{2.3.21}$$

When the perimeter of the layers is known, the number of wires in an arbitrary layer can be calculated from equation 2.3.22. In addition, the overall number of all wires can be calculated from equation 2.3.23. In the equation, p is the total number of all the layers. [51]

$$n_i = \frac{L_i}{\sqrt{A_3}} \tag{2.3.22}$$

$$\sum_{i=1}^{p} n_i = N_t \cdot N_s \tag{2.3.23}$$

[51] mentions that the wire diameter can often be very small. Because of this, some layers may be combined. The combination includes the winding layer and the insulation layer. From equation 2.3.24 and equation 2.3.25, the width of the winding layer and the width of the insulation layer can be calculated, respectively. In the equations, m is the number of layers for the single wire.

$$d_{ave} = d \cdot m \tag{2.3.24}$$

$$\delta_{ave} = d \cdot m \tag{2.3.25}$$

As a final remark, [51] also mentions that the very first layer at the slot wall should be made out of the slot liner, insulating paint and the epoxy resin. While the rest of the insulating layers are made out of the epoxy resin and the insulating paint only. The thermal conductivity coefficient of the layers can be calculated as shown in equation 2.3.26, using the materials that exists in the layers. In the equation, δ_i is the thickness related to each individual insulating material and k_i is the thermal conductivity coefficient related to each of the insulating materials for the layer. [51]

$$k_{eq} = \sum_{i=1}^{n} \delta_i / (\sum_{i=1}^{n} \delta_i / k_i) \tag{2.3.26}$$

2.3.4 Thermal resistance of the rotor

The thermal rotor models in the literature vary, as the rotor geometry and rotor type differs for different electrical machines. The ModHVDC machine is a permanent magnet machine with surface mounted magnets. Because of this, only literature that uses the same type of rotor and magnets have been considered in this section.

[31] makes a simplified thermal model of a PM motor for an electric vehicle and used the hollow cylinder equation, shown as equation 2.3.1, to model the thermal resistance in both the rotor core and the rotor magnets. However, a slight modification is made when calculating the thermal resistance of the magnets, in order to account for the retaining sleeve. The modified hollow cylinder equation is shown as equation 2.3.27. In the equation, r_2 and r_1 is the radius of the magnets and the rotor core, respectively. N_{pol} is the number of poles, θ is the angle of one pole in radians, k_m is the thermal conductivity of the magnet material and L_p is the length of the magnets in the axial direction. The hollow cylinder method is also found in [19] and [44]. [19, 31, 44]

$$R_{mag} = \frac{ln(r_2/r_1)}{N_{pol} \cdot \theta \cdot k_m \cdot L_p} \tag{2.3.27}$$

[19] points out that there will be a contact resistance between the rotor core surface and the magnets. In addition, it seem to be generally agreed in the reviewed literature that the thermal resistance of the shaft is only considered for the axial direction.

2.4 Thermal contact resistances

The reviewed literature have stated that contact resistances (or also called interface thermal resistance) in electrical machines may add up to large thermal resistances. Because of this, contact resistances should be included in the thermal modelling process for an accurate temperature estimation. In electrical machines, there are mainly three interfaces where contact resistance have been included. This is in the slot area, between the frame and the stator yoke and between the magnet and the rotor core. [1, 19, 29, 37, 44, 55–57]

[55] makes clear that the contact resistance is a complex function, based on the materials hardness, pressure applied at the interface, smoothness of the surface, air pressure within the gap, thermal expansion and so on. This means that it is very hard to determine an accurate value for these types of thermal resistances. However, it is stated in both [55] and in [29] that smoother and softer surfaces equivalates to smaller equivalent gaps. Thereby resulting in a smaller thermal resistance. [58] gives a very clear statement on the importance of ensuring good contact between interfaces, stating that expensive conducting materials are a total waste of effort and cost if the interfaces are made inadequately. [1, 55, 58]

Most commonly in electrical machines, the contact resistance is modelled as a pre-defined or measured interface gap. The thermal resistance of these interface gaps can be calculated by $R_c = \frac{g_e}{k_g A_g}$[44]. Where g_e is the gap length, k_g is the thermal conductivity of the gap and A_g is the area of the gap. The utilization of this method can be found in [19, 29, 37, 44, 55] and more. Different equivalent gaps for given material-to-material interfaces can be found in research papers and in any heat transfer text book. For example [58] and [43], to mention two. [1]

A table displaying equivalent gap lengths for some material-to-material interface is found in [55] and [29], both citing the the work from Mills[59]. The table is adapted as table 2.4.1 for this thesis. An other method used to find the thermal contact resistance, is by using the equivalent conductance. Using the fact that $R = 1/G$, where G is the equivalent conductance [19].

Table 2.4.1: *Equivalent gap lengths for some material-to-material interfaces. Table adapted from [29].*

Interface	**Equivalent conductance** $[W/m^2/C]$	**Equivalent gap length** **[mm]**
Ceramic-Ceramic	500-3000	0.0087-0.0052
Ceramic-Metal	1500-8500	0.0031-0.0173
Graphite-Metal	3000-6000	0.043-0.0087
Aluminum-Aluminum	2200-12000	0.0022-0.0012
Stainless-Aluminum	3000-4500	0.0058-0.0087
Iron-Aluminum	4000-40000	0.0006-0.0060
Copper-Copper	10000-25000	0.0010-0.0026

2.5 Different cooling methods and techniques

In this section, a literature study on relevant cooling methods and techniques is done. The goal is to find methods and techniques that can be used in the ModHVDC machine. As airflow in the air gap already has been investigated earlier in this thesis, the section mainly focuses on other techniques. Cooling ducts and channels are investigated first, before looking into cooling in the rotor.

2.5.1 Cooling ducts & channels

A seemingly popular cooling method for high power density electrical machines, is the use of cooling ducts or channels. These ducts or channels are in some cases referred to as water-jackets. The literature gives a wide variety of ducts and channels, depending on the need of the specific machine. As for the fluid flow in the air gap, the difficult aspect is to determine the convective heat transfer coefficient based on the Nusselt number. However, [17] and [55] gives some useful correlations to determine the Nusselt number for ducts and channels of different shapes. Note that both [17] and [55] references [60] for the correlations. Figure 2.5.1 illustrates an electrical machine with round ducts implemented in the stator yoke, with one duct for every other stator slot. [33] also uses round ducts in both the stator and the rotor. Figure A.0.3 in appendix A, is taken from [33] and shows where these round ducts are implemented.

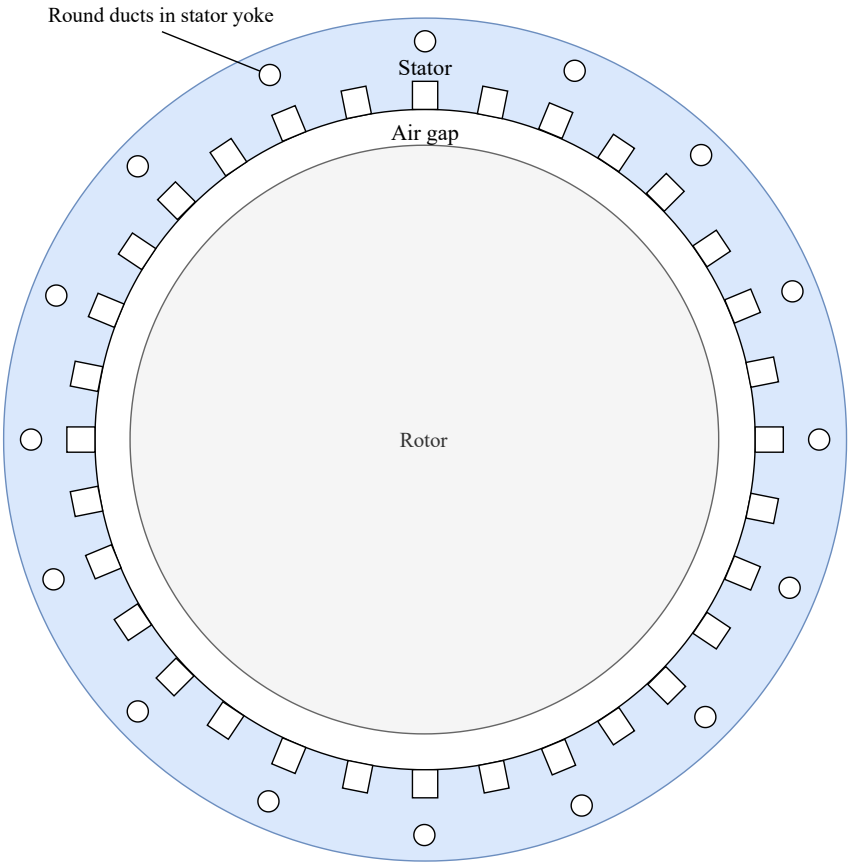

Figure 2.5.1: *Illustration of round ducts in stator yoke. It can be seen that one duct is used for every other slot in the stator.*

According to [17] and [55], the Nusselt number for laminar flow in a circular/round channel, a rectangular channel and a channel in a concentric cylinder can be calculated from equation 2.5.1, equation 2.5.2 and equation 2.5.3, respectively. Note that only [55] specifies that these correlations are used for enclosed channels. In the equations, D_h is the hydraulic diameter, L is the length of the surface, H is the channel height and W is the channel width. Both [17] and [55] also emphasises that these correlations take entrance length correction into account. This means that the correlations takes into account the distance the fluid needs to travel after entering the channels, before the temperature and velocity are fully developed. Equation 2.5.1 can also be found used in [61], specifying that the correlation is used for a Prandtl number of $P_r \geq 5$. While equation 2.5.2 is utilized in [20, 54]. In addition, [55] and [61] makes the statement that the Reynolds number for these correlations should be calculated as shown by equation 2.5.4. In the equation, v is the velocity of the fluid and μ is the dynamic viscosity of the fluid. [17, 55, 61]

$$N_u = 3.66 + \frac{0.065 \cdot (D_h/L) \cdot R_e \cdot P_r}{1 + 0.04 \cdot \left((D_h/L) \cdot R_e \cdot P_r^{2/3}\right)} \tag{2.5.1}$$

$$N_u = 7.49 - 17.02 \cdot \frac{H}{W} + 22.43 \cdot \left(\frac{H}{W}\right)^2 - 9.94 \cdot \left(\frac{H}{W}\right)^3 + \frac{0.065 \cdot (D_h/L) \cdot R_e \cdot P_r}{1 + 0.04 \cdot \left((D_h/L) \cdot R_e \cdot P_r^{2/3}\right)} \tag{2.5.2}$$

$$N_u = 7.54 + \frac{0.03 \cdot (D_h/L) \cdot R_e \cdot P_r}{1 + 0.016 \cdot \left((D_h/L) \cdot R_e \cdot P_r^{2/3}\right)} \tag{2.5.3}$$

$$R_e = \rho \cdot D_h \cdot \frac{v}{\mu} \tag{2.5.4}$$

When the flow in these channels become turbulent, a new correlation is used by both [17] and [55]. The correlation is shown as equation 2.5.5 and is valid for Reynolds numbers in the range of $300 < R_e < 10^6$. However, [17] points out that the flow for round and rectangular channels are considered laminar for a Reynolds number of $R_e < 2300$. For concentric channels the flow is laminar for a Reynolds number of $R_e < 2800$. This means that between the turbulent limit of $R_e = 3000$ and these, a transition flow is found. If this is the case, [17] explains that a weighted average between laminar flow and turbulent flow should be calculated based on the Reynolds number. In the correlation, the factor f is a friction factor that can be calculated as shown in equation 2.5.6 for smooth walls. [17, 55]

$$N_u = \frac{f}{8} \cdot \frac{(R_e - 1000) \cdot P_r}{1 + 12.7 \cdot (f/8)^{0.5} \cdot (P_r^{2/3} - 1)} \tag{2.5.5}$$

$$f = (0.790 \cdot Ln(R_e) - 1.64)^{-2} \tag{2.5.6}$$

In the above correlations, the hydraulic diameter for the channels are also needed. According to [17] and [55], the hydraulic diameter for concentric cylinders are calculated as shown in equation 2.5.7. Where h_{gap} is the length across the gap. For round or rectangular channels, the hydraulic diameter is four times the cross section area, divided by the perimeter. Giving equation 2.5.8 for rectangular channels and equation 2.5.9 for round channels. It is also important to note that these hydraulic diameters assume that the channels are completely full. [17, 20, 55]

$$D_{h_{conc}} = 2 \cdot h_{gap} \tag{2.5.7}$$

$$D_{h_{rect}} = \frac{4 \cdot H \cdot W}{2(H + W)} = \frac{2 \cdot H \cdot W}{H + W} \tag{2.5.8}$$

$$D_{h_{circ}} = \frac{4(\pi \cdot r^2)}{2\pi \cdot r} = 2r = D \tag{2.5.9}$$

Both [17] and [20] claims that the above correlations can be used for spiral or helical ducts. However, [62] uses a slightly more complex correlation when modelling a spiral cooling channel with good accuracy. An illustration of a helical or spiral duct, adapted from [62], is shown as figure 2.5.2. In the correlation, a critical Reynolds number is calculated as shown in equation 2.5.10. In the equation, D_c is an equivalent curve diameter for the helical duct. D_c can be calculated as shown in equation 2.5.11. Here, D is the diameter of the spiral itself, h is the spacing between each turn in the spiral and d is the diameter of the duct. In addition to the critical Reynolds number, the actual Reynolds number is calculated as previously shown in equation 2.5.4.

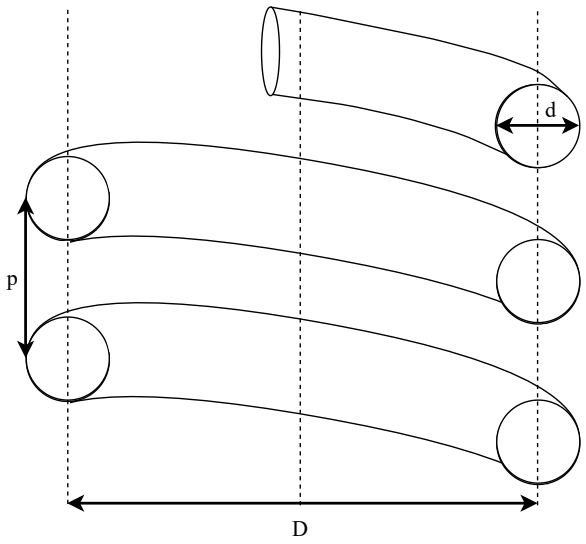

Figure 2.5.2: *Illustration of a spiral/helical duct with geometric designations. The figure is remade from [62].*

$$R_{e_c} = 2300\left(1 + 8.6(\frac{d}{D_c})^{0.45}\right) \tag{2.5.10}$$

$$D_c = D\left(1 + (\frac{p}{\pi \cdot D})^2\right) \tag{2.5.11}$$

[62] then uses the critical Reynolds number and the actual Reynolds number to check if the flow is laminar or turbulent. If the actual Reynolds number is lower than the critical value, a laminar flow correlation is used. This correlation is shown as equation 2.5.12. Note that this correlation uses P_r as the Prandtl number at bulk temperature and P_{r_w} as the Prandtl number with wall temperature. The exponent m, is calculated from equation 2.5.13. [62]

$$N_u = \left(3.66 + 0.08\left(1 + 0.8\left(\frac{d}{D_c}\right)^{0.9}\right)R_e^m \cdot P_r^{1/3}\right) \cdot \left(\frac{P_r}{P_{r_w}}\right)^{0.14} \tag{2.5.12}$$

$$m = 0.5 + 0.2903 \cdot \left(\frac{d}{D_c}\right)^{0.194} \tag{2.5.13}$$

If the flow becomes turbulent, which [62] defines as $R_e > 2.2 \cdot 10^4$, the correlation shown as equation 2.5.14 is used. The undefined variable in this correlation, is the pressure loss coefficient "ξ". The pressure loss coefficient can be calculated as shown by equation 2.5.15. As a final remark, [62] mentions that if the actual Reynolds number is between the critical value and the turbulent value a weighted average should be calculated. This should be done by using $R_e = R_{e_c}$ in equation 2.5.12 and the critical value for equation 2.5.14, before using interpolating. [62]

$$N_u = \frac{R_e \cdot P_r \cdot \xi/8}{1 + 12.7\sqrt{\xi/8} \cdot (P_r^{2/3} - 1)} \cdot \left(\frac{P_r}{P_{r_w}}\right)^{0.14} \tag{2.5.14}$$

$$\xi = \frac{0.3164}{R_e^{0.25}} + 0.03 \cdot \left(\frac{d}{D_c}\right)^{0.5} \tag{2.5.15}$$

2.5.2 Cooling in the rotating shaft

Since the rotor of electrical machine are rotating, it may be more complex to find a suitable cooling solution. In the reviewed literature, the most common method used to cool the rotor, seem to be a wet rotor solution. A wet rotor solution implies that the rotor is in direct contact with a fluid, that has high heat transfer capabilities and thereby dissipating the heat efficiently. However, as [63] points out, this may increase the friction losses in the machine in addition to increasing the risk of short circuits or even corrosion.

Another cooling solution for the rotor, that is described in [61, 63–67] among others, is an indirect cooling method where a hollow shaft is used. In the hollow shaft, fluids like water, air or oil can be pumped or otherwise forced through, to give high heat dissipation. As for the other cooling methods earlier described, the most difficult aspect of this cooling method, is to find the heat transfer coefficient. [63] also emphasises that since the rotor is a rotating part, both the rotational and the axial flows must be considered for the correlation used. An important observation is that this shaft cooling method is mostly used in high-speed applications. The Reynolds numbers for axial and rotational flow can both be calculated as shown by equation 2.5.4, using the respective fluid velocities in m/s. [61, 63–67]

Figure 2.5.3, taken from [65], illustrates the use and flow path for fluid in a hollow shaft. It can be seen that a rotating coupling is used at the inlet and outlet.

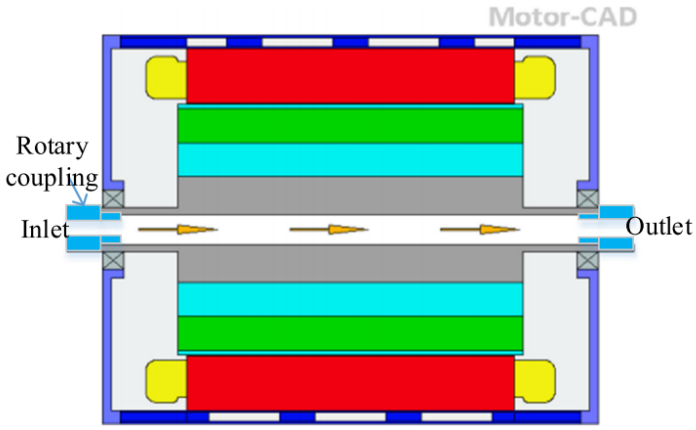

Figure 2.5.3: *Illustration of hollow shaft cooling. Figure taken from [65].*

[63] uses the correlation shown as equation 2.5.16 for low Reynolds numbers and equation 2.5.17 for higher Reynolds numbers in the rotating hollow shaft, citing the work from [68]. In the context of these correlations, equation 2.5.16 is valid for $1.6 \cdot 10^3 < R_{e_r} < 2.77 \cdot 10^5$ and $0 < R_{e_a} < 3 \cdot 10^4$, where R_{e_a} is the axial Reynolds number and R_{e_r} is the rotational Reynolds number. While equation 2.5.17 is valid for $R_{e_r} > 2.77 \cdot 10^5$. In [68], the convection inside a rotating cylinder with axial airflow is studied. With the use of experimental identification techniques and numerous models, suitable correlations was defined for both low Reynolds numbers and high Reynolds numbers. [68] also makes clear that for high rotational Reynolds

numbers, the convection is dominated by the rotating air flow. Resulting in equation 2.5.17. [63, 68]

$$N_u = 0.01963 R_{e_a}^{0.9285} + 8.5101 \cdot 10^{-6} \cdot R_{e_r}^{1.4513} \tag{2.5.16}$$

$$N_u = 2.85 \cdot 10^{-4} \cdot R_{e_r}^{1.19} \tag{2.5.17}$$

In [61] it is however claimed that the existing correlations used for hollow shafts are not applicable, if oil is the cooling fluid. Here, the convective heat transfer coefficient is investigated for a high speed PMSM with oil in the hollow shaft of the rotor. Using several models and CFD, a correlation is purposed. The correlation is shown as equation 2.5.18. [61] makes clear that the correlation developed, is only investigated for a rotational Reynolds number in the range of $2375 < R_{e_r} < 1.75 \cdot 10^5$, a Prandtl number ranging $145 < P_r < 712$ and a axial Reynolds number between $30 < R_{e_a} < 80$. Because of the low axial Reynolds number, the only considerable parameter becomes the rotational Reynolds number. It is also stated that this correlation could be used for numerous geometrical channels and flow rates, in both the axial and rotational direction. [61]

$$N_u = 3.811 \cdot 10^{-3} \left(\frac{1}{R_{e_r} \cdot P_r} \right)^{-0.641} \tag{2.5.18}$$

Another correlation used for hollow shaft cooling, with water as the fluid, is thoroughly investigated and described in [65]. In the article, both CFD models and a test rig has been used to find an expression for the Nusselt number. [65] states that the correlation should be valid for an axial Reynolds number between $3521 < R_{e_a} < 10\,563$ and a rotational Reynolds number between $0 < R_{e_r} < 16\,890$. The correlation is shown as equation 2.5.19. [65] point out that the heating of the fluid from the inlet to the outlet, is taken into account by the exponent of the Prandtl number.

$$N_u = 7.438 \cdot 10^{-3} \cdot R_{e_a}^{0.09683} \cdot P_r^{0.4} + 9.183 \cdot 10^{-5} \cdot R_{e_r}^{1.358} \cdot P_r^{0.4} \tag{2.5.19}$$

Chapter 3

Modelling

This chapter introduces and explains the methods and models that are used to illustrate the ModHVDC machine. First, an evaluation of the heat transfer coefficient in the rotor-stator air gap is done. The heat transfer from the frame to the ambient air is then modelled. After, the thermal equivalent model is built, starting by defining nodes and then each thermal resistance that is used. In addition, an explanation of how the losses are added to the circuit is done. The chapter proceeds with an explanation of how the FEM model is made. The last sections in this chapter, is used to introduce several cooling techniques that are implemented in the models to cool the ModHVDC machine. Keep in mind that only 2D-models are made in this thesis.

3.1 Thermal convection coefficient in rotor-stator air gap

As a physical prototype nor a fully functional 3D model is made of the modHVDC machine, it can be hard to predict the convection coefficient in the rotor-stator air gap. However, based on geometrical similarities with the correlations presented in the literature study, the convection coefficient in the rotor-stator air gap is estimated.

It is not yet known if there will be through-flowing air in the air gap, or if there will be airflow due to the rotating rotor only. Hence, three convection coefficients are investigated. One where air flow in the axial direction only, is considered. The second where only the rotation of the rotor is considered and the last where both axial air flow and air flow due to rotation is considered.

To be able to choose one of the correlations, the geometric factors Γ, η, e/R_1 is calculated based on the geometry of the reference machine. Giving $\Gamma = 100$, $\eta = 0.997$ and $e/R_1 = 0.003$. These geometrical factors are calculated as shown in the literature, section 2.1.2. As mentioned earlier, the reference machine is described in appendix B.

A MATLAB-script containing all the calculations for the convective heat transfer coefficients in the rotor-stator air gap, is shown in appendix E.

3.1.1 Convection coefficient with axial airflow only

The convection coefficient when only considering axial airflow, is found using the same method as described in section 2.1.1. Equation 2.1.2 and equation 2.1.3 are used to find two Nusselt numbers, before the average between these is used in equation 2.1.1 to decide the convection coefficient. The resulting convection coefficient is plotted as a function of the axial air flow velocity. The plot is shown as figure 3.1.1. In the figure it can be seen that the convection coefficient greatly increases for higher axial airflow velocities, reaching almost $100 W/m^2K$ for an airflow velocity of 20 m/s.

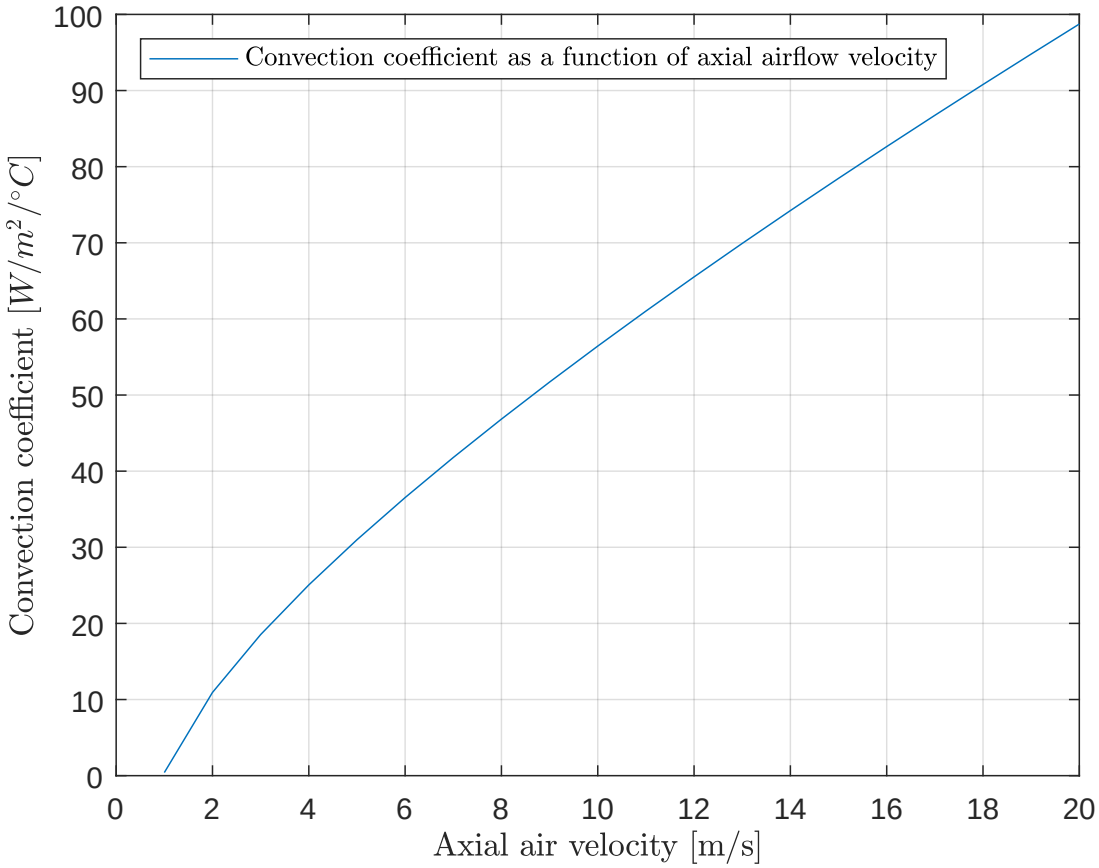

Figure 3.1.1: *Convection coefficient in the air gap, with axial airflow only.*

3.1.2 Convection coefficient based on airflow due to rotation only

Based on Γ, η and e/R_1, the correlation used is chosen from the most fitting correlation displayed in table 2.1.1. Studying the table it becomes clear that none of the correlations perfectly fits the reference machine. Because of this, the two correlations closest to that of the reference machine, is considered. These are the correlations from Becker and Kaye[22] and the one from Bjorklund and Kays[25]. In addition, the correlation from Aoki et al.[26] does not require knowledge of the geometrical factors of the machine and has also been considered. These three correlations have been used, calculating the corresponding convection coefficient as a function of rotor rotational speed in RPM. The resulting convection coefficients have been graphed together in figure 3.1.2, in addition to the average value. It is clear that higher rotational speed gives higher convection coefficients. However, the magnitude is far lower than for the convection coefficient considering axial airflow.

All the correlations used, have a validity given by the Taylor number. Using equation 2.1.6 to calculate the highest Taylor number due to rotation (10 RPM, given by reference machine), the Taylor number is calculated to $T_a = 1.66 \cdot 10^4$. This is within all the upper limitations for the correlations used.

In section 2.1.2, a different method to calculate the convection coefficient in the rotor-stator air gap than the correlations presented in table 2.1.1, was also described. The method involved equation 2.1.10 and equation 2.1.11. When calculating the convection coefficient with this method, the results became very similar to the Becker an Kaye correlation and has therefore been removed from the graph in figure 3.1.2, in an attempt to make the figure easier to read.

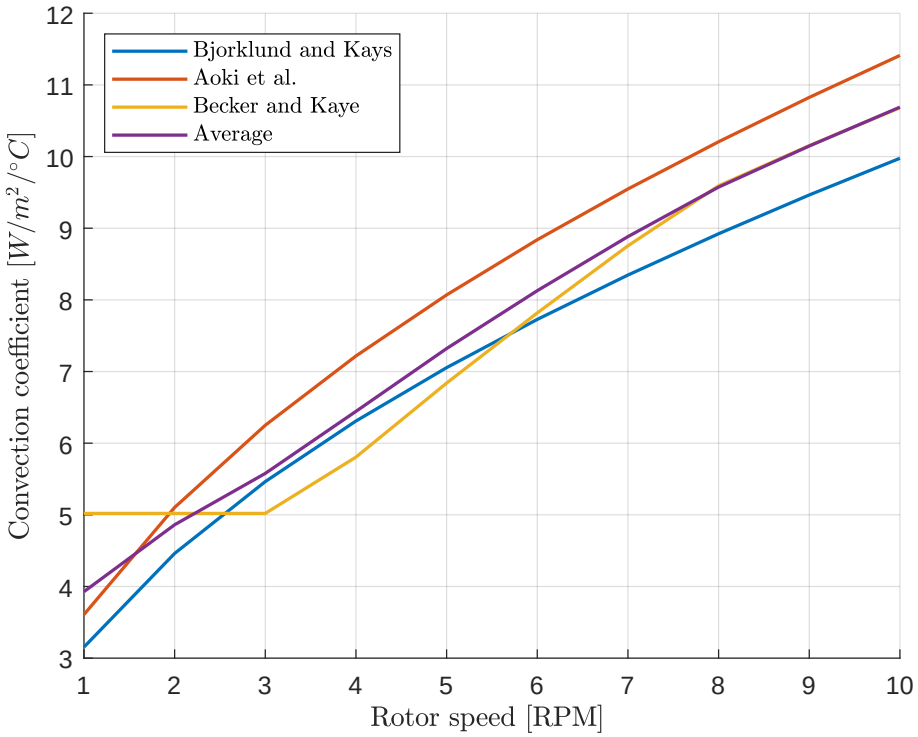

Figure 3.1.2: *Convection coefficient in the air gap, with airflow due to rotating rotor only. Three different correlations are used and displayed, in addition to the average value.*

3.1.3 Considering both rotation of rotor and axial forced airflow

When considering both rotation of the rotor and forced axial air flow, table 2.1.2 can be used to find a fitting correlation for the convection coefficient. Based on the cylindrical gap aspect ratio, η, there are three correlations that are fairly close to the reference machine. However, for this model, the Reynolds number becomes relatively high for medium to high axial air flow velocities. While the Taylor number, calculated by equation 2.1.16, is relatively low. Because of this, the correlation made by Gazley et al. is considered to be the most relevant. Keeping the rotational speed at nominal value (10 RPM), the forced air flow velocity was changed from 1m/s to 15m/s, while calculating the convection coefficient for each step. The resulting convection coefficient is displayed in figure 3.1.3. It can be seen that the convection coefficient almost has a linear relation to the axial flow velocity, when keeping the rotational speed of the rotor constant. The axial air flow velocity is the easiest parameter to change with regards to cooling of the machine and is therefore chosen as the dynamic factor in this correlation, instead of the rotor rotational speed.

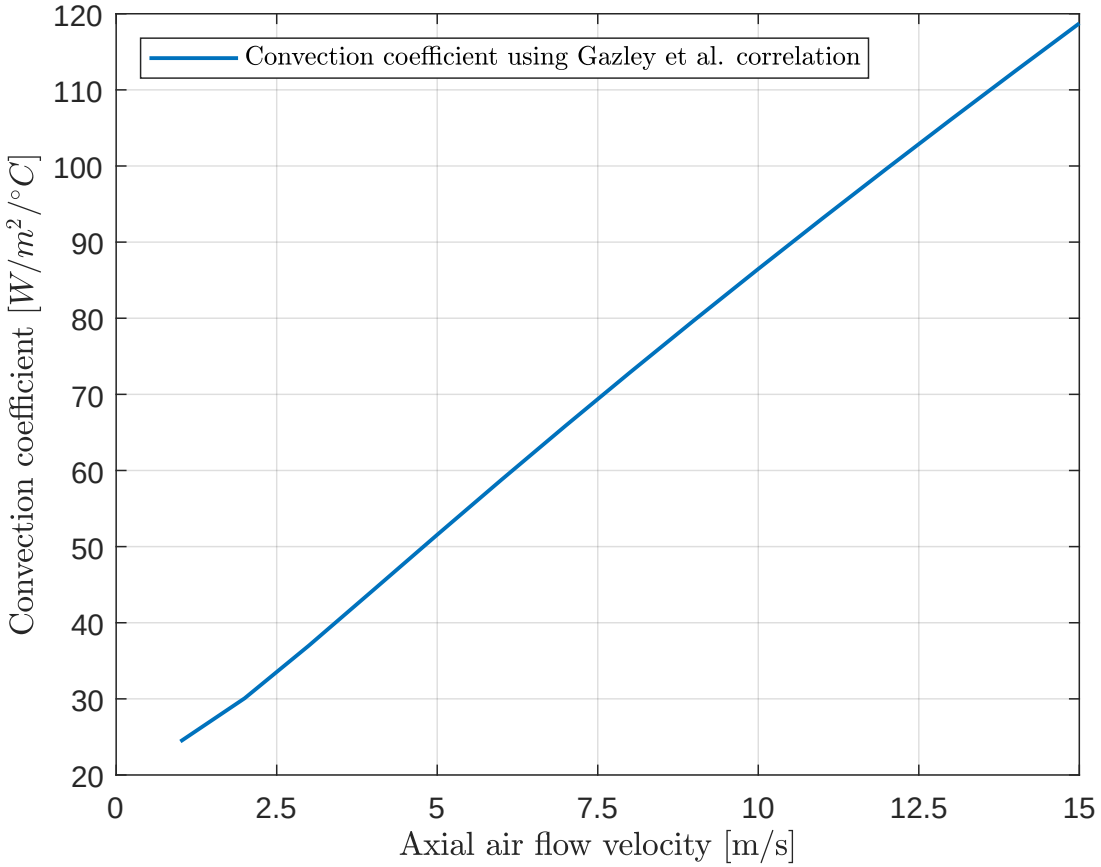

Figure 3.1.3: *Convection coefficient in the air gap with both axial air flow and air flow due to rotating rotor.*

3.2 Frame to ambient convection coefficient

The convection coefficient from the machine frame to the ambient, can be modelled as either natural convection or forced convection. As "worst case" scenario, the frame to ambient convection is modelled as natural convection only.

As explained in the literature section 2.2, the Grashof number and the Prandtl number is needed to calculate the natural convection coefficient. The Prandtl number can be set to $P_r = 0.7$, as earlier explained and the Grashof number is calculated from equation 2.2.2. Yielding $G_r = 6.64 \cdot 10^{11}$, for an ambient temperature of about $20°C$ and $\Delta T = 10°C$. In order to decide witch correlation to use in equation 2.2.1, the product of the Prandtl number and the Grashof number is needed. Yielding $P_r \cdot G_r = 4.85 \cdot 10^{11}$. From equation 2.2.1, the correlation $N_u = 0.129(G_r \cdot P_r)^{0.33}$ is chosen and the convection coefficient is calculated from equation 2.1.1. As the factor ΔT is an unknown factor in reality, the resulting convection coefficient has been plotted as a function of ΔT. This is displayed in figure 3.2.1. From the figure, it becomes clear that a ΔT of about $45°C$ is needed to achieve a convection coefficient of about $5W/m^2K$.

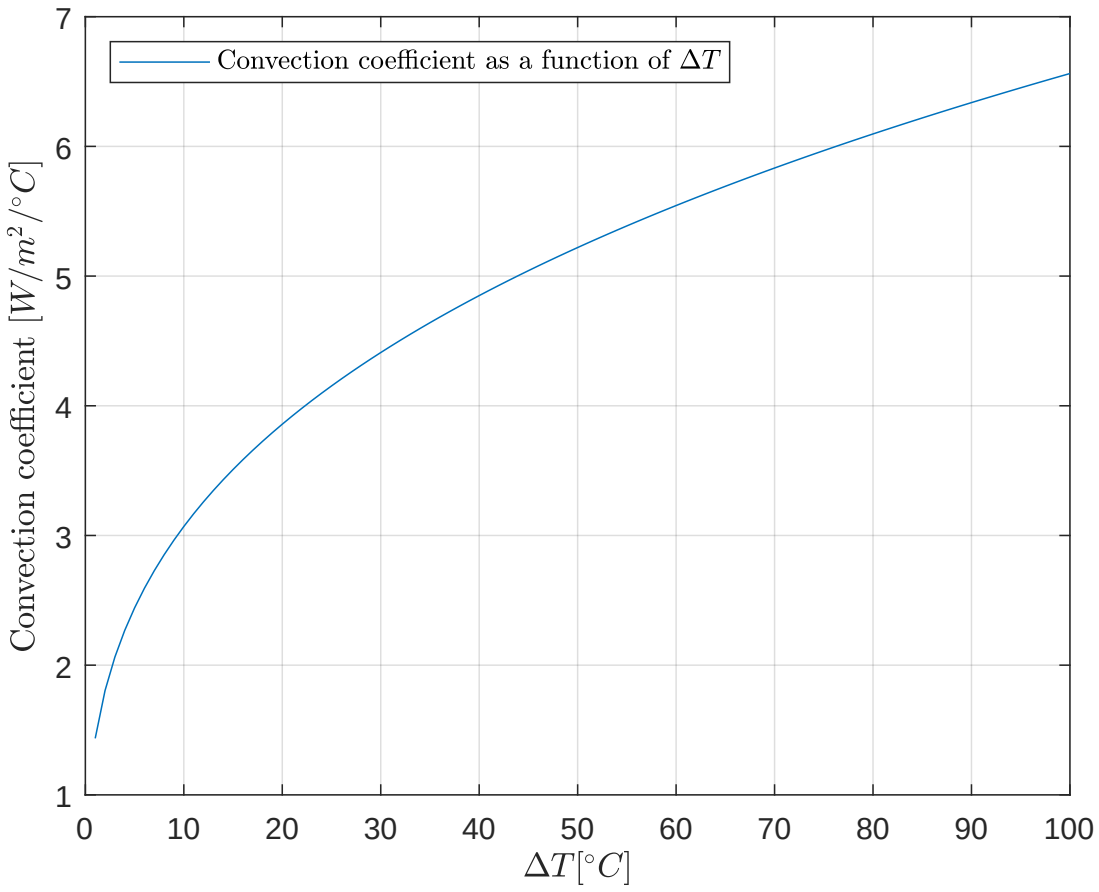

Figure 3.2.1: *Natural convection coefficient between frame and ambient as a function of ΔT.*

3.3 Thermal equivalent model

This section describes and illustrates how a base thermal equivalent model is made, based on the equations and methods shown in the literature section. The model made for this thesis is a 2D model, meaning that for all practical purposes the lengths in the axial direction has been ignored (same as setting L=1) when calculating the thermal resistances. Yielding the thermal resistance per unit length. In addition, no specific cooling method is added to the basic model. However, the temperature in the middle of the air gap is set to $40°C$ in order to get reasonable temperatures when solving the circuit. The main goal for the base model is to be compared with a FEM model with as low as possible difference in resulting temperatures. However, first the nodal placement is decided.

3.3.1 Nodal placement & base equivalent circuit

When making thermal models of electrical machines, the geometric symmetries in the machines are often used to make reduced and simplified models. Because of the geometric symmetries, a section of the machine that repeats itself can be modelled instead of the whole machine. For the ModHVDC machine, a section that repeats itself is equal to half a slot plus half a stator tooth. Figure 3.3.1 illustrates the section that is modelled, by two dotted lines. In the same figure the nodal placements can be seen. According to [7], it is important that the nodes are placed where an average temperature can be observed for a specific machine part or object. Because of this, all the nodes are placed at the midpoint of the respected machine part, in the radial direction. The nodes are shown as black dots in the figure. [1]

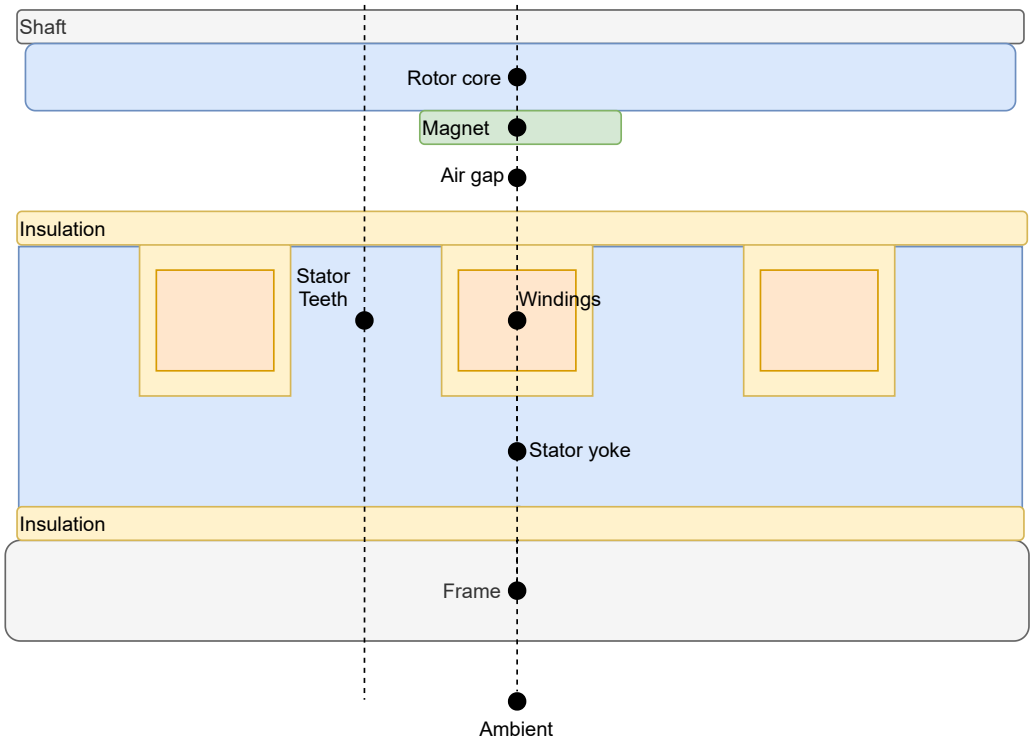

Figure 3.3.1: *Illustration of the modelled section of the ModHVDC machine, together with the nodal placement for the thermal model. The stator part of the figure was originally made in [1].*

The length between the dotted lines in figure 3.3.1, is defined by an angle, θ_s. This is because the machine is cylindrical in reality and not rectangular, as the figure might suggest. The angle θ_s is therefore used in later sections to scale the thermal resistances for the modelled section, as seen by equation 2.3.2 in the literature. Equation 3.3.1 is used to decide θ_s, where the length between the dotted lines is denoted $s = \frac{b_{ss}}{2} + \frac{b_{st}}{2}$. r is the radius at the winding node (same as stator teeth node) placement. Yielding $\theta_s \approx 0.016rad$. In reality, the angle would change depending on the radial position in the machine. However, θ_s is used in all thermal resistances that are scaled, as the geometry of the ModHVDC machine is large. [1]

$$\theta_s = \frac{s}{r} \tag{3.3.1}$$

Between the nodes, there are equivalent thermal resistances. Figure 3.3.2 is made to illustrate the general thermal equivalent circuit, including all the nodes. All the resistances in the figure are composed of several smaller sub-resistances. In addition, the figure illustrates how the losses in the machine are added to the respective nodes as current sources. Black resistances indicates purely conductive resistances, while blue resistances indicates that the resistance has elements of convection applied to one or more of the sub-resistances.

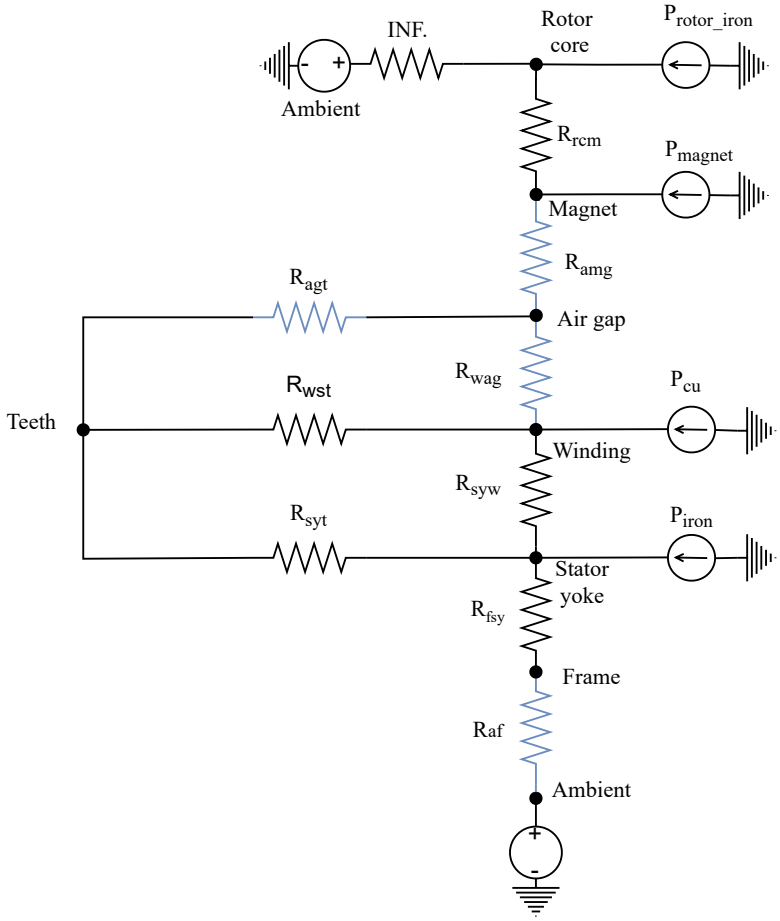

Figure 3.3.2: *General thermal equivalent circuit for the ModHVDC machine. The resistances in the figure consists of several smaller sub-resistances. The stator part was originally made in [1].*

In figure 3.3.2 it can be observed that the circuit starts (from the bottom) at ambient temperature, going through the whole machine and ends at ambient temperature at the other side of the rotor core. The ambient temperature at the rotor core is connected through an infinitely large resistance, meaning that no heat will flow in this direction. The only reason for this resistance, is to make the circuit a closed loop. In reality, some heat would flow in the axial direction and eventually reach the surrounding air and ambient temperature.

Table 3.3.1 is made for the reader to get a better understanding of the general thermal resistances shown in figure 3.3.2. Every individual sub-resistance that make up the resistances in table 3.3.1, are presented and described in the following sections.

Table 3.3.1: *Description of the thermal resistances for the general thermal network displayed as figure 3.3.2.* R_{af} *to* R_{agt} *has the same description in [1].*

Thermal resistance name	Description
R_{af}	Resistance between ambient air and middle of machine frame
R_{fsy}	Resistance between the middle of the machine frame and stator yoke
R_{syw}	Resistance between stator yoke and windings
R_{wag}	Resistance between windings and the start of the air gap
R_{syt}	Resistance between stator yoke and stator teeth
R_{wst}	Resistance between windings and stator teeth
R_{agt}	Resistance between stator teeth and the start of the air gap
R_{amg}	Resistance between Air gap and the middle of the magnet
R_{rcm}	Resistance between magnet and the middle of rotor core
INF.	Infinite resistance between rotor core and ambient temperature

3.3.2 Frame-to-ambient & frame thermal resistance

From the machine frame surface, there is a convective thermal resistance to the ambient air surrounding the machine. As explained in section 3.2, this convective thermal resistance is modelled with natural convection only. The thermal resistance for a given ΔT between the ambient and the surface of the machine frame, can easily be calculated. First, the correlation described in section 3.2 is used to find the convective heat transfer coefficient. Then, the thermal resistance can be calculated using the hollow cylinder equation. Resulting in equation 3.3.2.

$$R_{amb} = \frac{2\pi}{\theta_s} \cdot \frac{1}{2\pi r_m \cdot h_{amb}} \tag{3.3.2}$$

However, as the convection coefficient, h_{amb}, is dependent on the temperature difference between the frame and the ambient, this thermal resistance is modelled as a non-linear resistance. This is done by first making a new expression for h_{amb}. Starting from the definition of the Grashof number, inserted into the natural convection correlation shown as equation 2.2.1 and the base equation for the convection coefficient, equation 2.1.1. The process is shown in equation 3.3.3.

The Prandtl number and k_{air} are chosen from the ambient air temperature, which is set to $30°C$.

$$
\begin{aligned}
G_r &= \frac{\beta \cdot g \cdot \Delta T \cdot \rho^2 \cdot L^3}{\mu^2} = C \cdot \Delta T \\
\Rightarrow N_u &= 0.129(C \cdot \Delta T \cdot P_r)^{0.33} \\
\Rightarrow h_{amb} &= N_u \frac{k_{air}}{D_h} = \frac{0.129 \cdot C^{0.33} \cdot \Delta T^{0.33} \cdot P_r^{0.33} \cdot k_{air}}{D_h}
\end{aligned}
\tag{3.3.3}
$$

This equation for the convection coefficient is added to the model made in Simulink, by an algebraic loop. The loop calculates a new value for h_{amb} until stable temperatures are reached, meaning ΔT becomes constant. This is implemented using the analogy to electrical circuits, using the fact that U=RI becomes ΔT=Rq[43], where q is the heat flow. The subsystem made in Simulink is displayed as figure 3.3.3. In the figure it can be seen that the surface temperature of the frame is measured, before h_{amb} and consequently R_{amb} is calculated. Then, ΔT is measured between the positive and negative terminals and the heat flow, q, is calculated. A controlled current source is then used to control the heat flow through the resistance. As new values for q is calculated, so will new values for the temperature of the surface and ΔT be obtained, until q becomes constant. The subsystem contains the calculations, while the resistance itself has two ports that are connected as a normal resistance in the thermal equivalent circuit.

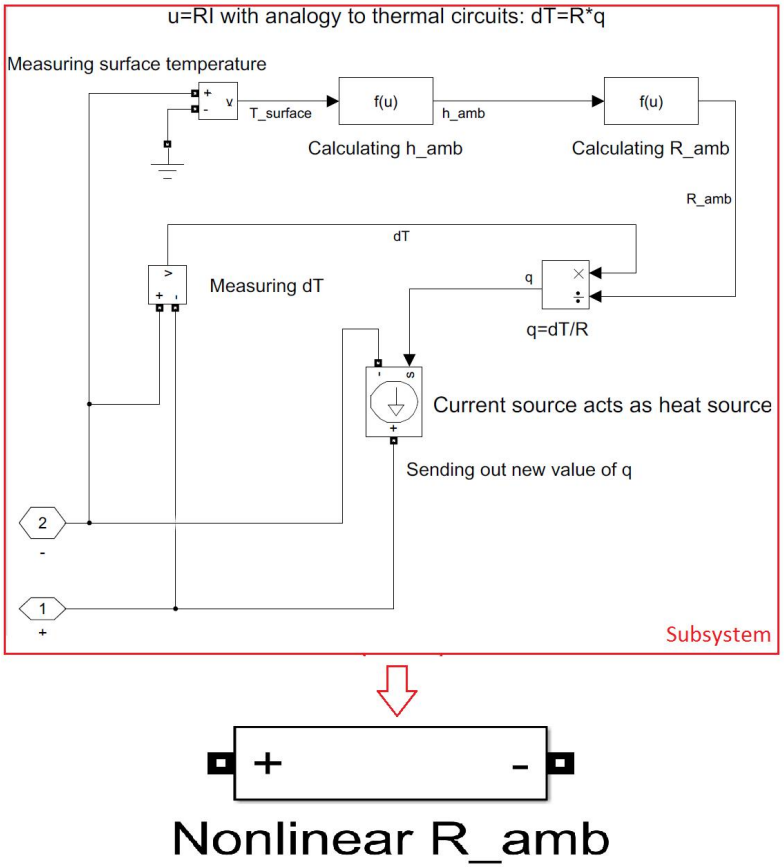

Figure 3.3.3: *Illustration of how the nonlinear thermal resistance, R_{amb}, is made in Simulink.*

The thermal resistance of the frame, can be modelled as a hollow cylinder. Yielding equation 3.3.4 [1]. Knowing the thermal resistance of the frame and the thermal resistance to the ambient, the total resistance between the ambient and the frame node can be calculated as shown in equation 3.3.5.

$$R_{fr} = \frac{ln(\frac{fr_o}{fr_i})}{2\pi \cdot k_{fr}} \cdot \frac{2\pi}{\theta_s} \tag{3.3.4}$$

$$R_{af} = \frac{1}{2} R_{fr} + R_{amb} \tag{3.3.5}$$

3.3.3 Insulation between frame and stator

As mentioned earlier, the frame and the stator are insulated from each other in the ModHVDC design. This means that a thermal resistance finds place between the frame and the stator, consisting of insulation material. As this insulation finds place around the whole machine, the hollow cylinder equation can be used to model the thermal resistance. Yielding equation 3.3.6[1]. The denotation "o" refers to the outer insulation around the stator.

$$R_{ins_o} = \frac{ln(\frac{r_{ins_o}}{r_o})}{2\pi \cdot k_{ins}} \cdot \frac{2\pi}{\theta_s} \tag{3.3.6}$$

3.3.4 Stator yoke and teeth

As explained in the literature study, both the stator yoke and the stator teeth can be modelled by the modified versions of the hollow cylinder equation. Yielding equation 3.3.7 for the thermal resistance of the stator yoke and equation 3.3.8 for the thermal resistance of the stator teeth. [1]

$$R_{sy} = \frac{ln(\frac{r_o}{r_{is}})}{2\pi \cdot k_f \cdot k_{sy}} \cdot \frac{2\pi}{\theta_s} \tag{3.3.7}$$

$$R_{st} = \frac{ln(\frac{r_{is}}{r_i})}{2\pi \cdot k_{st} \cdot k_f \cdot p_{st}} \cdot \frac{2\pi}{\theta_s} \tag{3.3.8}$$

The factor k_f in equation 3.3.7 and equation 3.3.8 comes from the utilization of the useful stator length, calculated by equation 2.3.4. Yielding $l_u = k_f \cdot 1$, since a 2D model is made. $k_f = 0.95$ is used for the stator iron, as explained in the the literature study in section 2.3.1.

In addition, the factor p_{st} can be calculated from equation 3.3.9. Taking into account the stator slots. In the equation, the area is used instead of the volume, because of the 2D modelling.

$$p_{st} = \frac{A_{st}}{A_{st} + A_{ss}} \tag{3.3.9}$$

For the stator teeth model, it is also desirable to model the thermal resistance in the tangential direction. This is done by looking at the stator teeth as rectangles and using the normal equation for thermal resistances, shown as equation A.0.1 in appendix A. Yielding equation 3.3.10[1].

$$R_{st_t} = \frac{b_{st}}{k_{st} \cdot d_{st}} \tag{3.3.10}$$

The total resistance between the frame node and the stator yoke node can then be calculated as shown in equation 3.3.11. Note that the thermal resistance of the frame and yoke are divided by 2, since both the nodes are placed in the middle. [1]

$$R_{fsy} = \frac{R_{fr}}{2} + R_{ins_o} + \frac{R_{sy}}{2} \tag{3.3.11}$$

Following the same logic, the total resistance between the stator yoke node and the stator teeth node can be found using equation 3.3.12. [1]

$$R_{syt} = \frac{R_{sy}}{2} + \frac{R_{st}}{2} \tag{3.3.12}$$

3.3.5 Slot and windings thermal resistance

The stator slot consists of insulation and windings. The windings themselves consists of copper coils, which again consists of copper turns and turn-to-turn insulation. Because of this, it is desirable to model the turn-to-turn insulation and not the whole winding as copper, as insulation material has a high thermal resistance. This can be done by modelling the windings in the slot with one equivalent thermal resistance in the radial direction and one equivalent thermal resistance in the tangential direction. An illustration of the stator slot with two turns in the tangential direction and three turns in the radial direction, is shown as figure 3.3.4. N_t is the number of turns in the tangential direction, N_r is the number of turns in the radial direction, w_r is the width of the windings in the radial direction, w_t is the width of the windings in the tangential direction and t_{iso} is the thickness of the turn-to-turn insulation. Since each copper turn is insulated separately, the thickness of the insulation between each copper turn becomes $2 \cdot t_{iso}$. Note that residual air pockets that may occur in a real machine has been ignored.

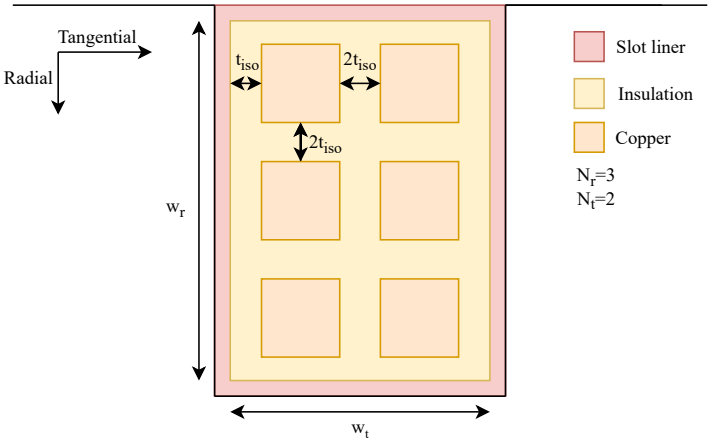

Figure 3.3.4: *Illustration of the windings in the slot with two turns in the tangential direction and three turns in the radial direction. The dimension in the figure is not realistically scaled.*

The equivalent thermal resistances is therefor dependent on the number of turns in the radial and the tangential direction, the insulation thickness around each turn and the width of the windings in both the radial and tangential direction. In addition, there is a thermal resistance in the copper itself. However, the thermal resistance of the copper is neglected as the thermal resistance of the insulation material is much higher ($R_{iso} >> R_{cu}$). The equivalent thermal resistances of the windings can then be calculated from equation 3.3.13 and equation 3.3.14. in the tangential and radial direction, respectively. In the equations, $t_{cu,r}$ and $t_{cu,t}$ is the total thickness of the copper coils in the radial and tangential direction.

$$R_{w,t} = \frac{(t_{iso} \cdot 2 \cdot N_t)}{k_{iso} \cdot t_{cu,r}} \tag{3.3.13}$$

$$R_{w,r} = \frac{(t_{iso} \cdot 2 \cdot N_r)}{k_{iso} \cdot t_{cu,t}} \tag{3.3.14}$$

The total thickness of the copper coils can be found by using equation 3.3.15, for the radial direction and equation 3.3.16, for the tangential direction.

$$t_{cu,r} = w_r - (t_{iso} \cdot 2 \cdot N_r) \tag{3.3.15}$$

$$t_{cu,t} = w_t - (t_{iso} \cdot 2 \cdot N_t) \tag{3.3.16}$$

The parameters $w_r = 118mm$ and $w_t = 56.7mm$ are known from the reference machine and t_{iso} can for now be assumed to be $t_{iso} = 0.13mm$. The parameters that need to be decided are N_r and N_t. If a maximum thickness of one coil in the tangential direction is assumed to be $10mm$, an estimate of the number of turns in the tangential direction is $N_t \approx 6$. The coils in the radial direction is usually thinner and may have a maximum thickness of 5mm[2]. When this is assumed, the number of turns in the radial direction becomes $N_r \approx 24$. This means that the total number of turns in the windings becomes $N_{turns} = N_t \cdot N_r = 144$.

When the total resistance in the tangential direction and the radial direction in the slot is known, a modified H-equivalent can be made for the windings in the slot. Following the description in the literature section. The difference to the method shown in the literature study, is that this H-equivalent is made for the windings (with turn-to-turn insulation) only and not the whole slot. An illustration of the H-equivalent is shown as figure 3.3.5[1]. The H-equivalent is directly implemented in the Simulink thermal equivalent circuit.

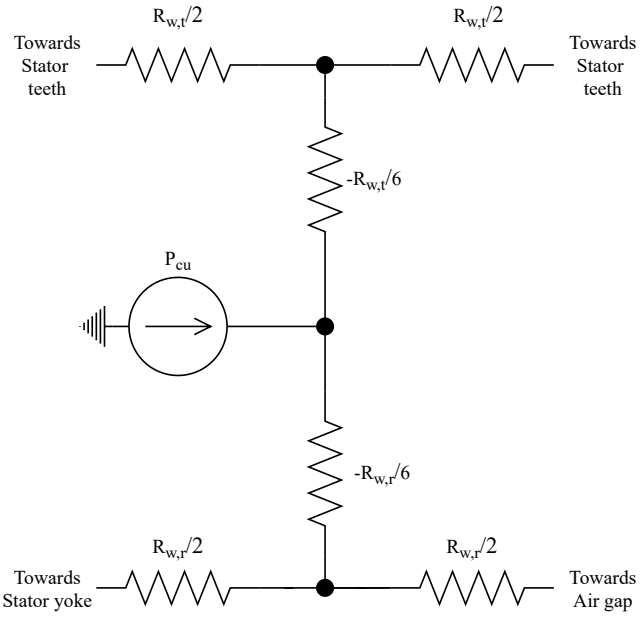

Figure 3.3.5: *Thermal H-equivalent of the windings with turn-to-turn insulation. [1]*

In addition to the winding equivalent resistances, the slot liner thermal resistance need to be included for a complete thermal slot model. The slot liner is modelled as a rectangle around the windings, with the same thickness in every direction. This is indicated in figure 3.3.4. The slot liner thermal resistances in the radial and tangential direction, can therefore be calculated as shown in equation 3.3.17 and equation 3.3.18, respectively.

$$R_{liner,r} = \frac{d_{ins}}{w_t \cdot k_{ins}} \tag{3.3.17}$$

$$R_{liner,t} = \frac{d_{ins}}{w_r \cdot k_{ins}} \tag{3.3.18}$$

The total thermal resistance between the winding node and the stator teeth node, R_{wst}, can be calculated as shown in equation 3.3.19[1]. Likewise, the total thermal resistance between the stator yoke node and the winding node, can be calculated as shown in equation 3.3.20[1]. The resistance $R_{liner,r}$ is multiplied by 2, as only half a slot i modelled (w_t in equation 3.3.17 becomes $w_t/2$). This is done to get a better cohesion between the FEM model and the thermal equivalent circuit. Note that $k_{iso} = k_{ins} = 0.25W/mK$, as the insulation material for both the slot liner and the turn-to-turn insulation is assumed to be mica-backed tape. Table B.0.10 in appendix B shows the thermal properties of mica-backed tape. R_t and R_r can be calculated as shown in the literature chapter.

$$R_{wst} = \frac{1}{2}R_{st_t} + R_t + R_{liner,t} \tag{3.3.19}$$

$$R_{syw} = \frac{1}{2}R_{sy} + R_r + R_{liner,r} \cdot 2 \tag{3.3.20}$$

3.3.6 Inner insulation around the stator

As mentioned earlier, there is an insulation layer around the stator. This means that the insulation layer also exists between the stator teeth and the air gap. Using the same method as for the outer insulation layer, the thermal resistance can be calculated as shown in equation 3.3.21. [1]

$$R_{ins_i} = \frac{ln(\frac{r_i}{r_{ins_i}})}{2\pi \cdot k_{ins}} \cdot \frac{2\pi}{\theta_s} \tag{3.3.21}$$

3.3.7 Air gap

As shown in section 3.1, there are several ways to model the airflow in the air gap and thereby the thermal resistance of the air gap. However, this base model does not consider any specific cooling methods. Therefore, the air gap thermal resistance is modelled as shown in section 3.1.2, where the air flow is due to the rotation of the rotor only. In addition, it is assumed that the temperature in the middle of the air gap is kept at $40°C$. This is done in order to get reasonable temperature values, as no cooling in the machine could give unreasonable high temperatures. Again, the main purpose of this base model is to be compared with a FEM model.

The literature describing the method seen in section 3.1.2, states that the heat exchange in the air gap can be seen as conduction only. Because of this, equation 3.3.22 is used to model the thermal resistance, which is the hollow cylinder equation. However, instead of using the thermal conduction coefficient of air in the equation, the convective heat transfer coefficient is used. As seen in figure 3.1.2, the average value of the convection coefficient in the air gap is about $h_{ag} = 10.8W/m^2K$ for the nominal speed of 10rpm. This value is therefore used to calculate the thermal resistance in the air gap.

$$R_{ag} = \frac{log((r_{mag} + d_{ag})/r_{mag})}{2\pi \cdot h_{ag}} \cdot \frac{2\pi}{\theta_s} \tag{3.3.22}$$

The total resistance between the air gap node and the stator teeth, can be calculated as shown in equation 3.3.23. While the total resistance between the air gap node and the winding node can be calculated as shown in equation 3.3.24. In the total resistance between the air gap node and the winding node, the fraction $\frac{s}{b_{ss}/2}$ can be seen. This fraction is used because the section modelled, only includes half the width of the slot. This is also true for the stator teeth width, scaling equation 3.3.23 by $\frac{s}{b_{st}/2}$. [1]

$$R_{agt} = \frac{R_{ag}}{2} + R_{ins_i} \cdot \frac{s}{b_{st}/2} + \frac{R_{st}}{2} \tag{3.3.23}$$

$$R_{wag} = \frac{R_{ag}}{2} + R_{ins_i} \cdot \frac{s}{b_{ss}/2} + R_r \tag{3.3.24}$$

3.3.8 Rotor

The rotor model consists of the thermal resistance in the rotor magnets, in addition to the thermal resistance of the rotor core. The thermal resistance of the rotor magnets can be modelled as shown in the literature study, yielding equation 3.3.25. The factor p_{mag}, is used to scale the thermal resistance based on the percentage of the angle θ_s that is occupied by the magnet. Meaning that 80% of the section tangential length is occupied by the magnet for a value of $p_{mag} = 0.8$. This is illustrated in figure 3.3.6. The rotor core is modelled as a hollow cylinder, yielding equation 3.3.26.

$$R_{mag} = \frac{ln(r_{mag}/r_{core})}{N_{pol} \cdot \theta_{mag} \cdot k_{mag}} \cdot \frac{N_{pol} \cdot \theta_{mag}}{\theta_s \cdot p_{mag}} \tag{3.3.25}$$

$$R_{rotor-core} = \frac{ln(r_{core}/r_{shaft})}{2\pi \cdot k_{core}} \cdot \frac{2\pi}{\theta_s} \tag{3.3.26}$$

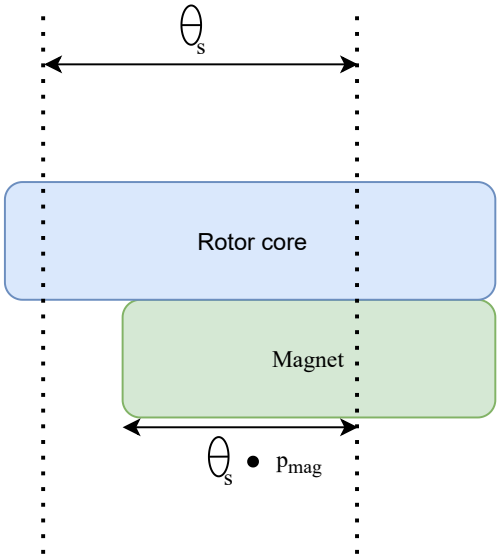

Figure 3.3.6: *Illustration of how the thermal resistance of the magnet is scaled based on its percentage within the modelled section.*

There is also a contact resistance that finds place between the rotor yoke surface and the magnets. The PM magnets are a ceramic compound called NdFeB and the rotor yoke is made of steel, as described by the reference machine in appendix B. In section 2.4, table 2.4.1, an equivalent gap length and an equivalent thermal conductance for the ceramic-metal interface is suggested. The equivalent conductance is suggested to be between 1500 to 8500 W/m^2K. Because of this, the mean value of $G = 5000W/m^2K$ is used when calculating the resulting thermal contact resistance. Yielding equation 3.3.27.

$$R_{contact_{RM}} = \frac{1}{G} \tag{3.3.27}$$

The total resistance from the rotor core node to the magnet node, R_{rc}, can then be calculated as shown in equation 3.3.28.

$$R_{rc} = \frac{1}{2}R_{mag} + \frac{1}{2}R_{rotor-core} + R_{contact_{RM}} \tag{3.3.28}$$

The total resistance between the magnet node and the air gap node, can be calculated from equation 3.3.29. Keep in mind that both nodes are placed in the middle in the radial direction.

$$R_{m-ag} = \frac{1}{2}R_{mag} + \frac{1}{2}R_{ag} \tag{3.3.29}$$

In addition, there are significant losses in the permanent magnets. The losses are added in the magnet node, where the average temperature can be found.

3.3.9 Implementing losses

In thermal equivalent circuits, losses can be modelled as current sources that injects a heat flow in the circuit. For this thesis, three main sources of losses are considered. These are copper losses in the windings, magnet losses in the PM magnets and the core losses in the stator. Solveig[3] has calculated the total copper losses and the stator core losses in the ModHVDC machine, as show in in table B.0.2 in appendix B. These losses are used, when recalculating the losses for the modelled section of the machine in this thesis. [1]

The section that is modelled for this thesis, makes up only half a slot. Equation 3.3.30 is therefore used to calculate the resulting volumetric loss for this half slot. Using $P_{cu} = 435\,500W$ as the total copper losses in the machine. The length of the copper is assumed to be as long as the entire machine, yielding $l_m = 1,5m$. In the equation, Q_s is the number of slots. [1]

$$P_{cu_{pr.vol}} = \frac{P_{cu}}{A_{cu} \cdot l_m \cdot Q_s} \cdot \frac{1}{2} \tag{3.3.30}$$

Assuming that the whole slot consists of copper, the copper losses in W/m can be found as $P_{cu_{pr.vol}} \cdot A_{slot}$. Resulting in $P_{cu_{2D}} = 380W/m$. Note that the importance of modelling the losses at this stage, is to get reasonable losses for the model and not to get a 100% accurate representation of the actual losses in the machine. In reality, the losses are not evenly spread across all windings at the same time and the whole slot does not consist of copper. [1]

The magnet losses are at this point in the ModHVDC project not known. However, other students that have worked on the project, have indicated that the magnet losses are significant and may be as high as a third the copper losses. Because of this, the magnet losses are defined as $\frac{1}{3}$ of the copper losses. Yielding $P_{mag_{2D}} \approx 126.5W/m$. These magnet losses are found using an unsegmented magnet design. If the magnets were segmented, meaning that each pole is laminated, the losses could be significantly reduced. [2]

In table B.0.2 in appendix B, the total core losses are displayed as $P_c = 55\,537W$. These losses finds place in both the rotor core and in the stator. Therefore, these losses should be modelled as two separate current sources in the equivalent circuit. One connected to the stator node and the other connected to the rotor core node. The total core losses per volume can be calculated as shown in equation 3.3.31. Where the total area of the core, $A_{core_{tot}}$, can be calculated as shown in equation 3.3.32. [1]

$$P_{c_{pr.vol}} = \frac{P_c}{A_{core_{tot}} \cdot l_{core}} \tag{3.3.31}$$

$$\begin{aligned} A_{core_{tot}} &= A_{stator_{yoke}} + A_{rotor_{core}} + A_{teeth} \\ A_{core_{tot}} &= (\pi \cdot r_o^2 - \pi \cdot r_{is}^2) + (b_{st} \cdot d_{ss} \cdot Q_s) + (\pi \cdot r_{core}^2 - \pi \cdot r_{shaft}^2) \end{aligned} \tag{3.3.32}$$

The losses for the modelled stator section can then be found from equation 3.3.33 [1], by comparing the area of the stator section to the total area of core material and multiplying with the total stator core material area to get W/m. The stator section area is calculated as shown in equation 3.3.34[1], since only half a tooth is inside the section that is being modelled. Yielding $P_{c_{stator}} \approx 4.1W/m$ [1]. Following the same logic, the losses implemented in the rotor core is calculated by equation 3.3.35. Where the area of the rotor core inside the section, is calculated as shown in equation 3.3.36. Yielding $P_{rotor_{core}} \approx 3.1W/m$.

$$P_{c_{stator}} = P_{c_{pr.vol}} \cdot \frac{A_{stator}}{A_{core_{tot}}} \cdot (A_{stator}) \tag{3.3.33}$$

$$A_{stator} = \pi \cdot r_o^2 \cdot \frac{\theta_s}{2\pi} - \pi \cdot r_{is}^2 \cdot \frac{\theta_s}{2\pi} + \frac{b_{st} \cdot d_{ss}}{2} \tag{3.3.34}$$

$$P_{rotor_{core}} = P_{c_{pr.vol}} \cdot \frac{A_{rotor_{core_s}}}{A_{core_{tot}}} \cdot (A_{rotor_{section}}) \tag{3.3.35}$$

$$A_{rotor_{section}} = \pi \cdot r_{core}^2 \cdot \frac{\theta_s}{2\pi} - \pi \cdot r_{shaft}^2 \cdot \frac{\theta_s}{2\pi} \tag{3.3.36}$$

3.3.10 Base thermal equivalent circuit in Simulink

Now that all thermal resistances have been described for the base model, a base thermal equivalent circuit can be modelled. Simulink is used to model the circuit, meaning that the circuit is simulated and not solved by using equations. Solving the circuit this way, makes it easy to implement cooling systems or modifications later on. Using the correlation from heat transfer to electric circuits, voltage sources are used as constant temperature sources, current sources are used to inject losses as heat flows and electrical resistances are used as thermal resistances. The average temperature of each part of the machine can be found by measuring the voltage at the respective node. The measured temperatures are then imported to the MATLAB work space. The model made in Simulink is shown as figure 3.3.7. In the figure, each machine part has been given a color in an attempt to make it easier for the reader to familiarize themselves with the model. Green is used for the rotor, blue for the air gap, red for the slot with windings, pink for the stator teeth, purple for the stator yoke and grey for the frame. As mentioned earlier, and shown in the figure, the thermal equivalent model is made as a closed loop by adding an infinite thermal resistance between the end of the rotor core and the ambient temperature.

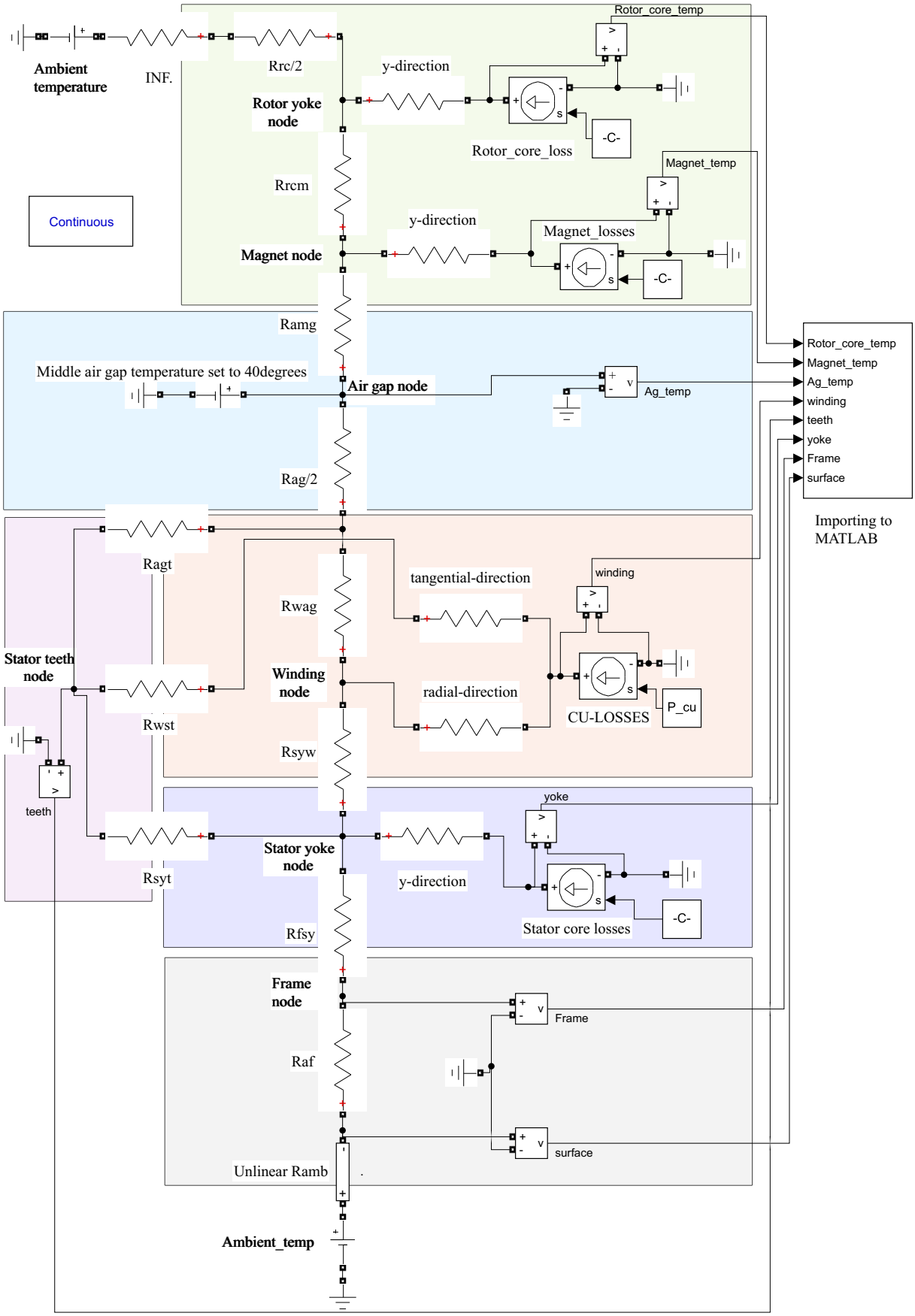

Figure 3.3.7: *Base thermal equivalent model made in Simulink.*

3.4 Thermal FEM model

In order to compare and verify the thermal equivalent circuit, a FEM model of the ModHVDC machine is made. The model is first made to mirror the base thermal equivalent model, before any modifications are done. The FEM model is made in the software COMSOL multiphysics, which is a well recognized tool for electrical machine modelling. The FEM model made is also made as a 2D model. Additional models are also made in this section, in order to verify some of the methods that are used.

3.4.1 FEM model of ModHVDC section

Before implementing any heat transfer mechanisms in the FEM model in COMSOL, the geometry of the machine is made. That is, the geometry of the earlier described section defined by the angle θ_s. The geometry of the section made in COMSOL, is illustrated by figure 3.4.1. After the geometry is modelled, the material properties and heat transfer mechanisms are added.

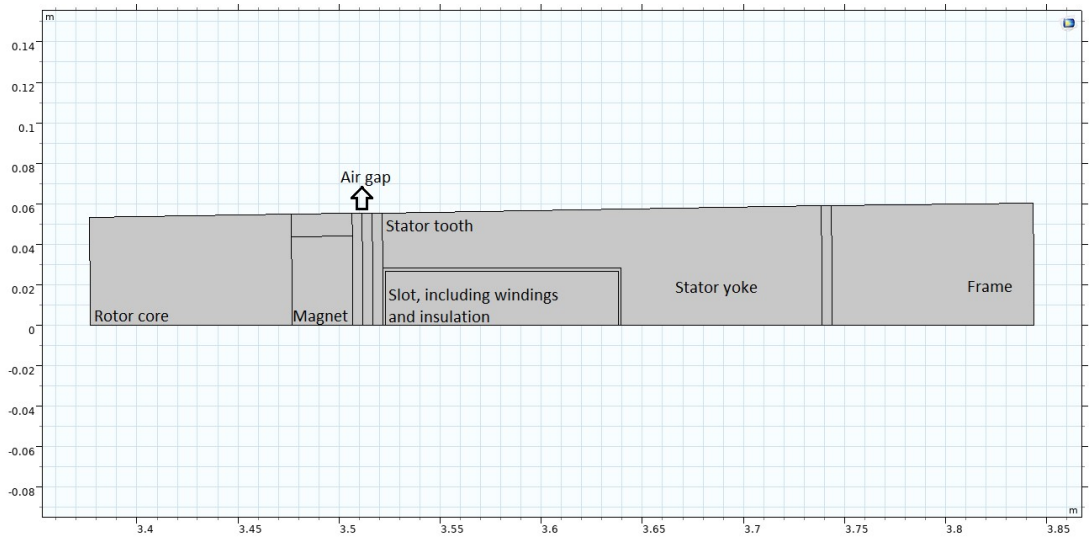

Figure 3.4.1: *2D FEM model of the ModHVDC section made in COMSOL.*

COMSOL multiphysics offers a wide variety of materials and thereby material properties to implement in models, chosen from a built in material library. Because of this, the material properties for the stator and rotor iron, the frame aluminum, some of the properties for air in the air gap and for the insulation material was taken directly from the material library. However, the thermal conductivity of air and of the insulation material have been changed from the original value in COMSOL. For the insulation material, the thermal conductivity is assumed to be equal to mica-backed tape, with $k_{ins} = 0.25W/m^2K$[1]. The thermal conductivity of the air in the air gap was set to $k_{air} = 10.8W/mK$, as earlier explained in section 3.3.7. In addition, the material library in COMSOL lacked material properties for the NdFeB magnets and the equivalent thermal conductivity of the slot material need to be calculated. The values given in table B.0.6 in appendix B, is therefore used for the magnets. The most notable and important

property is the thermal conductivity of $k_{mag} = 7.7W/mK$. The equivalent thermal conductivity of the slot material is outlined in the next paragraph.

In section 3.3.5, it was described how equivalent thermal resistances in the tangential and radial directions for the equivalent slot material was defined. In COMSOL, the user have the ability to define the thermal conductivity for a material in the x and y-directions. However, the equivalent thermal conductivity in the tangential and radial directions must first be calculated. Using the general equation for thermal resistances, the total resistance in the tangential direction can be written as equation 3.4.1, where $W_r^{'}$ is equal to $t_{cu,r}$. Rewriting equation 3.4.1 to be solved for $k_t^{'}$ and then implementing the thermal resistance in the tangential direction (as shown in equation 3.3.13), equation 3.4.2 is made. However, this equation does not consider the whole length in the radial direction, meaning that the actual equivalent thermal conductivity in the tangential direction, $k_t^{''}$, is found by weighing it with the actual length. Resulting in equation 3.4.3. Doing the same derivation for the radial direction, the equivalent thermal conductivity in the radial direction is found by equation 3.4.4. For the model made in COMSOL, the equations yield $k_t^{''} = 8.19W/mK$ and $k_r^{''} = 4.49W/mK$. In order to verify that this method is a valid approximation for the slot equivalent material, a FEM model including the turns in the slot is made in section 3.4.2 and then compared in the result section.

$$R_{tot_t} = \frac{1}{k_t^{'}} \cdot \frac{W_t}{W_r^{'}} \tag{3.4.1}$$

$$\begin{aligned} k_t^{'} =& \frac{1}{R_{tot_t}} \cdot \frac{W_t}{W_r - 2N_r \cdot t_{iso}} \\ \Rightarrow k_t^{'} \overset{3.3.13}{=}& \frac{k_{iso} \cdot W_t}{t_{iso} \cdot 2N_t} \end{aligned} \tag{3.4.2}$$

$$k_t^{''} = \frac{W_r^{'}}{W_r} \cdot k_t^{'} \tag{3.4.3}$$

$$k_r^{''} = \frac{W_t^{'}}{W_t} \cdot k_r^{'} \tag{3.4.4}$$

The heat transfer mechanisms is modelled by using a built in module called "Heat transfer in Solids". The modules gives the user a wide variety of options to model heat transfer mechanisms. Among these, are the ones used for the particular model made in this thesis. The module "Heat sources" is used to model losses, Heat flux is used to model convection effects, Thermal contact is used to model contact resistance, Temperature to set a constant temperature at a boundary and finally Thermal insulation, which is used to set boundaries where there will be no heat flowing through.

The losses in the machine are implemented as heat sources in the model, by selecting the area where the heat should be injected. This is illustrated in figure 3.4.2. As can be seen from the figure, the losses are defined in W/m^3. Equation 3.3.30 is used for the copper losses, resulting in $P_{cu_{pr.vol}} \approx 122\,000 W/m^3$[1]. As mentioned earlier, the magnet losses are about 1/3 of the copper losses. Yielding $P_{mag_{pr.vol}} = 40\,650 W/m^3$. To find the losses in W/m^3 for the rotor core and the stator iron, an evaluation of the areas is done. Equation 3.4.5 and equation 3.4.6[1] is used to calculate the losses for the rotor core and the stator iron, respectively. Keep in mind that the areas are used instead of volumes, as this is a 2D model. Yielding $P_{rotor_{iron}} = 59 W/m^3$ and $P_{stator_{iron}} = 61 W/m^3$.

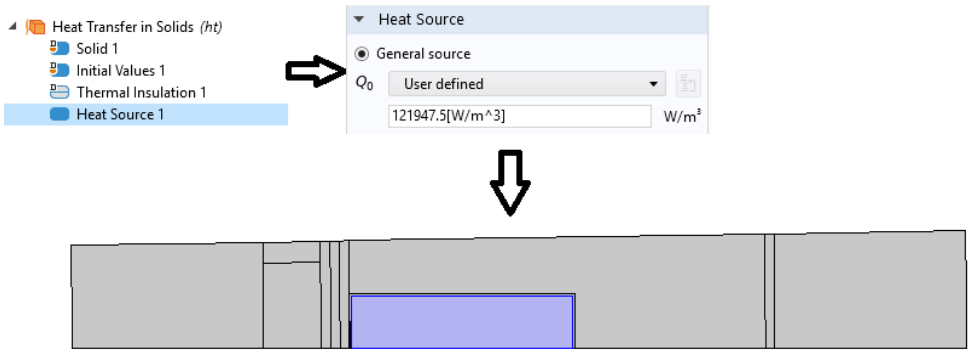

Figure 3.4.2: *Illustration of how losses are implemented as heat sources in COMSOL.*

$$P_{rotor_{iron}} = P_{c_{pr.vol}} \cdot \frac{A_{rotor_{section}}}{A_{core_{tot}}} \tag{3.4.5}$$

$$P_{stator_{iron}} = P_{c_{pr.vol}} \cdot \frac{A_{stator_{section}}}{A_{core_{tot}}} \tag{3.4.6}$$

As shown in section 3.3.2, the thermal resistance between the frame surface and the ambient air is a nonlinear resistance. By defining the thermal resistance as a heat flux in COMSOL, the resistance can be easily implemented when the nonlinear equation for the heat transfer coefficient is known. This is because the equation for the heat transfer coefficient can be directly defined in COMSOL. Using an ambient temperature of $30°C$, equation 3.3.3 was implemented in the FEM model in order to have a thermal resistance and heat flow between the frame and the ambient air.

The final thermal resistance to be defined in the FEM model, is the contact resistance between the magnet and the rotor core. Similarly to the convection between frame and ambient, the contact resistance can easily be implemented when the equivalent layer conductance is known for the interface. As mentioned in section 3.3.8, the equivalent conductance for the interface between steel and ceramic is $G = 5000W/m^2K$ on average. This value is directly implemented by using the "Thermal Contact" appliance and selecting the interface boundary in the COMSOL model. Note that the radiation conductance has been set to zero.

Finally, the temperature in the middle of the air gap is set to $40°C$ by using the "Temperature" appliance. As explained in section 3.3, the temperature in the air gap for the base model is set to $40°C$ in order to get reasonable temperatures when comparing the thermal equivalent model and the FEM model. This is because no active cooling methods have been implemented at this point.

3.4.2 FEM Slot model with winding turns

As mentioned in the last section, the method used to model the equivalent thermal conductivity of the slot, is just an approximation. Because of this, a FEM model that includes the turns with turn-to-turn insulation is made, in order to verify that the approximation is valid. For this model, only the stator is considered, as the slot is the important part. In addition, the temperature in the air gap is still set to $40°C$. This is because the goal for the model is to identify the conduction within the slot, and not the overall temperature in the machine.

Figure 3.4.3 shows the model made in COMSOL. The model is made with 24 turns in the radial direction and three turns in the tangential direction, as only half a slot is considered in the section of the machine that is modelled. As explained in section 3.3.5, the thickness of insulation between the slot liner and the first turn is t_{iso} and the thickness of the insulation material between each turn is $2t_{iso}$. This is illustrated in figure 3.3.4. The slot insulation material has been given the thermal conductivity of $k_{iso} = 0.25W/mK$. All the other properties in the model are the same as explained in the previous section. The resulting temperatures are compared with the model with an equivalent slot conductance in the result chapter.

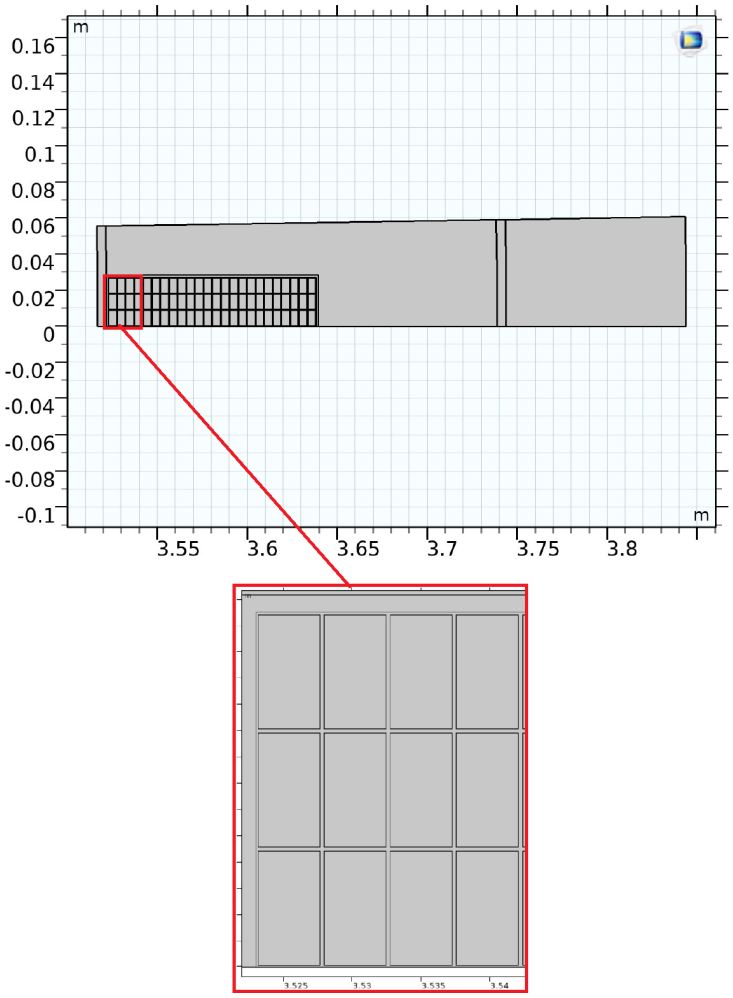

Figure 3.4.3: *FEM model with turns and turn-to-turn insulation.*

3.5 Convection coefficient for hollow shaft cooling

In section 2.5.2, a cooling method based on fluid flow through a hollow shaft was introduced. Three different correlations were presented for different cooling fluids. The first, shown as equation 2.5.16 and equation 2.5.17, uses air inside the hollow rotor shaft. The second, shown as equation 2.5.18, uses oil as the fluid. While the third method uses water and is shown as equation 2.5.19.

The geometry of the ModHVDC machine in this thesis is relatively large for an electrical machine, whereas the shaft itself has a radius of $3.38m$. Because of this, it would not make sense to use a large percentage of the shaft as a cooling channel. At least not for oil or water as fluid, because of the power that would be needed to pump these fluids through the shaft. With this in mind, the cooling channel in the hollow shaft has been given a maximum diameter of $0.5m$. This means that roughly 7% of the shaft is hollowed out to make room for the cooling fluid. This may indicate that a hollow shaft solution is not suitable for the ModHVDC machine due to the large geometry, but is nevertheless studied in this thesis.

The material properties used for air is listed in table B.0.5 in appendix B. The values for $20°C$ are used. The properties of water and oil can be found in table C.0.1 and C.0.2 in appendix C, respectively. Note that Silicone SF94 is the oil type that is listed in this table and thereby used in the correlation. The Prandtl number used for water is $P_{r,water} = 7$, as this is the Prandtl number of water at $20°C$ according to [65]. For the oil, the Prandtl number is calculated to be $P_{r,oil} = 305$ by using equation C.0.1.

First, the rotational Reynolds numbers are calculated for the three methods at 10 RPM, using equation 2.5.4. The fluid velocity in the rotational direction is calculated as $v_r = \omega \cdot r$. The results are shown in table 3.5.1, in addition to the limits for the correlation used. By studying the table, it becomes clear that only the water solution violates the limits for the correlation used at nominal rotational speed.

Table 3.5.1: *Resulting rotational Reynolds number for different fluids in a hollow shaft cooling solution. Values are calculated based on the nominal rotational speed of the ModHVDC machine, which is 10RPM. The limitations for the correlations used are also displayed.*

Fluid in the hollow shaft	R_{e_r} **at 10 RPM**	**Limit for correlation**
Air	$8.61 \cdot 10^3$	$1.60 \cdot 10^3 < R_{e_r} < 2.77 \cdot 10^5$
Oil	$4.29 \cdot 10^3$	$2.38 \cdot 10^3 < R_{e_r} < 1.75 \cdot 10^5$
Water	$73.54 \cdot 10^3$	$0 < R_{e_r} < 16.89 \cdot 10^3$

Further, the heat transfer coefficient resulting from the correlations, are plotted as a function of fluid velocity in the shaft. Since the rotational Reynolds number for the air correlation is within acceptable values for the nominal speed, the heat transfer coefficient is plotted as a function of axial flow velocity. While the heat transfer coefficient for the water and oil correlations are plotted as a function of RPM. Oil is plotted as a function of RPM and not axial flow velocity, because the correlation used only considers the rotational Reynolds number. However, the axial

Reynolds number is set as $R_{e_a} = 80$ to be within the limits of the correlation. The resulting heat transfer coefficients are shown as figure 3.5.1. In the figure. the red vertical line indicates the upper limit for the Reynolds number allowed for the correlation. The middle plot, which is the correlation where oil is used, does not contain the red line as the Reynolds number never reaches the limit.

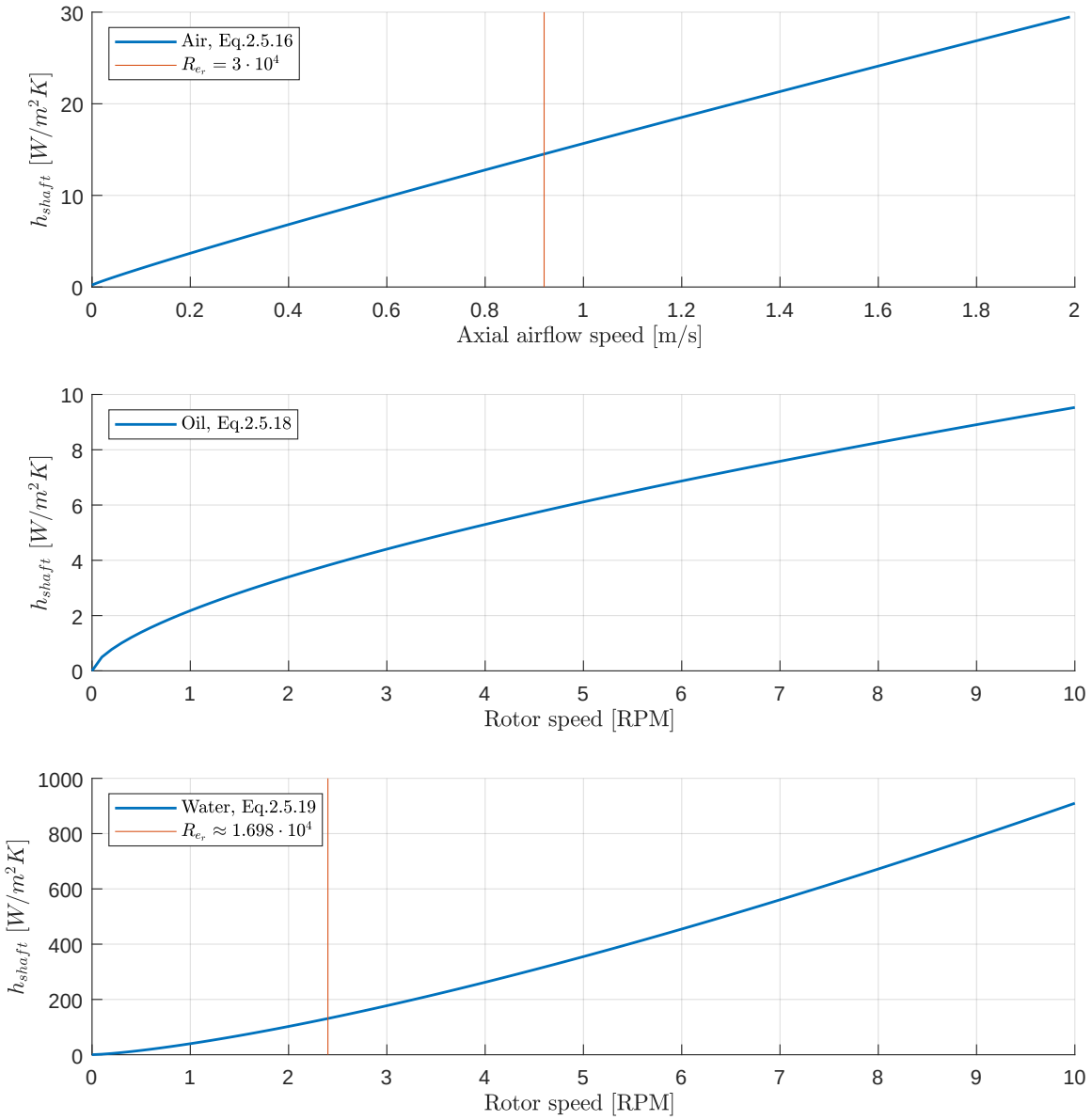

Figure 3.5.1: *Three plots showing the convection coefficient in the hollow shaft for three different fluids. Air, oil and water. The red line indicates the maximum allowed Reynolds number for the correlation used.*

From figure 3.5.1, it can be seen that the maximum heat transfer coefficient for the three correlations becomes $h_{shaft,a} = 14.37 W/m^2K$ for air in the shaft, $h_{shaft,o} = 9.53 W/m^2K$ for oil and $h_{shaft,w} = 123.70 W/m^2K$ for water. The low heat transfer coefficient for air and oil, might suggest that the correlations used does not fit the ModHVDC machine geometry.

3.6 Convection coefficient for cooling ducts in stator

In section 2.5.1, three correlations for cooling ducts of different geometry were presented. These were round, rectangular and concentric cooling ducts. In this section, the convection coefficient for cooling ducts in the stator is investigated. Because of this, only the rectangular and round ducts are considered as concentric ducts does not make sense in the stator. The correlation used for round ducts, is shown as equation 2.5.1 and the correlation used for rectangular channels is shown as equation 2.5.2.

First, it is investigated which type of duct that should be used in the stator. An optimal cooling duct for the stator is, thought to be a cooling duct with a low area and a high convection coefficient. This is because removing a large area of the stator may impact the electromagnetic design of the machine. The direct impact on the electromagnetic design is however not investigated further in this thesis.

By plotting the convection coefficient as a function of fluid velocity for both duct types, it can be seen that rectangular ducts yields a much higher convection coefficient than round ducts for the same area used. This was done both for Silicone oil and for water, yielding the same conclusion. Figure 3.6.1 illustrates the convection coefficient as a function of fluid velocity in a round duct and a rectangle duct for the same area, as an example. In the example, Silicone oil is used a fluid medium. The sudden jump in convection coefficient for the round duct, is due to the flow becoming turbulent and equation 2.5.5 is used. The material properties can be found in appendix C. From the figure, it is clear that a rectangular duct is more efficient. Because of this, it has been decided that rectangular cooling ducts should be used in the stator.

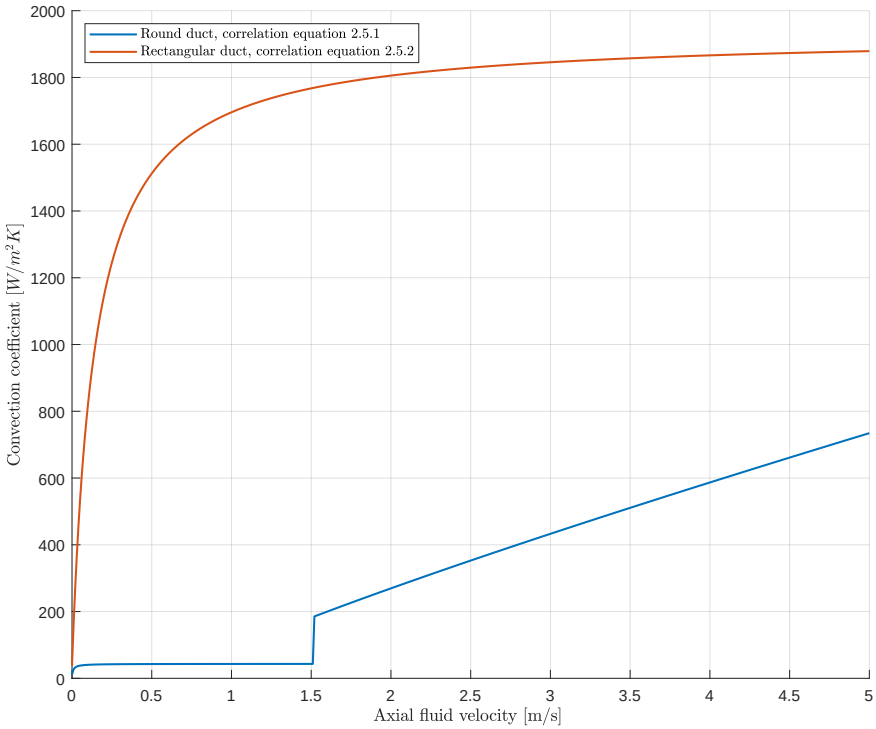

Figure 3.6.1: *Convection coefficient as a function of fluid velocity for a round duct (Blue) and a rectangular duct (Red) in the stator with the same area.*

The total area of the stator section is calculated from equation 3.3.34 to be $60400mm^2$. To avoid hollowing out a large part of the stator material and thereby impacting the electromagnetic design of the machine, it is decided that $400mm^2$ can be used for stator duct cooling. By a trial and error approach, it was found that the rectangular duct correlation (equation 2.5.2) yields the highest convection coefficient for a low height/width ratio. Because of this, the height of the rectangular channel is set as $H = 0.01m$ and the width is set to $W = 0.04m$. However, the area of the duct or the height/width ratio is not fully optimized.

The resulting heat transfer coefficient as a function of fluid velocity is plotted for water, Silicone KF96 oil and air. The plots are shown as figure 3.6.2. From the figure, it becomes clear that water and oil yields a much higher heat transfer coefficient than air. However, at the maximum speed of 10m/s, the Reynolds number for air is still not near the limit for the correlation. The upper limit for the Reynolds number in the correlation used is $R_e = 1 \cdot 10^6$, as described in section 2.5.1. This means that higher fluid velocities could be used to reach a higher convection coefficient, if air is used as fluid medium in the rectangular duct.

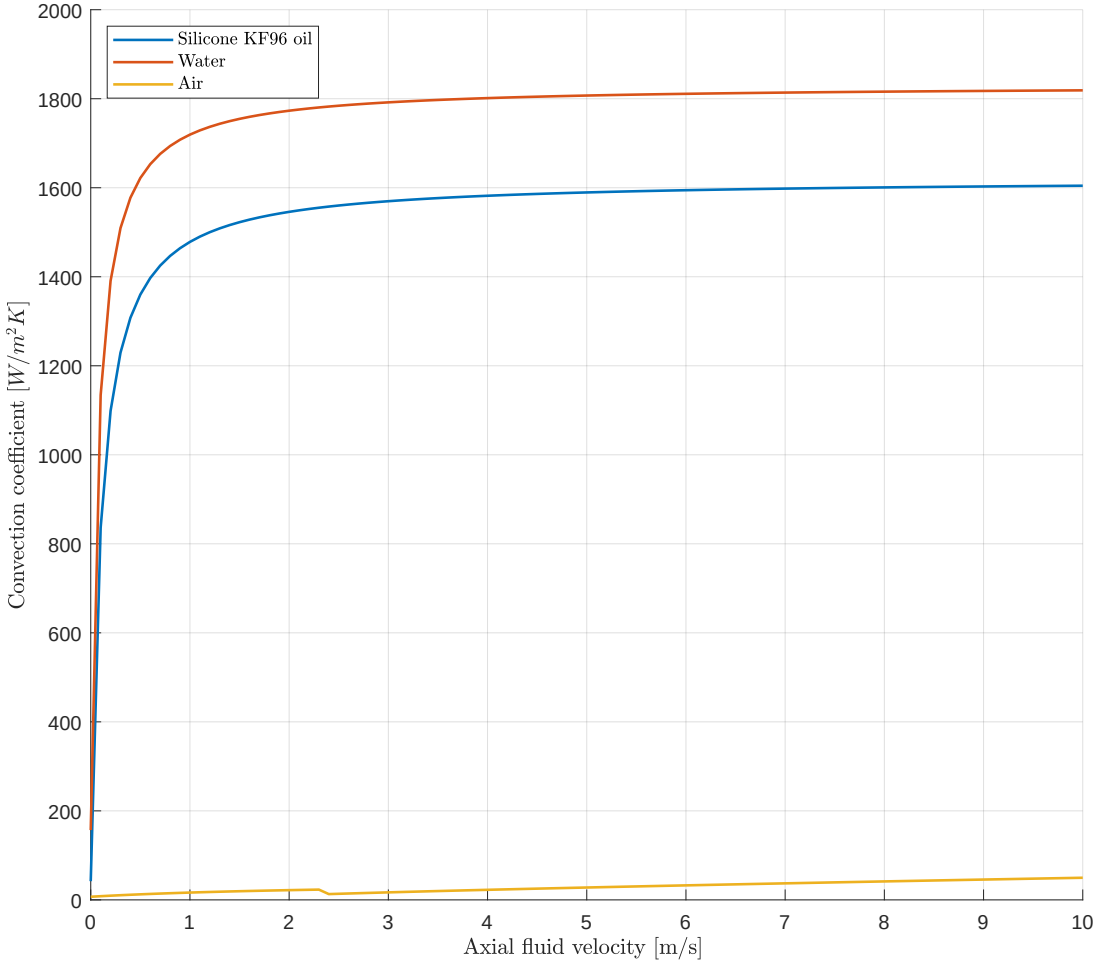

Figure 3.6.2: *Convection coefficient in a rectangular duct of $400mm^2$ for three different fluid mediums, using the correlation shown as equation 2.5.2. The fluids used are Silicone KF96 oil, Water and Air.*

3.7 Convection coefficient for concentric duct at stator surface

As described in the previous section, a concentric cooling duct does not make sense in the stator. However, a concentric cooling duct between the stator surface and the inner frame of the machine, might be a possible solution. As mentioned in several times, there is an insulation layer between the stator surface and the frame because of the fact that the stator is floating on HVDC. In fact, as shown in table 1.2.1, the highest voltage between the stator and the frame (earth) will be equal to $V_{DC}/2 = 50kV$ for the reference machine. By removing this insulation layer, the area can be used as a cooling duct for the ModHVDC machine. However, it must be made sure that short circuits does not occur between the stator surface and the frame. For this method, air is used as fluid in the concentric gap. In addition, a fastening mechanism would be necessary, in order to attach the stator to the frame. However, this fastening mechanism or the effects it may imply, is not further investigated in this thesis.

In order to ensure that a short circuit across the cooling gap does not occur, the Paschens law and curve for air can be used. The Paschens law is shown as equation 3.7.1[69] and yields the electric breakdown voltage between two surfaces where gas is present. A figure from [69], showing the breakdown voltage of air as a function of the pressure spacing product, is attached in appendix A as figure A.0.2. In equation 3.7.1, pd is the pressure spacing product given in bar·cm. [69]

$$V_b = 6.72\sqrt{pd} + 24.36 \cdot (pd) \tag{3.7.1}$$

Assuming a pressure of 1bar and a concentric gap distance of 2cm, the breakdown voltage of air becomes $V_b = 58.2kV$. Approximately the same value can be found by observing the Paschens curve in figure A.0.2. Since the resulting breakdown voltage is higher than the voltage across the gap, short circuits can be avoided. Because of this, a gap distance of $2cm$ is used.

Using the correlation for concentric ducts, shown as equation 2.5.3, the Nusselt number and thereby the convection coefficient for laminar flow is found. When the flow becomes turbulent, equation 2.5.5 is used. The resulting convection coefficient is plotted as a function of axial fluid velocity in the concentric gap and displayed as figure 3.7.1. From the figure, it becomes clear that the flow in the concentric gap becomes turbulent for very low speeds, indicated by the sudden jump in convection coefficient. For higher fluid velocities, a relatively high convection coefficient can be achieved. The highest Reynolds number occurs at the highest fluid velocity. However, the Reynolds number only reaches $5.3 \cdot 10^4$, which is within the given limit for the correlation.

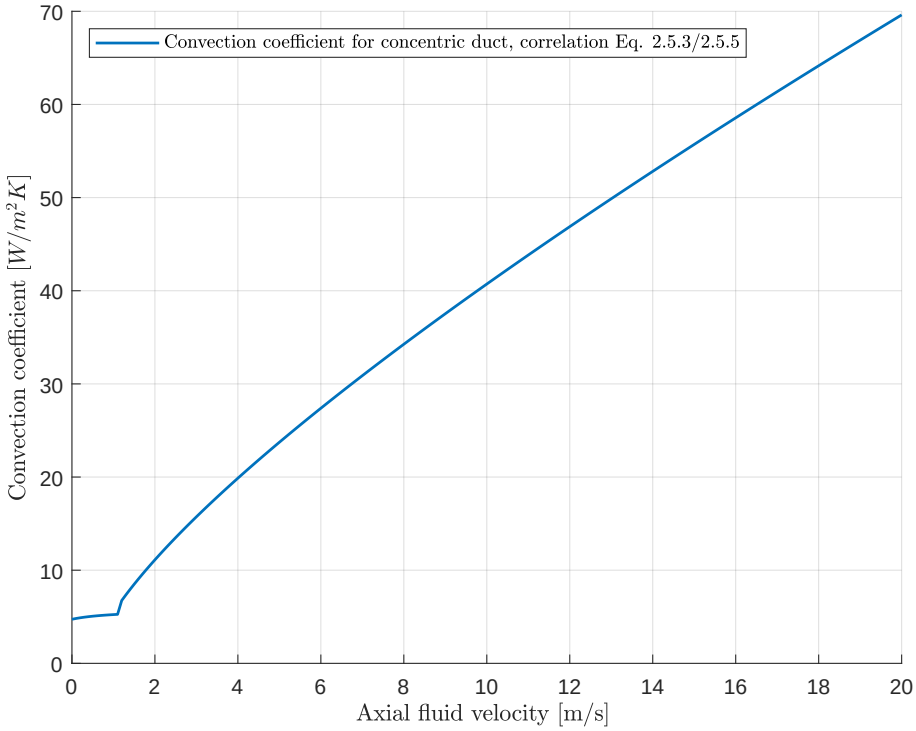

Figure 3.7.1: *Convection coefficient for a concentric duct between stator surface and frame. The correlation used for laminar flow is shown as equation 2.5.3 and for turbulent flow equation 2.5.5 is used.*

Taking this cooling method one step further, the surface perimeter and area of the stator can be increased. In doing so, the surface where convection takes place increases and more heat will be dissipated/removed from the stator. One way to increase the surface perimeter of the stator is to make wave shaped cooling fins on the surface. The wave shaped cooling fins also removes some of the stator area, which could affect the electromagnetic design of the machine. This is however not further investigated in this thesis.

Designing these wave shaped cooling fins can be done easily, however the danger of short circuits is still present. Because of this, the peaks of the waves should be at the $2cm$ gap distance between the surface of the stator and the frame. An illustration of how this might look is shown as figure 3.7.2. In the figure, the parameter P_p is the peak-to-peak height for the waves.

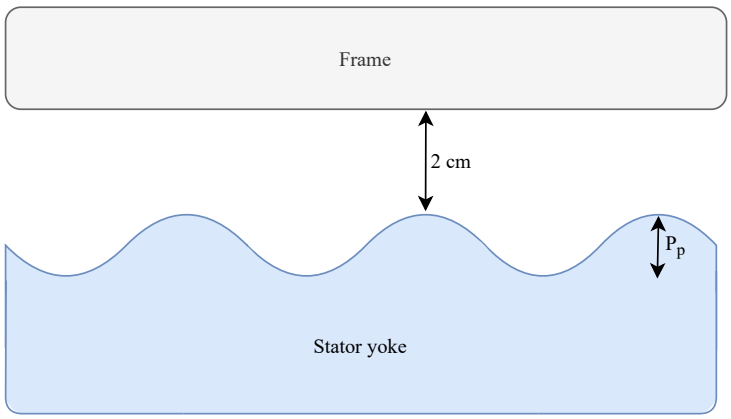

Figure 3.7.2: *Illustration of a stator with wave shaped cooling fins at the surface. The waves makes the perimeter of the surface longer, yielding a larger area of which convection may take place.*

Simplifying the sinusoidal waves as triangle waves, the new perimeter and the relative increase in area can be easily calculated. If two full waves are allowed within the modelled section of the ModHVDC machine, the waves can be illustrated as shown by figure 3.7.3. Keeping in mind that the perimeter of the modelled section is $s = 0.0576m$. From the figure, it can be easily seen that y can be found from Pythagoras, yielding equation 3.7.2. The new perimeter is then found as shown in equation 3.7.3. From the equations, it is clear that the parameters that may be changed to yield larger perimeter and area, is the frequency of the waves and the peak-to-peak height of the waves. Finally, the relative change can be found from equation 3.7.4.

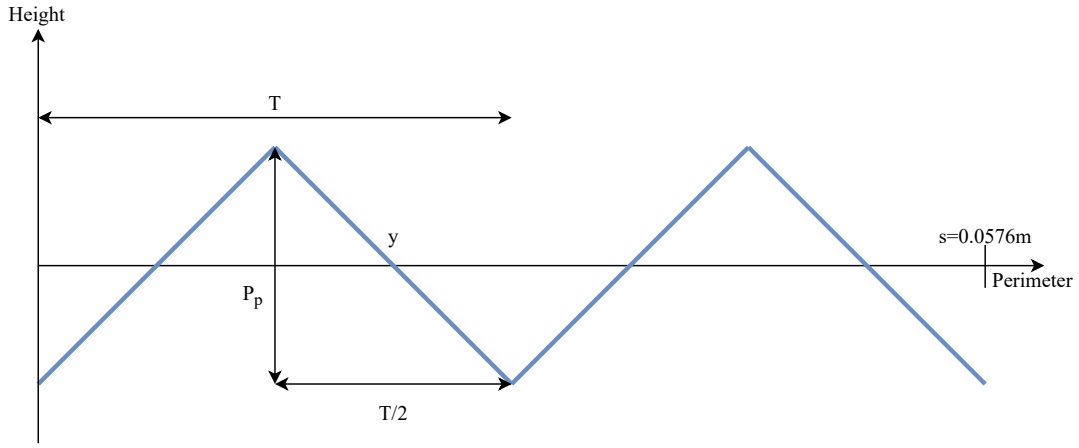

Figure 3.7.3: *Illustration of how the stator surface waves are simplified as triangular waves.*

$$y = \sqrt{P_p^2 + (T/2)^2} \tag{3.7.2}$$

$$s_{new} = 4 \cdot y = 4 \cdot \sqrt{P_p^2 + (T/2)^2} \tag{3.7.3}$$

$$s_{rel} = \frac{s_{new}}{s} = \frac{4 \cdot \sqrt{P_p^2 + (T/2)^2}}{s} \tag{3.7.4}$$

Allowing for a peak-to-peak distance of 10mm, the relative increase in perimeter is calculated to be $s_{rel} = 1.22$. This means that the perimeter and surface area is increased by 22%.

In addition, a new hydraulic diameter should be used because of the waved fins. The mean distance between the frame and the stator yoke is now $2cm + 10mm/2 = 0.025m$. By still assuming the duct as a concentric duct, the hydraulic diameter can be calculated as shown in equation 2.5.7. The concentric duct correlation, equation 2.5.3, is used for laminar flow and equation 2.5.5 is used for turbulent flow. Figure 3.7.4 illustrates the resulting convection coefficient. It can be observed that the waves have a minimal effect on the convection coefficient, as the convection coefficient as a function of fluid velocity is almost the same for the two cases with and without cooling fins. However, it is also important to note that the frequency of the waves, nor the peak-to-peak distance has been optimized. Although the convection coefficient is about the same as the case without cooling fins, the area of which convection takes place has increased. This means that more heat will be dissipated and removed from the machine.

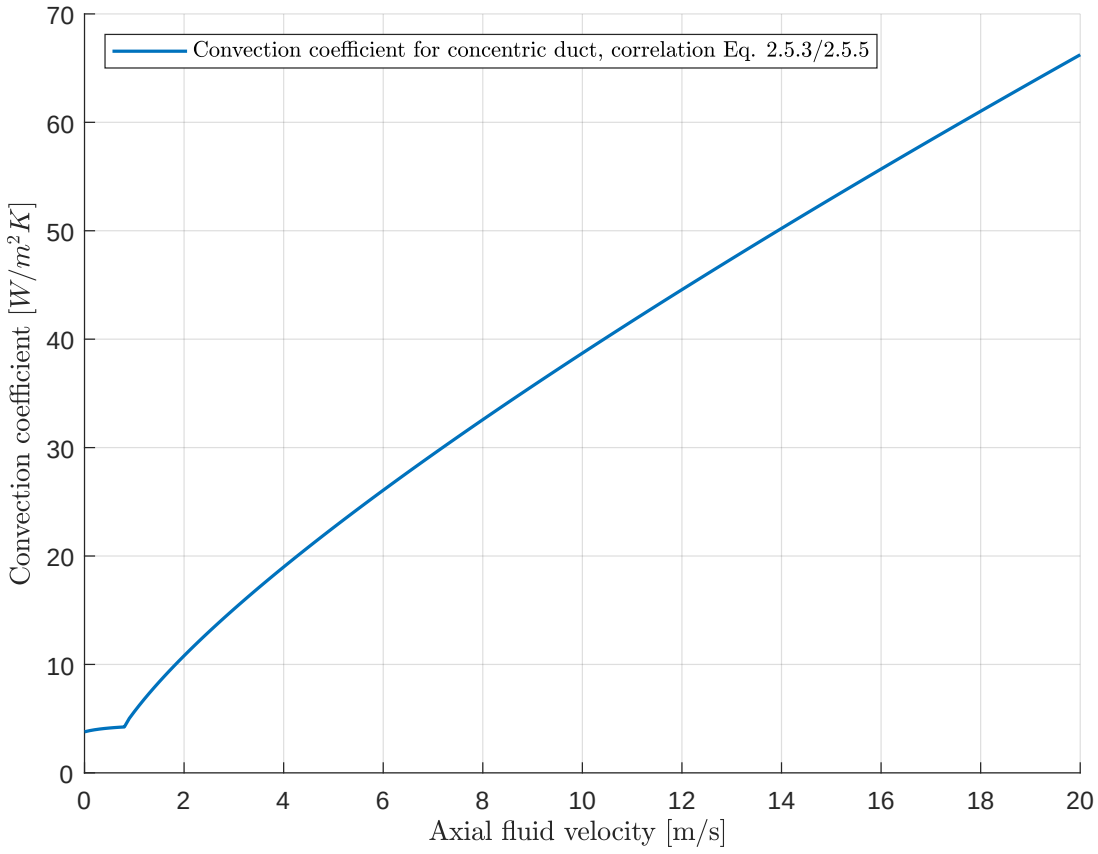

Figure 3.7.4: *Convection coefficient for a waved concentric duct between stator surface and frame.*

3.8 Implementing cooling methods in the thermal models

Now that different cooling methods have been introduced, they are implemented in the thermal equivalent circuit and the FEM model in COMSOL. Through an iterative approach, it was found that no single cooling method was sufficient to yield acceptable temperatures in the winding/slot or in the magnets. Because of this, a combination of two or more cooling methods are implemented at the same time. In this section, it is explained how the methods are implemented in the models. The resulting temperatures are displayed in the result chapter.

3.8.1 Hollow shaft cooling and rectangular duct in stator

A possible combination of cooling techniques, is hollow shaft cooling in the rotor and rectangular duct cooling in the stator. For both these methods, the highest heat transfer coefficient was found when the fluid medium was water. Because of this, and because it does not make sense to have two different fluid mediums, it was decided to implement these cooling methods using the heat transfer coefficients found for water cooling.

In the FEM model, the cooling methods can be easily implemented by making the geometry of the ducts and directly defining the heat transfer coefficients on the related surfaces. The rectangular duct is placed in such a way that the middle of the duct meets the middle of the stator slot, in the tangential direction. This means that only half the width of the duct is considered in the modelled section. Meaning that a height of $H = 0.01m$ and a width of $W = 0.02$ is used in the models. In addition, the duct is placed in the middle of the stator yoke in the radial direction. The placement for the duct has in no way been optimized, as this is done purely for an easier comparison between the thermal circuit and the FEM model. A discussion on the topic can be found in the discussion chapter, section 5.1.2. For the hollow shaft cooling, the shaft is assumed to be made of aluminum and modelled as a part of the rotor. The resulting FEM model is shown as figure D.0.1 in appendix D. The figure also illustrates how far away the hollow shaft actually is from the heated parts of the machine. Further implying that this cooling method may be a poor choice for the ModHVDC machine. The convection coefficient for the hollow shaft is set to $h_{shaft} = 123.7W/m^2K$, as explained in section 3.5. The convection coefficient for the duct in the stator is set to $h_{stator_{duct}} = 1800W/m^2K$, as this can be achieved for water cooling in such a duct, according to figure 3.6.2 in section 3.6. The ambient (or external temperature) of the cooling fluids are assumed to be $30°C$, as COMSOL demand the external temperature as an input variable. This is also done for all other cooling implementations.

For the equivalent circuit model, some new thermal resistances need to be calculated. The cooling duct in the stator have three surfaces where convection takes place, meaning that there are three heat paths and three thermal resistances that need to be calculated and implemented in the base thermal equivalent circuit. The resistances are calculated by using the base equation for convective thermal resistance, shown as equation A.0.2 in appendix A. These resistances are implemented as three resistances in parallel. Figure 3.8.1 illustrates how these three resistances

are implemented in the thermal equivalent model, shown in the blue area. The figure is a small sample of the whole equivalent circuit. The figure shows that the resistances are connected to the stator yoke node, which is in the middle of the stator yoke. Finally, the constant temperature of $40°C$ in the air gap is removed.

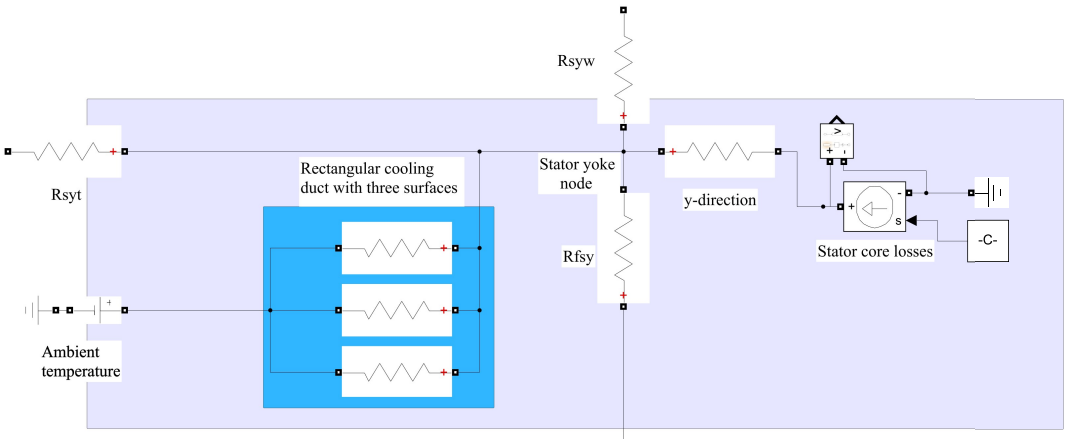

Figure 3.8.1: *Illustration of how a rectangular cooling duct is implemented in the base thermal equivalent circuit. The rectangular duct have three surfaces, that are illustrated with three thermal resistances connected in parallel as shown in the blue area.*

The hollow shaft cooling is implemented by making two new thermal resistances. First, the shaft has a conductive thermal resistance that is calculated by the hollow cylinder equation. In addition, there is convection on the innermost surface of the shaft, towards the fluid within the hollow shaft. This resistance is calculated as shown by equation 2.3.3. The total resistance of the shaft and the convection to the hollow shaft fluid, is connected to the rest of the circuit as shown in figure 3.8.2. Illustrated in the red box.

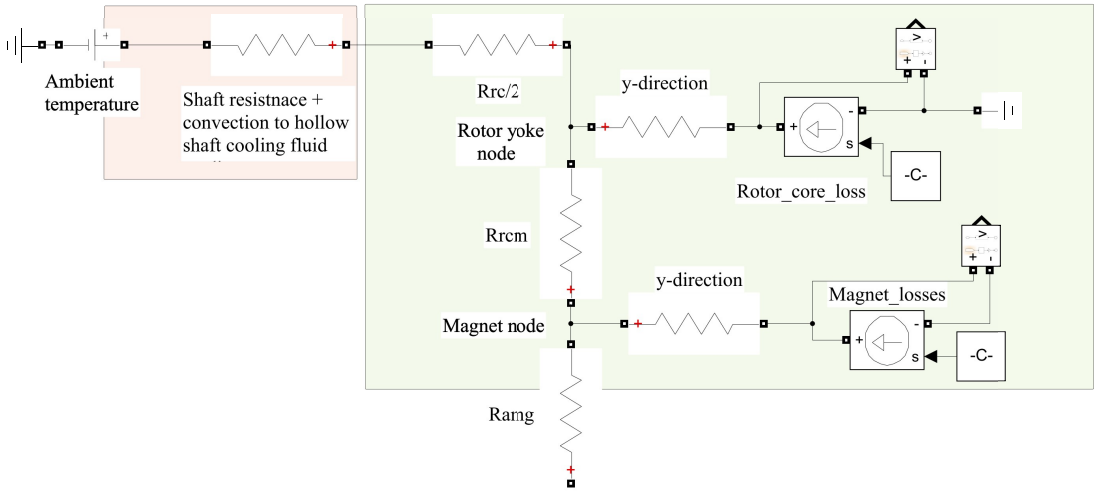

Figure 3.8.2: *Illustration of how the hollow shaft cooling method is implemented in the thermal equivalent circuit. Illustrated by the red area, where the total resistance of the shaft and the convective resistance is connected to the rest of the circuit.*

Finally, the constant temperature in the air gap is removed from the equivalent circuit. The whole equivalent circuit for for this cooling solution is shown as figure D.0.2 in appendix D.

3.8.2 Forced air cooling in the air gap and in rectangular duct in stator

Another combination of cooling methods, is forced air cooling in the air gap combined with air cooling in a rectangular duct in the stator. Again, the same fluid is used for both cooling methods, as it would not make sense to make several complete cooling systems with different cooling mediums.

The rectangular duct is implemented in the same way as described in the previous section, for both the FEM model and for the equivalent circuit. However, the convective heat transfer coefficient is changed. In figure 3.6.2, it can be seen that the convective heat transfer coefficient can reach about $h_{stator_{duct}} = 50W/m^2K$ for a fluid velocity of 10m/s. Note that this may be a conservative value, because the correlation allows for a higher Reynolds number, and thereby a higher heat transfer coefficient.

For the forced air cooling in the air gap, the convective heat transfer coefficient can be found by going back to section 3.1.3. Studying figure 3.1.3, it can be seen that the heat transfer coefficient for an airflow of about 10 m/s is $h_{ag} = 88W/m^2K$.

In the FEM model, the duct is implemented in the same way as before. However, with the new heat transfer coefficient. The cooling in the air gap is implemented by defining the convective heat transfer coefficient on the radial surfaces leading to the air gap. Figure 3.8.3 illustrates the resulting geometry of the FEM model. In addition, the temperature of the air gap is no longer set as a constant value.

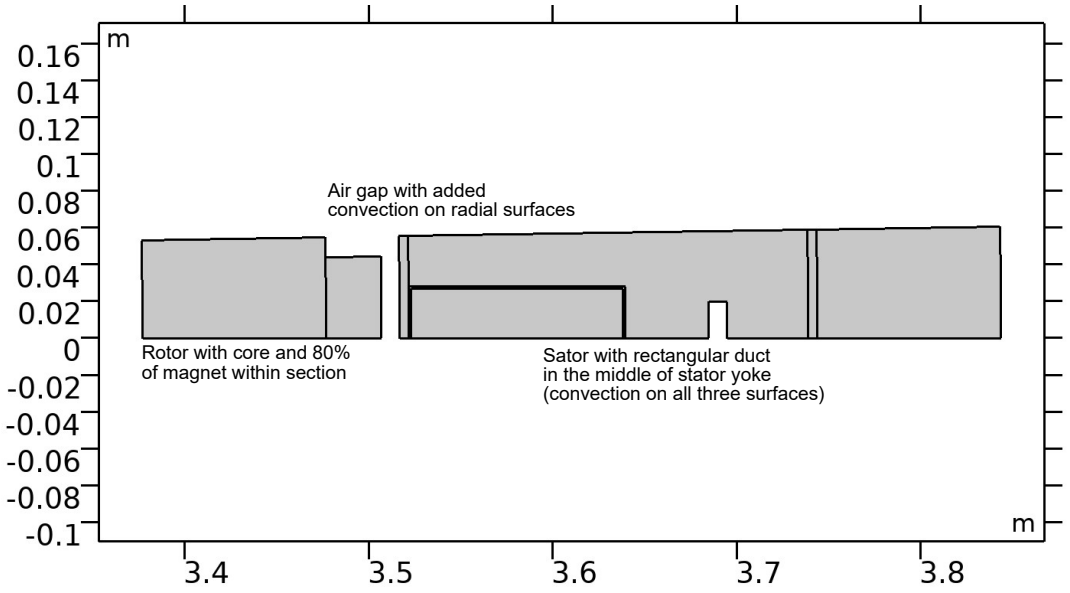

Figure 3.8.3: *Illustration of resulting FEM model for rectangular duct and air gap air cooling.*

The cooling in the air gap is implemented in the thermal equivalent circuit, by introducing two new thermal resistances. One for each of the surfaces leading towards the air gap, in the radial direction. The thermal resistances can be calculated by using the hollow cylinder equation, with a slight modification on the magnet surface. For the surface towards the stator, equation 3.8.1

is used. While for the surface towards the magnet, equation 3.8.2 is used. In equation 3.8.2 the modification factor p_m can be seen. This factor is used to take into account that only 80% of the magnet is within the modelled section and thereby the area of which convection takes place is reduced. In this case $p_m = 0.8$.

$$R_{ag_{stator}} = \frac{1}{2\pi \cdot (r_{mag} + d_{ag}/2) \cdot h_{ag}} \cdot \frac{2\pi}{\theta_s} \tag{3.8.1}$$

$$R_{ag_{magnet}} = \frac{1}{2\pi \cdot r_{mag} \cdot h_{ag}} \cdot \frac{2\pi}{\theta_s \cdot p_m} \tag{3.8.2}$$

Figure 3.8.4 illustrates how these new resistances, and thereby forced air cooling in the air gap, are connected and implemented in the base thermal equivalent model. Indicated by the purple area. As for all cooling methods, the constant temperature in the air gap, is removed. Additionally, the temperature at the air gap node is no longer measured. This is because it is assumed that all heat that is transported to the cooling fluid, is also transported out of the machine. The rectangular stator duct is connected in the exact same way as shown in figure 3.8.1. The whole equivalent circuit for this combined cooling solution is shown in appendix D, as figure D.0.3.

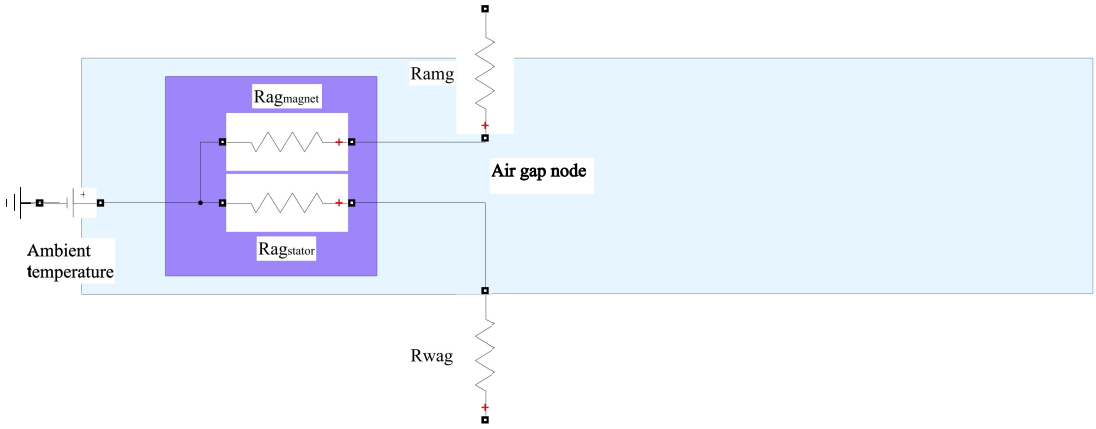

Figure 3.8.4: *Illustration of how forced air flow in the air gap is implemented in the thermal equivalent circuit. Illustrated in the pink area, where two new resistances are introduced.*

3.8.3 Cooling duct in stator and concentric duct between stator and frame

For the next investigated cooling solution, rectangular cooling duct in the stator and a concentric duct between the stator surface and the frame is implemented. In section 3.7, the convection coefficient for the concentric duct was investigated. However, only air was used as fluid. Because of this, air is used as fluid for this combined cooling method. For now, a concentric duct without waves is implemented. The constant temperature in the air gap is removed.

The rectangular duct in the stator is implemented in the same way as described in the previous combined cooling method. Using $h_{stator_{duct}} = 50W/m^2K$. Look back to figure 3.8.1 and section 3.8.1 for a complete description of how the duct is implemented in both the FEM model and the thermal equivalent circuit.

In the FEM model, the concentric duct is implemented by removing the insulation between the stator and the frame, in addition to removing frame material until a gap length of $2cm$ is reached. The gap length of $2cm$ is used to avoid short circuits, as explained in section 3.7. The convection coefficient is then defined on the surfaces in the radial directions. From figure 3.7.1, it can be observed that the convection coefficient can reach as high as $70W/m^2K$ for a fluid velocity of 20m/s. However, as a conservative choice $h_{con_{duct}} = 50W/m^2K$ is used. The resulting geometry of the FEM model can be seen as figure 3.8.5.

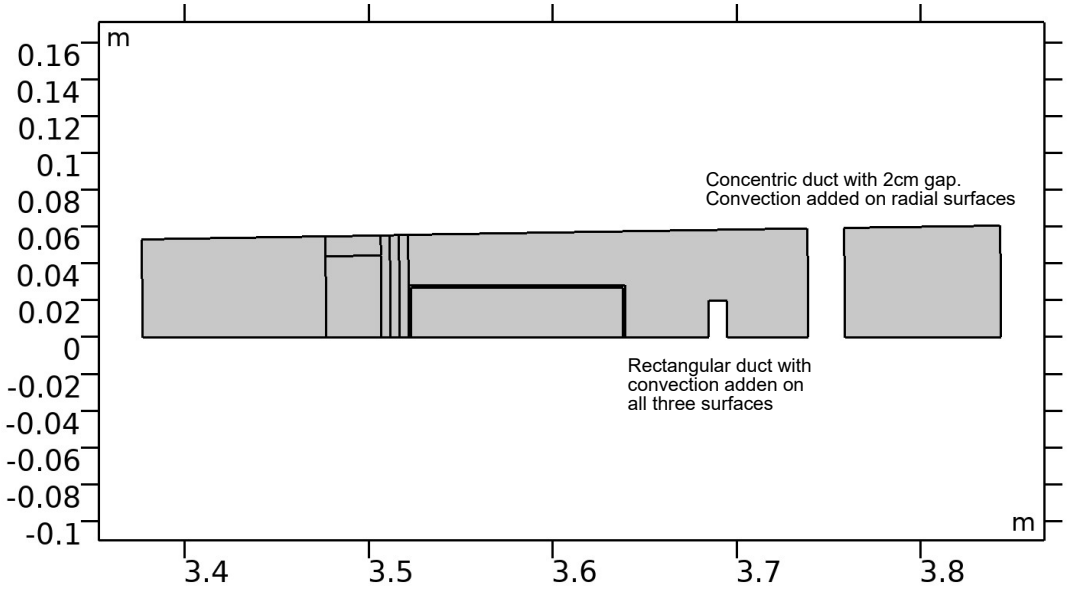

Figure 3.8.5: *Cooling combination with rectangular duct in stator and concentric duct at stator surface, The concentric duct has a gap length of 2cm to avoid short circuits.*

As mentioned, the rectangular duct is implemented in the same way as earlier described. For the concentric duct, two new resistances are calculated. These are calculated from the hollow cylinder equation for convection, shown as equation 2.3.3. The convective resistance between the surface of the stator and the cooling fluid is named $R_{ss_{duct}}$ and the convective resistance between the frame and the cooling fluid is called $R_{fr_{duct}}$. The calculation of these and all other resistances can be found in the attached MATLAB-script in appendix E. In addition, some small

modifications are done to the base model, in order to implement the cooling method at the right placement. The resistance R_{fsy}, which is equal to $\frac{1}{2}R_{sy} + \frac{1}{2}R_{fr} + R_{inso}$ is split into two separate resistances. In addition, the resistance of the insulation, R_{inso}, is removed since this resistance no longer exists. Figure 3.8.6 illustrates the resulting circuit between the frame and the stator. Where the implementation of the concentric duct between the stator surface and the frame can be seen in the purple area. The complete equivalent circuit for this combined cooling method can be found as figure D.0.4 in appendix D.

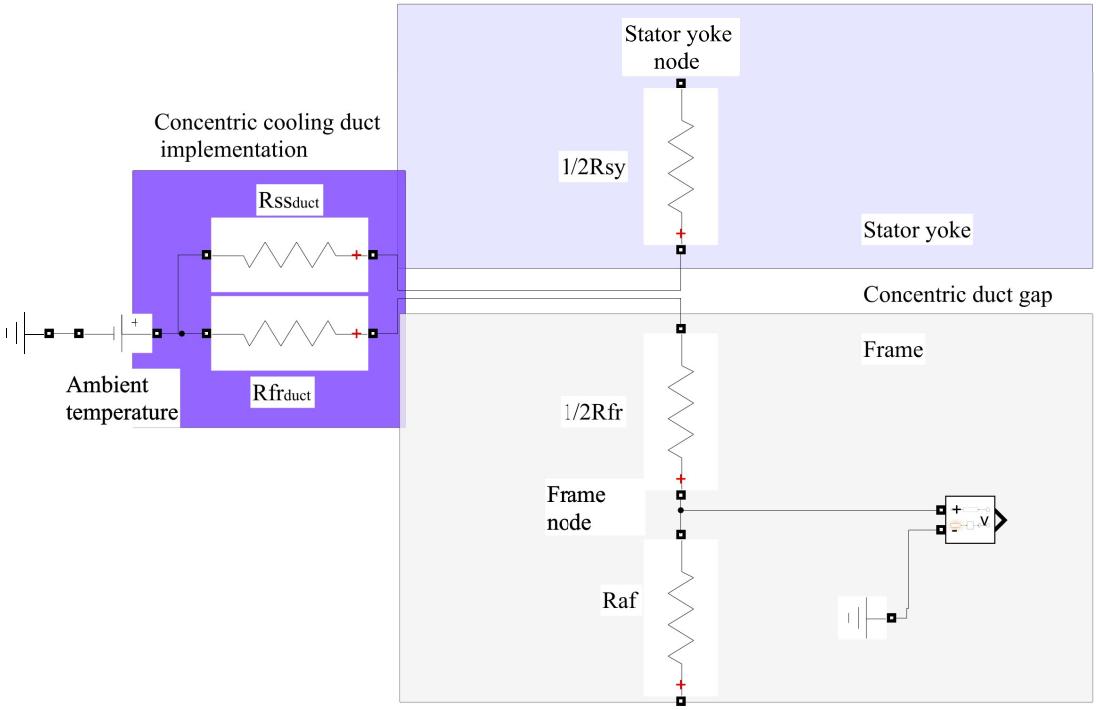

Figure 3.8.6: *Resulting part of the equivalent circuit with concentric cooling duct between stator surface and frame. The implementation of the cooling duct can be seen in the purple area.*

3.8.4 Air cooled air gap and concentric duct between stator and frame

The last cooling combination developed in this thesis, is an air cooled air gap combined with an air cooled concentric duct between the stator surface and the frame. Two models for this cooling combination are made. One without waved cooling fins at the stator surface and one with a waved cooling fin surface. This is done in order to evaluate the effects of the waved cooling fin surface on the resulting temperatures.

Both an air cooled air gap and an air cooled concentric duct have been presented previously. The two methods are implemented in the exact same way as before, using $h_{ag} = 88W/m^2K$ for the air gap and $h_{con_{duct}} = 50W/m^2K$ for the concentric duct. For a full explanation of how the methods are implemented in the FEM model and in the equivalent circuit, see section 3.8.2 and section 3.8.3. The resulting FEM model is shown as figure 3.8.7, while the whole equivalent circuit can be found as figure D.0.5 in appendix D. As explained earlier, the temperature in the air gap is no longer measured, as it is assumed that all heat transferred to the air gap is transferred out of the machine.

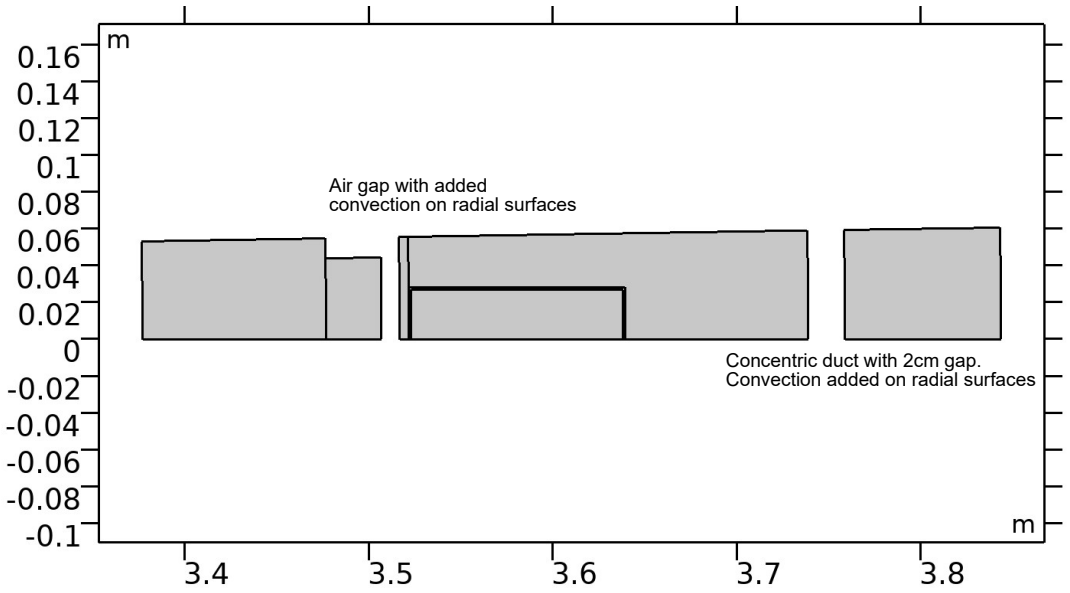

Figure 3.8.7: *FEM model with air gap and concentric duct on stator surface cooling.*

Taking the concentric duct method one step further, waved cooling fins are implemented at the stator surface. This is done to increase the area of which convection takes place. This method was elaborated on in section 3.7, where the heat transfer coefficient for two waves within the modelled section was investigated.

Implementing the waved cooling fins in the FEM model is easy, as the geometry of the waved fins can be directly made on the stator surface. The peak of the waved surface makes for a 2cm gap between the stator and the frame, in order to avoid short circuits. In addition, the peak-to-peak distance for the waves are $P_p = 10mm$. In section 3.7, figure 3.7.4, the convection coefficient for the concentric duct with waved cooling fins is shown. From the figure, it can be seen that the convective heat transfer coefficient for this method can be set to $h_{con_{duct}} = 50W/m^2K$. While the convective heat transfer coefficient of the air gap is still $h_{ag} = 88W/m^2K$. The resulting FEM model is shown as figure 3.8.8.

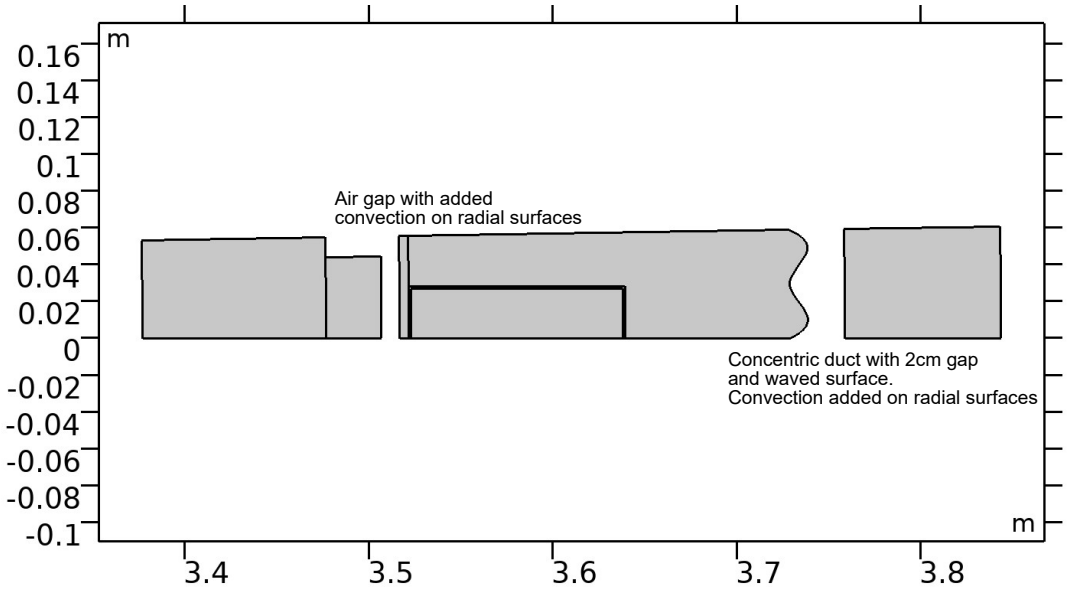

Figure 3.8.8: *FEM model with air gap and concentric duct cooling with waved stator surface.*

For the thermal equivalent model, the structure and connections are the same as before. However, the resistance $R_{ss_{duct}}$ is calculated with a slight modification. The increase in area can be seen as a decrease in thermal resistance, leading to equation 3.8.3. s_{new} can be calculated as shown in equation 3.7.3.

$$R_{ss_{duct}} = \frac{1}{2\pi \cdot (r_{inso} - 0.01) \cdot h_{con_{duct}}} \cdot \frac{2\pi}{\theta_s} \cdot \frac{s}{s_{new}} \tag{3.8.3}$$

Chapter 4

Results

In this chapter, the results from this thesis are presented. The chapter starts with a comparison of the two different FEM models made of the stator, with and without turns and turn-to-turn insulation. After the comparison, the base model made both as a FEM model and an equivalent circuit is, compared to verify the validity of the models. Then, the resulting temperatures for the different cooling methods are presented. The most important temperatures that should be paid additional attention to, finds place in the copper/slot node and in the magnets. The maximum temperatures of these are $150°C$ and $80°C$, respectively, as shown in appendix B. From the results, it can be seen that several cooling solutions are applicable to the ModHVDC machine, yielding acceptable temperatures.

4.1 Model with turns and insulation in slot vs equivalent thermal conductivity

As elaborated on in the modelling chapter, section 3.4.2, two methods are used to model the stator slot material. The first and most simple method, is to model the slot material as one square block with equivalent thermal conductivity in the radial and tangential directions. The second method, is to model the slot with turns of copper and an insulation layer around each turn. In this section, the resulting temperatures for the two methods are presented. The maximum temperatures in this comparison is of little importance, as no cooling solutions are implemented in the models. The goal is to verify the simplification, that is the equivalent conductivity method.

Figure 4.1.1 and figure 4.1.2 displays the resulting temperature pattern in the stator for the two methods. Where figure 4.1.1 includes the turns and turn-to-turn insulation and figure 4.1.2 uses the equivalent thermal conductivity method. Comparing the figures, it can be seen that the temperature distribution in the stator segment is about the same for both methods. In addition, only a difference of $2°C$ in maximum temperature within the slot can be observed. Whereas the turn-to-trun model yields a maximum temperature of $195°C$ and the equivalent conductivity model yields a maximum of $193°C$. As an other remark, it can also be observed that the maximum temperature within the slot occurs at about the same spot.

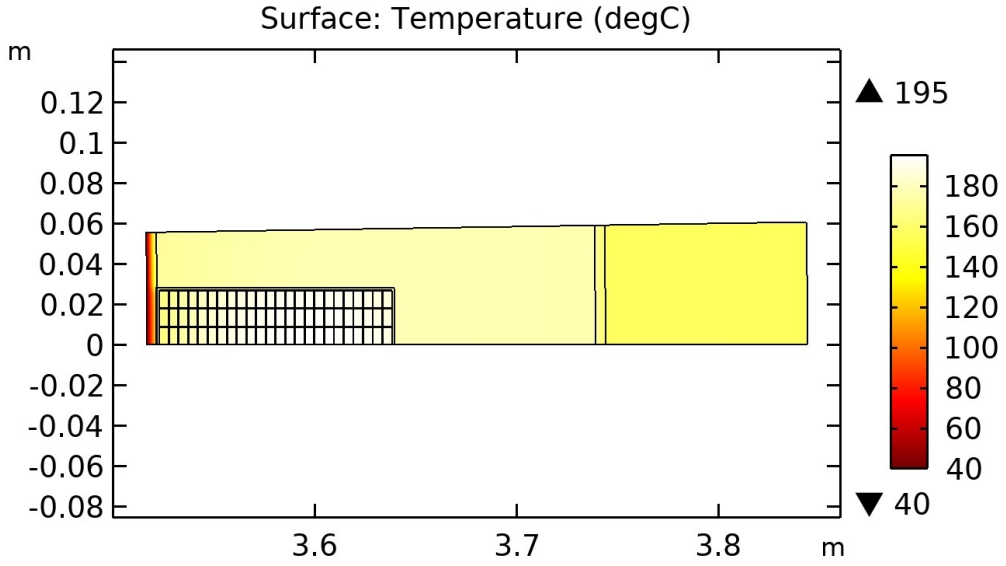

Figure 4.1.1: *Temperature distribution in the stator when including copper turns and turn-to-turn insulation in the slot.*

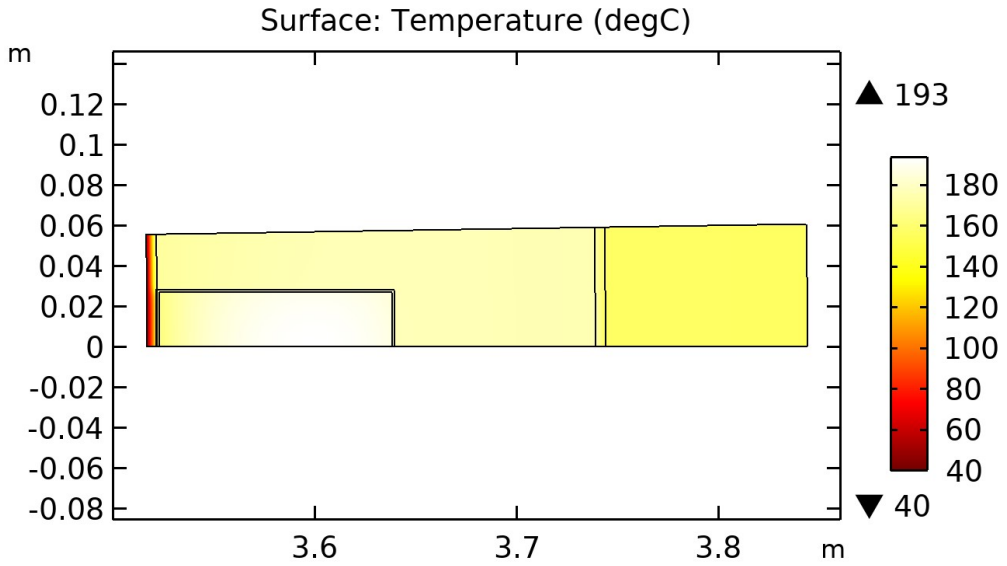

Figure 4.1.2: *Temperature distribution in the stator when using equivalent thermal conductivity.*

The built-in surface average temperature measurement tool in COMSOL, is used to find the average temperatures in the stator section. Table 4.1.1 lists the resulting temperatures, in addition to the simulation time for both methods. Studying the table, it becomes even more clear that there are very small differences between the two methods. The largest difference is seen in the winding/slot node, with only a $1.3°C$ difference in the average temperature. This is equal to a 0.7% difference between the methods. An other interesting observation, is that the simulation time for the method with turns and insulation is about 7 seconds longer than the equivalent thermal conductivity method. This might not sound like much, but is actually a difference of about 108%. In all other results presented, the method with equivalent thermal conductivity is used.

Table 4.1.1: *Comparison of temperatures in the stator section with turns and insulation in the slot versus equivalent thermal conductivity for the slot material.*

Node	With turns & insulation $[°C]$	With equivalent thermal conductivity $[°C]$	ΔT $[°C]$	ΔT [%]
Ambient	30	30	-	-
Frame	156.8	156.4	0.4	0.3
Yoke	176.6	176.1	0.5	0.3
Winding/slot	187.1	185.8	1.3	0.7
Teeth	175.4	174.9	0.5	0.3
Air gap	40	40	-	-
Simulation time	$\approx$ 10 [s]	$\approx$ 3[s]	$\Delta t = 7[s]$	-

4.2 Base model comparison between equivalent circuit & FEM model

Before a comparison is done, the thermal resistances for the equivalent circuit are calculated. The thermal resistances for the base equivalent circuit are calculated as described in the equivalent model section, section 3.3. The resulting resistances are displayed in table 4.2.1. The calculation of these resistances and the sub-resistances they are a result of, can be seen in a MATLAB-script attached appendix E. For the resistance from the frame surface to the ambient, R_{amb}, the final value is gives, as this is a nonlinear resistance.

Table 4.2.1: *Thermal resistances for the base thermal equivalent circuit.*

Parameter	Value [mK/W]
R_{amb}(nonlinear)	2.2752
R_{af}	0.0035
R_{fsy}	0.3533
R_{syt}	0.0401
R_{syw}	0.4372
R_{wst}	0.0769
R_{wag}	1.1551
R_{agt}	0.7368
R_{ag}	0.0167
R_{amg}	0.0524
R_{rcm}	0.0564
R_{rc}	0.0242

From the results, it becomes clear that the largest thermal resistance in the base model finds place between the frame surface and the ambient air. This is as expected, since the resistance was modelled in a conservative way. Only considering the natural convection at the surface. The second largest resistance finds place between the winding/slot node and the beginning of the air gap. This may indicate that the thermal resistance in the radial direction within the slot is high. This makes sense, when keeping mind that most of the turns finds place in the radial direction. Generally, the resistances that include convection or insulating material are observed to be larger than the purely convective resistances without insulating material. The exception is with the thermal resistance of the air gap itself. This may be due to the method used to calculate the thermal resistance of the air gap, where a completely convective heat transfer was assumed.

Simulating the equivalent circuit made in Simulink, the average temperatures are found by measuring the voltage at each respective node. While the temperatures from the FEM model are found by using the surface average temperature tools available in COMSOL. The results are shown in table 4.2.2. In addition, the temperature distribution found in the FEM model is shown as figure 4.2.1.

The maximum temperature is found in the winding/slot node, reaching around $190°C$ on average. However, figure 4.2.1 shows that the highest temperature is $197°C$, meaning a difference of

$7°C$ between the peak temperature and the average temperature within the slot. The whole stationary part of the machine is observed to reach high temperatures, indicating that an efficient cooling system is needed in direct contact with the stationary part. While the rotating part of the machine is well within acceptable values. However, this is probably the due to the fact that the air gap temperature was set as a constant $40°C$. Again, these temperatures do not represent the real values in the machine. They however serve the purpose of comparing the equivalent circuit with the FEM model made of the same machine section.

Observing table 4.2.2, it becomes clear that the equivalent circuit and the FEM model correspond well. The highest deviation in resulting temperature is found in the winding/slot node, with a difference of only $1.7°C$. Yielding a percentage difference of only 0.89%. The lowest temperature difference is found in the stator yoke node. Where a difference of $0.2°C$ is observed. An interesting observation is that the percentage difference is highest in the rotor core node, with 3.48%. However, the temperature difference is only $1.6°C$. The temperatures from the equivalent circuit are all higher than the FEM model temperatures. With the exception of the air gap temperature. A discussion on the results is done in chapter 4.

Table 4.2.2: *Comparison of resulting temperatures from the base models. Both from the equivalent circuit made in Simulink and from the FEM model made in COMSOL.*

Node	**Equivalent circuit temperatures** [$°C$]	**FEM model temperatures** [$°C$]	**Temperature difference** [$°C$]	ΔT [%]
Frame	159.4	159.0	0.4	0.25
Stator yoke	179.4	179.2	0.2	0.11
Stator teeth	179.0	178.0	1.0	0.56
Winding/Slot	190.8	189.1	1.7	0.89
Air gap	40.0	40.9	0.9	2.22
Magnet	44.9	44.0	0.9	2.02
Rotor core	46.8	45.2	1.6	3.48

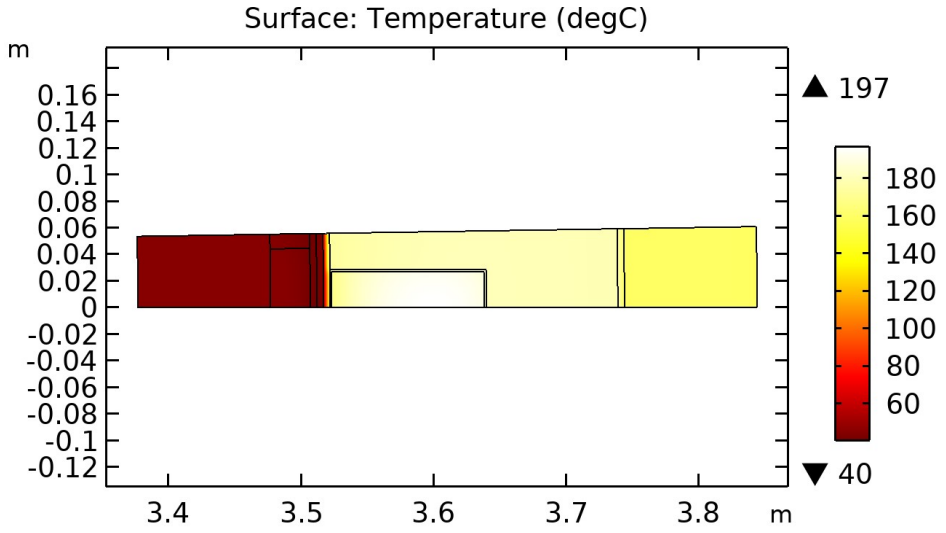

Figure 4.2.1: *Temperature distribution for the base FEM model made in COMSOL.*

4.3 Hollow shaft cooling and rectangular duct in stator

In this section, the results from the combined cooling techniques of hollow shaft and rectangular duct cooling are presented. As mentioned in the modelling section, the fluid used for this combined method is water. The resulting average temperatures in the ModHVDC machine from both the analytical thermal equivalent circuit and the FEM model, is displayed in table 4.3.1. Along with the maximum temperature for each part from the FEM model and the difference between the FEM model and the thermal equivalent circuit.

Table 4.3.1: *Temperatures from the combined cooling methods of hollow shaft cooling and rectangular duct in stator. The methods have been used with water as fluid medium.*

Node/placement	**Equivalent circuit temperatures** [$^\circ C$]	**FEM model temperatures** [$^\circ C$]	**Temperature difference** [$^\circ C$]	ΔT [%]	**FEM model max temp** [$^\circ C$]
Frame	35.10	35.59	0.49	1.40	35.60
Stator yoke	35.36	37.36	2.00	5.50	40.38
Stator teeth	50.79	51.87	1.08	2.10	58.12
Winding/Slot	71.64	71.42	0.22	0.31	84.86
Air gap	107.04	107.75	0.71	0.66	109.66
Magnet	110.44	111.02	0.57	0.52	111.14
Rotor core	110.81	110.64	0.17	0.15	112.06

Studying the table, it can be seen that the temperature in the magnets is far higher than the allowable maximum temperature of $80^\circ C$. This means that this cooling method is not sufficient for the ModHVDC machine. However, the slot/winding temperature is well within the limit and it can be observed a good coherence between the FEM model and the thermal equivalent circuit. Whereas a maximum difference of only $2.00^\circ C$ is observed. In addition, it is observed that the maximum temperatures from the FEM model can become somewhat higher than the average, where the largest difference can be observed in the slot. Here, a difference of $13.44^\circ C$ can be observed between the FEM average temperature and the FEM maximum temperature. Indicating that the hot spot should be given additional attention.

4.4 Forced air through air gap and rectangular duct in stator

The resulting temperatures from the combined cooling solution of forced air through the air gap and through a rectangular duct in the stator, is presented in this section. Table 4.4.1 presents the average temperatures obtained from the FEM model and the thermal equivalent model. In addition, the differences and the maximum temperatures from the FEM model are displayed.

Table 4.4.1: *Temperatures from the combined cooling situation of forced airflow in the air gap and air in rectangular duct in stator.*

Node/placement	**Equivalent circuit temperatures** [$°C$]	**FEM model temperatures** [$°C$]	**Temperature difference** [$°C$]	ΔT [%]	**FEM model max temp** [$°C$]
Frame	103.03	102.28	0.75	0.73	102.37
Stator yoke	112.40	112.50	0.10	0.09	114.34
Stator teeth	118.51	117.80	0.71	0.60	118.72
Winding/Slot	134.00	132.25	1.75	1.31	137.22
Air gap	-	-	-	-	-
Magnet	67.08	66.23	0.85	1.28	68.10
Rotor core	69.11	68.11	1.00	1.46	68.11

From the results, it can be seen that this cooling combination can be applied to the ModHVDC machine with acceptable temperatures. The maximum allowable temperature of the windings and the maximum allowable temperature of the magnets have not been reached. However, it can be seen that the whole machine reaches high temperatures and even the frame is over $100°C$. An other observation is that the coherence between the thermal equivalent model and the FEM model is very good. With a maximum difference of only $1.75°C$. In addition, it can be seen that the maximum temperature differs from the average by some degrees. However, only about $5°C$ at max in the slot/winding node. Figure 4.4.1 shows the resulting temperature distribution from the FEM model, in order to give a better visualisation of the temperatures.

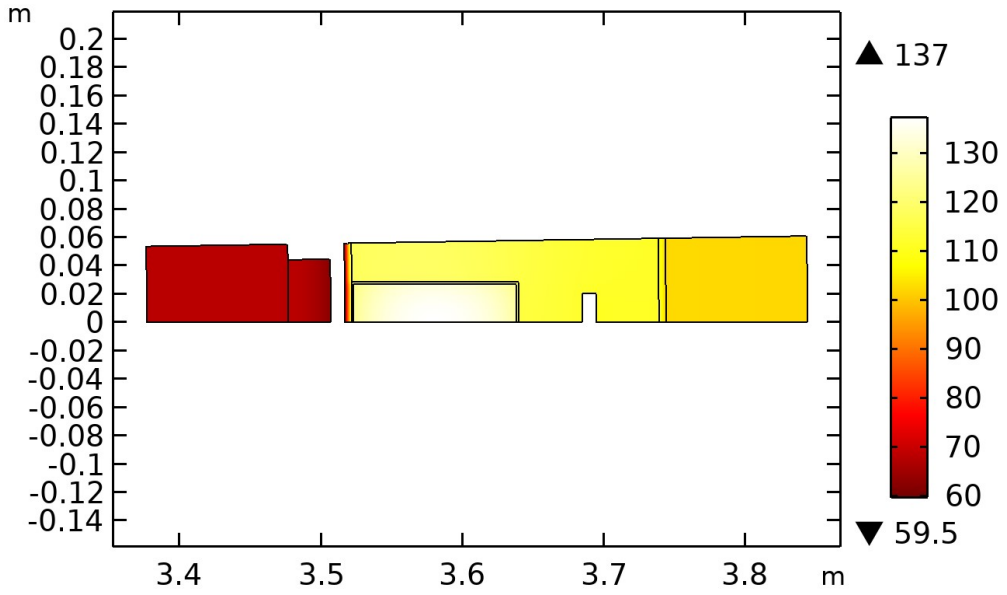

Figure 4.4.1: *Temperature distribution for forced air through air gap and rectangular duct in stator.*

4.5 Air cooled rectangular duct in stator and concentric duct on stator surface

The temperatures resulting from the combined cooling method of air cooled rectangular duct in stator and concentric duct between the stator surface and the frame, is presented in this section. The temperatures can be seen in table 4.5.1, where the nodal temperatures and the max temperature from the FEM model are presented.

Table 4.5.1: *Temperatures from the combined cooling methods of concentric duct between stator surface and frame and rectangular duct in stator. The methods have been used with air as cooling fluid.*

Node/placement	**Equivalent circuit temperatures** [$°C$]	**FEM model temperatures** [$°C$]	**Temperature difference** [$°C$]	ΔT [%]	**FEM model max temp** [$°C$]
Frame	30.00	30.00	0	0	30.00
Stator yoke	125.90	125.58	0.32	0.25	129.31
Stator teeth	142.42	142.63	0.21	0.15	149.58
Winding/Slot	163.89	162.81	1.08	0.66	178.81
Air gap	212.10	212.44	0.34	0.16	214.04
Magnet	217.04	216.50	0.54	0.25	217.97
Rotor core	219.06	217.53	1.53	0.70	217.67

The results show that the allowable max temperature for the windings and for the magnets have been violated. This means that this combined cooling method is insufficient for the ModHVDC machine. A temperature rise can be observed towards the center of the machine, possibly due to the lack of cooling around or near the magnet. Although the temperatures of the machine are high, the frame temperature is observed to be at ambient temperature. The coherence between the FEM model and the equivalent circuit is however excellent. Where a maximum difference of only $1.53°C$ can be observed in the rotor core node. In addition, the maximum temperature from the FEM model is once again observed to be over $10°C$ higher than the average temperature. The temperature distribution from the FEM model is shown in figure 4.5.1.

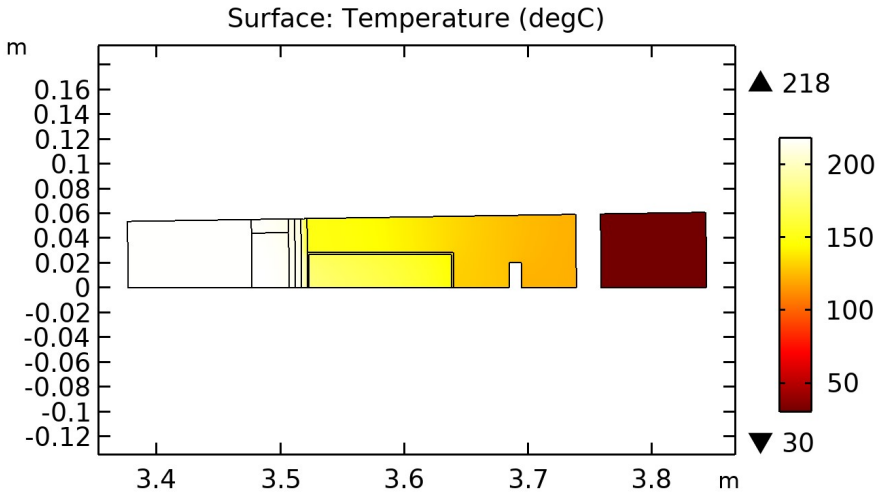

Figure 4.5.1: *Temperature distribution for the combined cooling methods of rectangular duct in stator and concentric duct at stator surface.*

4.6 Forced air through air gap and concentric duct at stator surface

In this section, the results from the combined cooling method of an air cooled air gap and air in a concentric duct between the stator and the frame is presented. First, the results in the case of a stator surface without waved cooling fins is presented. Then, the case where waved cooling fins are added on the stator surface is presented. Lastly, a comparison of the two methods is done.

For the first case, where no waves have jet been implemented, the resulting temperatures are shown in table 4.6.1. The nodal temperatures from the equivalent circuit, the average temperature from the FEM model and the maximum temperature from the FEM model are presented.

Table 4.6.1: *Temperatures from the combined cooling methods of concentric duct between stator surface and frame and forced air in air gap.*

Node/placement	**Equivalent circuit temperatures** [$°C$]	**FEM model temperatures** [$°C$]	**Temperature difference** [$°C$]	ΔT [%]	**FEM model max temp** [$°C$]
Frame	30.00	30.00	0.00	0.00	30.00
Stator yoke	111.73	110.90	0.83	0.75	112.64
Stator teeth	117.88	116.83	1.05	0.89	117.77
Winding/Slot	133.40	131.33	2.07	1.56	136.28
Air gap	-	-	-	-	-
Magnet	68.16	66.23	1.93	2.87	68.11
Rotor core	70.19	69.11	1.08	1.55	69.20

Studying the table, it can be seen that the temperatures are within the allowable range. With a slot/winding temperature of around $133°C$ and a magnet temperature of around $68°C$. This means that even before waved cooling fins are added on the stator surface, this combined cooling method can be applied to the ModHVDC machine. It is also observed that all temperatures of the thermal equivalent model is higher than the average from the FEM model, but lower (or about equal for the magnet and the rotor core) than the maximum value from the FEM model. Additionally, the difference between the equivalent circuit and the FEM model is very low. With a maximum difference of $2.07°C$ found in the winding/slot node. Indicating a good coherence between the analytically made model and the FEM model. For this combined cooling method, it can be observed that most of the machine becomes very warm. With a stator yoke temperature of over $100°C$. However, the frame itself is observed to be at only $30°C$. Figure 4.6.1 displays the temperature distribution in the modelled section.

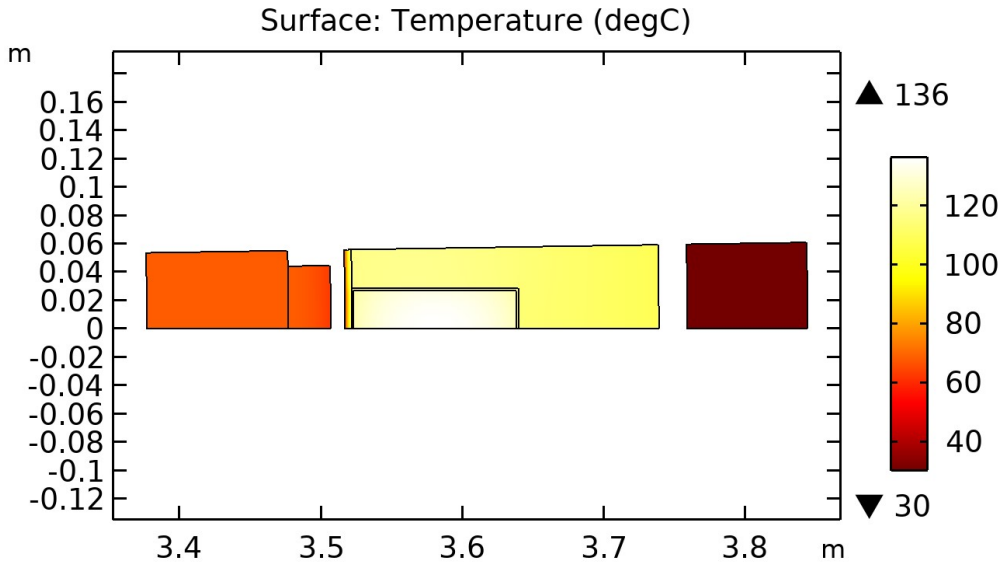

Figure 4.6.1: *Temperature distribution for the combined cooling method of air in air gap and in a concentric duct at stator surface.*

Table 4.6.2 shows the resulting temperatures when waved cooling fins are added on the stator surface. From the results, it becomes clear that all temperatures are within the allowable range. With a maximum temperature in the windings/slot of 125.47°C and a maximum temperature in the magnets of 68.11°C. The difference between the equivalent circuit and the FEM model is observed to be slightly higher than for the other implemented cooling methods. However, the maximum difference is only 2.60°C. The temperature distribution for the FEM can be seen in figure 4.6.2. In addition, a comparison of the waved cooling fin method and the method without fins, can be seen in table 4.6.3.

Table 4.6.2: *Temperatures from the combined cooling methods of concentric duct between waved stator surface and frame and forced air in air gap.*

Node/placement	**Equivalent circuit temperatures** [°C]	**FEM model temperatures** [°C]	**Temperature difference** [°C]	ΔT [%]	**FEM model max temp** [°C]
Frame	30.00	30.00	0.00	0.00	30.00
Stator yoke	101.71	99.18	2.53	2.52	101.04
Stator teeth	108.40	105.80	2.60	2.43	106.94
Winding/Slot	124.22	121.64	2.58	2.10	125.47
Air gap	-	-	-	-	-
Magnet	68.16	66.23	1.93	2.87	68.11
Rotor core	70.19	69.11	1.08	1.55	69.20

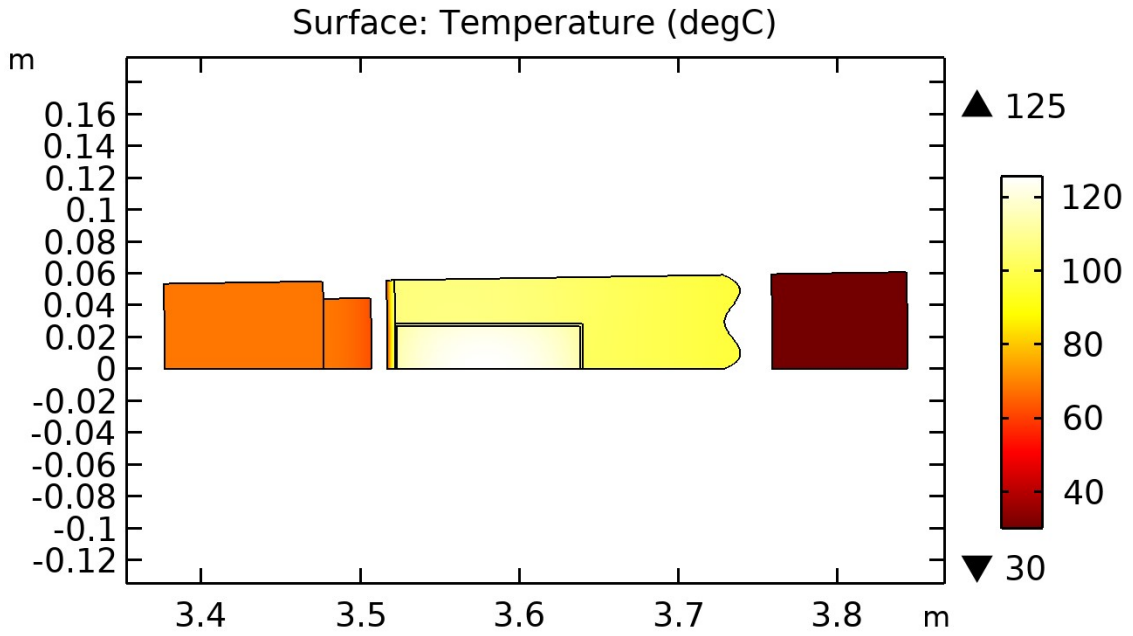

Figure 4.6.2: *Temperature distribution for the combined cooling method of air cooled air gap and concentric duct on a waved stator surface.*

Table 4.6.3 shows the resulting max temperature from the FEM models with and without waved cooling fins on the stator surface. It can be observed that the waved cooling fin method have reduced the temperature in all the stator parts of the machine. On average, the maximum temperature in the stator has been reduced by $11°C$. However, the rotor and frame are not affected by the waved cooling fins. The same can be said for the average temperatures, when comparing table 4.6.1 and table 4.6.2. In the modelling chapter, it was mentioned that the frequency and the depth of the waves have not been optimized. This indicates that a larger reduction in temperatures may be possible, if this cooling method is investigated further.

Table 4.6.3: *Comparison between max temperatures obtained from the FEM models for two stator surface methods. One where waved cooling fins on the stator surface is implemented and one without fins.*

Node/placement	**FEM model without cooling fins Max temp.** $[°C]$	**FEM model with waved cooling fins Max temp.** $[°C]$
Frame	30.00	30.00
Stator yoke	112.64	101.04
Stator teeth	117.77	106.94
Winding/Slot	136.28	125.47
Air gap	-	-
Magnet	68.11	68.11
Rotor core	69.20	69.20

Chapter 5

Discussion

In this chapter, discussions and evaluations on the methods, models and results from the thesis are done. The chapter starts with an evaluation of the cooling methods and how these are implemented. Then, a discussion on the effects of the waved cooling fins find place. Further, the impact on the electromagnetic design, optimization and further cooling methods are discussed. The equivalent thermal conductivity method versus the full slot model is then evaluated, before the differences between the FEM model and the analytical thermal equivalent circuit are discussed. The chapter finishes with a discussion and evaluation of the assumptions, limitations and simplifications made for the thesis.

5.1 Cooling methods and implementation

In section 3.8, it was mentioned that no single cooling method investigated yielded sufficient cooling for the ModHVDC machine. This implies that the ModHVDC machine is in need of a combination of several cooling methods, or other more sufficient and effective methods that have not been investigated in this thesis. Using a combination of cooling methods, sufficient solutions were found.

Going through the results from the different cooling methods, a trend can be seen. The methods that have implemented cooling on or close to both the magnet and the slot, have all yielded acceptable temperatures. While the methods where cooling techniques have been applied to only the stationary part of the machine or far away from the magnets, have all violated the allowable temperatures of either the magnets or the windings (or both). Clearly indicating that the ModHVDC machine should be cooled by techniques that are efficient in the magnet and slot areas. As should be expected, since the winding losses and the magnet losses stands for the majority of the losses in the machine. Further, this also indicates that the hollow shaft cooling method is not applicable to the ModHVDC machine, as have been hinted to throughout the thesis. Although, the size of the hollowed shaft have not been optimized.

A cooling method that has reached acceptable temperatures in the slot and magnets, is the combination of forced air in air gap and in a rectangular duct in the stator. However, this cooling solution yield very high temperatures in the whole stator and in the frame. With temperatures reaching as high as $102.4°C$ in the frame. These high temperatures may lead to other dangerous situations around the machine, for other equipment or for personal working in the area close to the machine. In addition, if the ModHVDC machine is placed in an enclosed room, such as the nacelle of a wind turbine, the ambient temperature may start to rise to higher temperatures and thereby increasing the overall temperatures of the machine. Alternatively, an additional effective ventilation system may be needed.

The most efficient cooling solution investigated, also avoids the problem with high temperatures in the frame. This is the combined cooling method of forced air through the air gap and through a concentric duct between the stator surface and the frame. The results form this cooling combination can be seen in section 4.6, where it can be observed that the maximum allowable temperature in the windings and in the magnets are acceptable. It can also be seen that the temperature of the stator is high, but that the temperature in the frame is only $30°C$. This result is however thought to be slightly wrong and at least a somewhat higher temperature in the frame is expected in reality. This is because the model does not allow for heat to flow between the stator and the frame, because of the concentric duct. In reality, the stator is fastened with an insulated fastening mechanism. Some heat will flow through these, heating the frame. Although, the effect of this may be very small due to the fact that the area around the fastening mechanisms are cooled by a forced cooling fluid. In addition, radiation is neglected. Radiation may increase the temperature of the frame somewhat. However, this cooling combination is thought to yield a acceptable frame temperature in reality too. A reason for this method to be the most efficient, is thought to be because the insulation layer at the stator surface is removed. Since the insulation material stands for a significant thermal resistance. This cooling method was also taken one step further, when waved cooling fins were implemented on the stator surface. A discussion on this can be found in section 5.1.1. Additionally, this combined cooling method is thought to be a cheap and simple method to implement in reality. This is because only air is used as cooling fluid for both the air gap and the concentric duct. Forced air flow in the air gap, is a cooling method that has been used and designed for many electrical machines in the literature, which makes it possible to find inspiration for an efficient way to implement this method. The concentric duct method has also been investigated in the literature. However, some challenges with regards to the mechanical design of the machine may occur if this method is used. This should probably be further investigated before deciding the final thermal management system.

An observation that is true for all cooling combinations, is that the maximum temperature may become significantly higher than the average temperature. Although, the maximum difference between average temperature and the maximum temperature is $13.44°C$ in this thesis. However, this should be kept in mind if a thermal equivalent circuit is used without a FEM model comparison. Especially, if the temperatures becomes close the the allowable maximum. This is

because the circuit only yields the average temperatures of the nodes, and not the maximum. Alternatively, this could be solved with additional equations too. This may be extremely important in the hot spot areas of the machine.

It should also be mentioned that not all possible cooling solutions have been investigated in this thesis. This means that other cooling techniques and combinations may be more effective for the ModHVDC machine, than the ones investigated in this thesis. However, useful observations and cooling combinations that are applicable to the ModHVDC machine, has been found in this thesis. A discussion on further investigation on cooling techniques is done in section 5.1.3.

5.1.1 Waved cooling fins vs stator surface without fins

In section 4.6, the results show that the most efficient cooling technique was further improved by adding waved cooling fins on the stator surface. Resulting in a reduced max temperature in the stator by $11°C$. This makes the method very interesting for the ModHVDC machine design and should probably be investigated further in the future. This is because the method has not been optimized in any way. Which indicates that the frequency of the waves or the peak-to-peak height of the waves could be changed for an improved design, thereby lowering the temperatures even further. The cost of making the sheets of the stator waved surface, should also be taken into account. Additionally, making waved cooling fins in the stator may affect the electromagnetic design of the machine. Because of this, a coupled thermal and electromagnetic model and simulation should be performed, when further investigating this cooling solution. Although, the effects is assumed to be low, as the area of the stator that is removed may be minimal. This is however depending on the peak-to-peak distance and the frequency of the waves.

From the results of the waved cooling fin method, it could be observed a slight increase in difference between the FEM model and the thermal equivalent circuit, compared to the other cooling methods. This is thought to be because an additional layer of complexity is added to the models. Additionally, when calculating the relative increase in area for the thermal equivalent circuit, the waves were simplified to a triangular shape, as explained in section 3.7. This simplification leads to a slight difference between the FEM model and the equivalent circuit. However, the largest difference between the two methods is only $2.58°C$.

5.1.2 Optimization and impact on electromagnetic design

As mentioned in the modelling chapter, the cooling methods implemented in the models are not optimized. Additionally, the impact on the electromagnetic design is not investigated in this thesis.

For the rectangular duct that was implemented in the stator, an evaluation on the placement and size should be done for further investigations and testing. It is thought that this cooling duct will be more efficient if the duct is moved closer to the slot itself, but this may however affect the electromagnetic design in a negative way. In addition, the size of the duct should also be optimized with regards to cooling and the electromagnetic design. If this is done, it is the author's belief that this cooling method can be improved. A coupled electromagnetic and thermal simulation of the FEM models could be done in an iterative approach, to optimize this rectangular duct in the stator. An other approach to optimize this cooling method, is to investigate if it is better to implement several rectangular or circular ducts in key positions within the stator. Extra attention should then be given to the electromagnetic design.

The hollow shaft solution could also be optimized. By for example making the hollow duct in the shaft larger, more fluid could be pumped through. This could decrease the thermal resistance between the heated parts and the fluid, because of less shaft material. In addition, a higher convective heat transfer coefficient may be achieved. However, if this is done, the hollow part of the shaft becomes very large and only air would be reasonable to use as cooling fluid. Additionally, larger pumping power would be needed to get a decent fluid velocity. Because of this, it is thought that this method should not be further investigated for the direct dive ModHVDC machine. That being said, maybe this solution is applicable to a geared version of the ModHVDC machine. In a geared version, the rotor diameter would be much smaller and thereby increasing the applicability of this hollow shaft method. A smaller diameter could lead to a better coherence with the correlations used for the hollow shaft. The resulting convection coefficient for the hollow duct, is as shown in figure 3.5.1, quickly reaching the Reynolds number limits for the correlations. With a smaller duct, it is thought that higher velocities could be used before reaching the maximum Reynolds number for the correlations.

A key parameter to be optimized, is the convection coefficients. In this thesis, correlations have been used to estimate the different convection coefficients and conservative values have been implemented. This has been done in an effort to make "worst case" scenarios, but should be optimized for further studies. However, a 3D model may be needed. This is because CFD simulations could be done when a 3D model of the machine is made. From CFD, more realistic convection coefficients can be found and then optimized by designing an efficient flow path and adjusting the fluid velocities. Another approach may be to make a real life model, this may however be more costly and time consuming. Using a real life model, temperatures could be measured at the related surfaces and in the cooling fluid. These temperature could then be used to calculate an equivalent thermal resistance between the surface and the cooling fluid.

In section 3.3.9 it was mentioned that the magnet losses that are implemented, results from an unsegmented magnet design. It was also mentioned that if the magnets were to be segmented, the magnet losses could be reduced significantly. As mentioned earlier, the cooling methods that have been implemented some distance away from the magnets, have all lead to a violation of the allowable temperatures. However, this might not be the case if segmented magnets were to be used instead. Additionally, this would mean that the cooling combinations that have yielded acceptable temperatures would be even more efficient. With the segmented magnets, the possibility for only one cooling method instead of a combination, may arise. This should therefore be further investigated in the future development of a complete cooling system. In reality, it is more likely the segmented magnet design that would be used in the ModHVDC machine[2].

5.1.3 Further investigation of cooling methods

As mentioned earlier, there may be several cooling solutions that are applicable to the ModHVDC machine, that have not been investigated in this thesis. If a 3D model is made, it opens for the possibility to further investigate some of the cooling solutions in this thesis, in addition to other cooling methods that have not been investigated yet.

An interesting cooling method, could be to implement cooling rods in the rotor or stator. These rods can often be made of copper, and can be cooled on the outside of the machine. Another cooling method that can be implemented in a 3D model, is the helictical duct introduced in section 2.5.1. This may be seen as a more complete cooling solution, as the whole spiral could be modelled. A third method, that is often mentioned in the literature, is spray cooling in the end winding region. This method have proved to be very effective to cool the windings in electrical machines. However, as the stator is floating on HVDC, short circuits may occur if the spray is not perfectly controlled to only hit the windings themselves. Because of this, the spray cooling method is thought to be a poor solution for the ModHVDC machine.

For most of the methods tested in this thesis, air has been used as the cooling fluid. However, for all the duct solutions other cooling fluids, such as water or oil could also be used. Using other cooling fluids may increase the cost, but they may also increase the heat dissipation in the machine. This could be further investigated in the future, if necessary. Other correlations may then need to be either defined, by using CFD simulations or with real life models.

5.2 Equivalent thermal conductivity vs full slot model

In section 4.1 of the result chapter, the complete slot model with turns and turn insulation, and the slot model using an equivalent thermal conductivity was compared. From the results, it was shown only a small difference in temperature between the two methods. Whereas the maximum deviation was $2°C$. Indicating that it is a valid approximation to calculate an equivalent thermal conductivity, instead of modelling a complete slot with turns and turn-to-turn insulation. An interesting observation, was the simulation time for the two methods. The simulation for the complete slot model took about 10 seconds, while the equivalent thermal conductivity method only took about 3 seconds. For the models made in this thesis, the time difference has an insignificant impact. However, if larger models of the ModHVDC machine is made, this may need to be considered. If a whole 3D model is made, including all the slots with windings included, a large reduction in simulation time would be achieved with the equivalent conduction method.

Additionally, the method used to find the equivalent conduction is straight forward and simple. This means that it can easily be applied to winding designs off all shapes and sizes. The method is therefore considered reasonably accurate, although the method is lacking in other areas. One of these is that the method does not consider the randomness of the windings, meaning that straight conductors and perfect placement within the slot is assumed. In addition, the residual air pockets that may find place between copper and insulation or between each turn has been neglected. This may be easily added to the method, if an equivalent air gap for the residual air is quantified. However, a real life model may be needed to quantify an equivalent air gap.

In section 2.3.3, a layered model of the slot with windings and insulation used in other publications was presented. This layered model for the slot is also used to show the temperature distribution within the slot and windings, like the equivalent conductivity method used in this thesis. Because of this, it is assumed that similar results would be obtained for both the methods. However, the layered method makes it easier to implement the residual air pockets that might find place in the slot. This is because the method introduces a impregnation goodness factor, as explained in section 2.3.3. However, information on the insulation is then needed.

5.3 Differences between FEM model and analytical model

Throughout the thesis and for all cooling methods implemented, a FEM model and an analytical thermal equivalent model have both been made. This has made it possible to constantly confirm that there is a correspondence between the FEM model and the analytical thermal equivalent model. The results indicate that the models are made in a satisfactory and appropriate manner. However, some small differences can be observed.

For the base model comparison presented in section 4.2, it can be seen a maximum difference of $1.7°C$ between the FEM model and the thermal equivalent model. For the models where cooling combinations have been implemented, a maximum difference between the FEM model and the equivalent of $2.58°C$ can be found. Interestingly, both the maximum differences finds place in the slot/winding node. The increase in difference, when cooling methods have been implemented, is thought to be because of the fact that both the FEM model and the thermal equivalent circuit get an increased complexity. However, a difference of $2.58°C$ is acceptable. Reasons for the observed differences between the FEM models and the thermal equivalent circuits are discussed below.

First, it is important to note that FEA and an analytically made equivalent circuit is fundamentally different. Whereas FEA is a numerical approach and the equivalent circuit is solved by defining thermal resistances analytically. A small difference will come from this fact alone. Both models are however dependent on the users understanding of the topic, as the models only yields as reliable results as the reliability of the inputs. For the simple geometry in this thesis however, the FEM model is thought to give a better indication than the thermal equivalent circuit. Although, the FEM model is no exact model neither[1].

The greatest contribution to the difference between the FEM model and the thermal equivalent model, is thought to be because of how the losses are added in the two methods. When making a thermal equivalent circuit, the losses are calculated and added as constant current sources that are connected to the circuit. In this thesis, only one current source is used for each loss mechanism, which is connected directly to the respective node in the circuit. This means that all heat is injected directly at the average temperature point. While in COMSOL, the user has the possibility to add the losses as heat sources over a given area, as shown in figure 3.4.2. This means that the losses are evenly distributed over the whole slot/magnet/stator etc. To get an even better coherence between the two methods, the equivalent circuit could be split into more sub-pieces. Allowing for the heat sources to be divided and connected in such a way that the heat is more evenly distributed. However, the difference between the FEM models and the thermal equivalent circuits is very small in this thesis, implying that the approximation used for the thermal equivalent circuit is valid.

In the thermal equivalent circuit, the thermal resistances in the tangential direction of the magnet, rotor core, stator yoke and frame have been ignored. This means that only the radial heat flow is considered in these parts. While the FEM model includes both the radial and tangential heat flow. This may have lead to a small difference in temperature, however only a minor impact on the models. Although, if a larger scale model of for example one whole module of the ModHVDC machine was made, these resistances should probably be included in the circuit as well. This may also be true for a full 3D model. [1]

A simplification, that has been made when making the models, is that contact resistance has only been included between the magnet and rotor surface. This is because only values for the ceramic-metal interface, was found in the reviewed literature. In reality, contact resistance will find place where all surfaces of different parts meet. This would be between the insulation around the stator and the stator itself, between the insulation around the stator and the frame and between the slot in the stator and the slot liner within the slot. Softer materials have a smaller contact resistance, according to the literature. Because of this, most of these contact resistances are assumed small and it may be acceptable to ignore them. However, the contact resistance in the slot area should probably be implemented for further studies. This is because one of the most important temperatures finds place in the windings within the slot. In addition, this resistance may be of important magnitude as well. This is assumed to impact the temperatures somewhat, but the models made in this thesis is however assumed to yield a good estimation.

5.4 Evaluation of assumptions, limitations and simplifications

In section 1.4, the main assumptions, limitations and simplifications made for this Master's thesis was introduced. The effect of these, alongside some additional assumptions that have been made throughout the thesis, is discussed under.

The most notable simplification and limitation for this thesis, is that all models made are 2D models. A key effect from this 2D modelling, is that the axial heat flow is neglected. The literature have shown that many thermal models of electrical machines also considers the end winding region and some aspects of axial heat transfer[1]. The end winding region could therefore be given some extra attention if a 3D model of the ModHVDC machine is made[1]. However, the literature also indicates that good estimations and reliable models can also be made as 2D models.

The 2D limitation makes it hard to implement/model complete cooling methods. As a result of this, no heat exchangers or external fans and so on is investigated in this thesis. This may not be necessary at this stage, because the methods used estimates the resulting convective heat transfer coefficients that these complete cooling systems would yield. Although, the complete system must of course be made at some point in the ModHVDC project.

Additionally, the 2D limitation makes it impossible to run CFD simulations, to investigate and decide the convective heat transfer coefficients. This is commonly done in the literature when cooling methods are designed, as the correlations used introduces uncertainties in the models. Because of this, it is recommended that a 3D model of the ModHVDC machine is made in order to perform CFD studies. However, the correlations used in this thesis have been used in other models with success, although they are only estimations that introduces uncertainties. It should also be mentioned that the heat transfer coefficients used in this thesis, have been chosen with care and conservative values have been implemented in the models. Hopefully resulting in temperatures that are possible to reach in a real life model of the ModHVDC machine. Some of the correlations used in this thesis also include the heating effect of the cooling fluid. This means that the length of the cooling channel and thereby the heating of the fluid in the axial direction, is considered when calculating the convective heat transfer coefficient. Resulting in more reliable heat transfer coefficients.

One of the key assumptions in this thesis, was mentioned to be that all heat transferred to the cooling fluid or out of the modelled section, is also transferred out of the machine. In reality, an efficient and reliable cooling system must be designed to remove most of the heat transferred from the heated parts of the machine. Although all the heat would not be transferred out of the machine, leading to slightly higher temperatures in reality. However, the effects of this is assumed to be small since conservative heat transfer coefficients are chosen and the heating of the cooling fluid is taken into account in some of the models made. However, a complete cooling system that actually allows the cooling fluid to have an entrance point and an exit, must at some point be designed.

The thesis only concentrates on the thermal aspects during the modelling procedure. This indicates that the electromagnetic design may be disturbed by some of the implemented cooling methods. This has no effect on the results presented in this thesis, but should be investigated when further developing a complete cooling system for the ModHVDC machine. A coupled thermal and electromagnetic model and simulation, should therefore be done in the future.

The rotor part of the model, is stationary in all simulations. In reality this is obviously not the case. However, this is thought to have a small effect on the resulting temperatures of the models made in this thesis. This is because it may rather be seen as a ”worst case” scenario that the magnets always are standing still directly across from the slot, since these are the two main sources of generated heat in the machine. However, for the FEM model in COMSOL, it is possible to make a dynamic model where the rotor is rotating. This could be done for further investigations and quantifying the effect that the rotation has on the temperature.

In section 1.4, it was mentioned that radiation effects have been neglected throughout the thesis. However, the literature mentions that radiation effects have a higher impact if the difference in temperature between two surfaces is high. From the results presented in chapter 4, it was observed that high temperature differences between the rotor and the stator may occur. In some situations, the frame of the ModHVDC machine also becomes very warm, increasing the radiation effects to the ambient. For the cooling methods where the insulation between the stator yoke and the frame has been removed, high temperature differences can be observed between the two surfaces. This may indicate that the effects of radiation should be added to the models for more realistic and accurate temperatures. However, it is still assumed that the effects of radiation is small when there exists a forced cooling fluid between the heated surfaces.

Lastly, it has been made clear that only stationary models and simulations have been made in this thesis. This means that transients have not been investigated. The consequence of this simplification, is therefore that the models in this thesis are unable to test the overloading capabilities of the ModHVDC machine. The transients may also be of interest for the complete cooling system, as it would indicate how much cooling the machine would need at start. during ramp up and in different loading scenarios. Information on how to regulate the thermal management system and the whole machine system during load changes and overloading could also be achieved, if transient models are made.

Chapter 6

Conclusion & Further work

This is the final chapter of this Master's thesis. In this chapter, conclusions are drawn based on the results and discussions from the thesis. The chapter is concluded with a suggestion of further work, that may be necessary or useful to the continuation of the thermal management system design for the ModHVDC machine and the project.

6.1 Conclusion

The main goal for this Master's thesis, has been to investigate different cooling solutions for the ModHVDC machine by making a thermal model of the machine. In doing so, answering the question "Is the ModHVDC concept possible to realize, with regard to thermal management?". This question has been answered by making two base thermal models. One analytical thermal equivalent circuit and one numerical FEM model. Then, different cooling solutions have been implemented and tested one at a time.

From the results presented in chapter 4, it was found that no single cooling method investigated yielded sufficient thermal management to the ModHVDC machine. However, by combining two cooling methods into a combined cooling solution, several different cooling solutions yielded acceptable temperatures. Acceptable temperatures meaning below the maximum temperature of $80°C$ in the magnet and $150°C$ in the windings. The cooling solutions have been implemented with conservative convection coefficients and have not yet been optimized, yielding conservative results. Because of this, the results show that the ModHVDC concept is indeed possible to realize, with regards to the thermal management aspect.

The most efficient cooling solution, was the combination of forced air through air gap and forced air through a concentric duct between the stator surface and the frame. When implementing the concentric duct, the insulation around the stator surface is removed. This means that a large thermal resistance is removed, leading to an easier thermal management of the ModHVDC machine. The concentric duct method was also taken one step further, when waved cooling fins were made on the stator surface. The waved fins increased the area of which convection takes

place, reducing the temperatures of the machine further. This makes this cooling method and combination very interesting for the ModHVDC machine. It is therefore recommended that this method is further investigated and optimized, in the further development of the thermal management system for the ModHVDC machine. The impact on the electromagnetic design also need to be quantified for an ideal design.

In reality, it is assumed that the magnet and rotor temperature may be decreased significantly. This is because the segmented magnet design would most likely by used. The losses in the magnets would therefore be lower than what is used in this thesis, leading to a lower temperature in the magnets and thereby the rotor. This further approves that the ModHVDC design is possible to realize.

There are of course several other cooling methods that are not mentioned in this thesis, that may be effective for the ModHVDC machine. However, several cooling methods investigated in this thesis, have proven to yield acceptable temperatures in the ModHVDC machine. The most effective method only uses air as cooling fluid, which is considered to be the cheapest and easiest systems to implement in real machines.

By comparing the analytical thermal equivalent circuit and the numerical FEM model, it was seen great coherence throughout the thesis. For the base model and for all the cooling solutions implemented, a maximum difference between the two methods of only $2.58°C$ was found. Verifying that the methods used are appropriate.

Although the models made in this thesis are believed to yield a good indication on the temperatures in the ModHVDC machine, they are not complete twins of reality. The models can easily be improved to yield more realistic temperature values, if some more considerations are taken. It has been mentioned several times that the effects of radiation has been ignored. Implementing this in the models would increase the reliability. In addition, it has been mentioned that contact resistance has only been added between the magnet and the rotor core surface. Adding contact resistances around the slot, is therefore something that is recommended when further developing the thermal management system.

6.2 Further work

As mentioned in the last paragraph of the conclusion, the models could yield more realistic temperature values if the effects of radiation and more contact resistances are added. A first step for further work, could therefore be to investigate if these effects are indeed necessary for a realistic model and if so, implement them in the existing models. [1]

Since the effects of contact resistance may be significant, it would be natural to do further investigations on the topic. A method that could be used to estimate the contact resistance, is to make a simplified experimental model. This experimental model could then be applied with a resistive load, to act as heat loss. The equivalent thermal resistances of the slot and for the contact resistance in the slot area could then be found, by measuring the resulting temperatures. In doing this, the method used to model the slot with windings in this thesis, could also be compared with the experimental model as well,

A simplification in this thesis, has been that the rotor position has been stationary in the simulations. In the FEM model made in COMSOL, the rotor can be made to rotate during the simulations. This could be implemented to see the effect on the resulting temperatures of the model and quantify if the simplification is valid or not.

Additionally, the models should be expanded to transient models. Doing this would give information on how to regulate the thermal management system during different loading scenarios and possible overloading. Such transient models is needed for the most efficient design of electrical machines, as they would indicate how to regulate the system as a whole.

Before making a complete 3D model, a coupled thermo-electric simulation could be done in COMSOL. This is should be done to investigate how the implemented cooling methods have affected the electromagnetic design of the machine. In doing so, some guidelines for how the cooling methods could be implemented without affecting the electromagnetic design too much could be made. A coupled analysis could of course also be done after making a 3D model as well.

Following the guidelines, an optimized size and position for different cooling ducts could be developed. In addition, the frequency and the peak-to-peak height for the waved cooling fins on the stator surface could be optimized.

To get more realistic convective heat transfer coefficients, CFD simulations could be used instead of correlations found in the literature. By using CFD, more reliable heat transfer coefficients can be found for the specific design of the ModHVDC machine. A 3D model where the flow paths of the cooling fluids are included, is then needed. This is a recommended step in the further development of the thermal management system for the ModHVDC machine. Alternatively, a real life model with the same dimensions could be used to decide the heat transfer coefficients.

If a 3D model is made, it would be possible to investigate several other cooling techniques. Among these, the helictical duct as mentioned before. As well as unlocking further optimization of all the cooling techniques that are being considered. In addition, a more realistic and complete picture on the temperature distribution in the machine could be seen.

The cost and applicability of the investigated cooling methods must also be evaluated, before making a complete thermal management system. This point also includes mechanical challenges they may occur for different cooling solutions. Other further works, could be to investigate the cooling methods for a geared version of the ModHVDC machine. As mentioned earlier, a geared version of the ModHVDC machine could have a much smaller geometrical design. This means that other cooling methods may be more appropriate, than for the direct drive version investigated in this thesis. It is the author's belief that the hollow shaft solution may be interesting to investigate with a geared design of the ModHVDC machine.

Bibliography

[1] Kristian Husmo Lyngved. *Preceding Specialization course TET4510 at NTNU. Where relevant literature studies and usefull models were made.*

[2] Pål Keim Olsen. *Associate professor at NTNU and Supervisor for this project.* Personal communication/discussions.

[3] Solveig Samseth Strand. *Electromagnetic Design of Modular Generators for Offshore Wind Power Applications.* eng. 2020.

[4] Pål Keim Olsen. NTNU et. al. *ModHVDC Research Application. Technical report.* 2018.

[5] Pål Olsen et al. "A Transformerless generator-converter concept making feasible a 100 kV light weight offshore wind turbine: Part I - The generator". In: Sept. 2012, pp. 247–252. ISBN: 978-1-4673-0802-1. DOI: 10.1109/ECCE.2012.6342816.

[6] Magnus Borgersen. "Master's thesis; Costum Design and Analysis of Modular High Voltage DC Generator". In: (2019). DOI: http://hdl.handle.net/11250/2623213.

[7] A thesis submitted for the degree of Doctor of Philosophy The University of Edinburgh Carlos Mejuto. *Improved Lumped Parameter Thermal Modelling of Synchronous Generators.* https://www.era.lib.ed.ac.uk/bitstream/1842/4612/1/Mejuto2010.pdf. (Accessed on 10/05/2020).

[8] J. Nerg, M. Rilla, and J. Pyrhonen. "Thermal Analysis of Radial-Flux Electrical Machines With a High Power Density". In: *IEEE Transactions on Industrial Electronics* 55.10 (2008), pp. 3543–3554. DOI: 10.1109/TIE.2008.927403.

[9] Bergman, Theodore L., Lavine, Adrienne S., Incropera, Frank. *Introduction to Heat Transfer, 6th edition.* 2011.

[10] D. A. Howey, P. R. N. Childs, and A. S. Holmes. "Air-Gap Convection in Rotating Electrical Machines". In: *IEEE Transactions on Industrial Electronics* 59.3 (2012), pp. 1367–1375. DOI: 10.1109/TIE.2010.2100337.

[11] Hosain, Lokman and Bel Fdhila, Rebei. "Air-Gap Heat Transfer in Rotating Electrical Machines: A Parametric Study". In: *Energy Procedia* 142 (Aug. 2017), pp. 4176–4181. DOI: 10.1016/j.egypro.2017.12.343.

[12] M. Fénot, Y. Bertin, E. Dorignac, G Lalizel. "A review of heat transfer between concentric rotating cylinders with or without axial flow, International Journal of Thermal Sciences". In: *ISSN 1290-0729* Issue 7 (2011), pp. 1138–1155, DOI: https://doi.org/10.1016/j.ijthermalsci.2011.02.013.

[13] Maunu Kuosa, Petri Sallinen, and Jaakko Larjola. "Numerical and experimental modelling of gas flow and heat transfer in the air gap of an electric machine". In: *Journal of Thermal Science* 13 (Aug. 2004), pp. 264–278. DOI: 10.1007/s11630-004-0041-4.

[14] Verlag des Vereins Deutscher Ingenieure in Düsseldorf Germany 1988. Fünfte Erweiterte Aufgabe. *VDI-Wärmeatlas: Berechnungsblätter für den Wärmeübergang, VDI Verlag.*

[15] F. Ahmed and N. C. Kar. "Analysis of End-Winding Thermal Effects in a Totally Enclosed Fan-Cooled Induction Motor With a Die Cast Copper Rotor". In: *IEEE Transactions on Industry Applications* 53.3 (2017), pp. 3098–3109. DOI: 10.1109/TIA.2017.2648780.

[16] P. Roy et al. "Thermal Representation of Interior and Surface Mounted PMSMs for Electric Vehicle Application". In: *IECON 2019 - 45th Annual Conference of the IEEE Industrial Electronics Society.* Vol. 1. 2019, pp. 1411–1416. DOI: 10.1109/IECON.2019.8927431.

[17] D. A. Staton and A. Cavagnino. "Convection Heat Transfer and Flow Calculations Suitable for Electric Machines Thermal Models". In: *IEEE Transactions on Industrial Electronics* 55.10 (2008), pp. 3509–3516.

[18] D. J. Powell. "Modelling of high power density electrical machines for aerospace". In: Submitted as a PHD thesis at the University of Sheffield. 2004.

[19] BJORN ANDERSSON. *Lumped Parameter Thermal Modelling of Electric Machines - Analysis of an Interior Permanent Magnet Synchronous Machine for Vehicle Applications.* https://odr.chalmers.se/bitstream/20.500.12380/185192/1/185192.pdf. Master of science Thesis.

[20] L. Cuiping et al. "Analysis of 3D static temperature field of water cooling induction motor in mini electric vehicle". In: *2011 International Conference on Electrical Machines and Systems.* 2011, pp. 1–5. DOI: 10.1109/ICEMS.2011.6073618.

[21] Zabdur Rehman and Kwanjae Seong. "Three-D Numerical Thermal Analysis of Electric Motor with Cooling Jacket". In: *Energies* 11 (Jan. 2018). DOI: 10.3390/en11010092.

[22] K.M. Becker, J. Kaye. "Measurements of diabatic flow in an annulus with an inner rotating cylinder". In: *Journal of heat transfer* 84 (1962), pp. 97–105. DOI: https://doi.org/10.1115/1.3684335.

[23] F. Tachibana, S. Fukui. "Convective heat transfer of rotational and axial flow between two concentric cyllinders". In: *Bulletin of JSME 7* (1964), pp. 385–391. DOI: https://doi.org/10.1299/jsme1958.7.385.

[24] Y. Yamada. "Resistance of a flow through an annulus with an inner rotating cyllinder". In: *Bulletin of JSME 5* (1962), pp. 302–310. DOI: https://doi.org/10.1299/jsme1958.5.302.

[25] F. Tachibana, S. Fukui, H. Mistumara. "Heat transfer in an annulus with inner rotating cylinder". In: *Bulletin of JSME 3* (1960), pp. 119–123. DOI: https://doi.org/10.1299/jsme1958.3.119.

[26] H. Aoki, H. Nohira, H. Arai. "Convective heat transfer in an annulus with an inner rotating cylinder". In: *Bulletin of JSME 10* (1967), pp. 523–532. DOI: https://doi.org/10.1299/jsme1958.10.523.

[27] K.S. Ball, B. Farouk, V.C. Dixita. "An experimental study of heat transfer in a vertical annulus with a rotating inner cylinder". In: *International Communications for Heat and Mass Transfer 32* (1989), pp. 1517–1527. DOI: https://doi.org/10.1016/0017-9310(89)90073-2.

[28] S.C. Tzeng. "Heat transfer in a small gap between co-axial rotating cylinders". In: *International Communications for Heat and Mass Transfer 33* (2006), pp. 737–743. DOI: https://doi.org/10.1016/j.icheatmasstransfer.2006.02.012.

[29] D. Staton, A. Boglietti, and A. Cavagnino. "Solving the more difficult aspects of electric motor thermal analysis". In: *IEEE International Electric Machines and Drives Conference, 2003. IEMDC'03.* Vol. 2. 2003, 747–755 vol.2.

[30] Therattil Mohanan, Vidya. "Thermal Modelling of Permanent Magnent Machines Using double layer winding - Strategies for cooling of PM motors in ship propulsion pods". In: (). DOI: http://hdl.handle.net/11250/2420571.

[31] Xiaofeng Ding, Madhur Bhattacharya, and Chris Mi. "Simplified Thermal Model of PM Motors in Hybrid Vehicle Applications Taking into Account Eddy Current Loss in Magnets". In: *Journal of Asian Electric Vehicles* 8 (Jan. 2010). DOI: 10.4130/jaev.8.1337.

[32] C. Gazley. *Heat transfer characteristics of the rotational and axial flow between concentric cylinders.* Trans. ASME 1985.

[33] Yew Chuan Chong. "Thermal analysis and air flow modelling of electrical machines". PhD thesis. June 2015.

[34] T.M. Kuzay, C.J. Scott. "Turbulent Heat Transfer Studies in Annulus With Inner Cylinder Rotation". In: *ASME. J. HeatTransfer* (1977). DOI: https://doi.org/10.1115/1.3450635.

[35] D.A. Simmers, J.E.R. Coney. "A Reynolds analogy solution for the heat transfer characteristics of combined Taylor vortex and axial flows". In: *International Journal of Heat and Mass Transfer* Volume 22, Issue 5 (1979). DOI: https://doi.org/10.1016/0017-9310(79)90116-9.

[36] R.N. Childs, A.B. Turner. "Heat transfer on the surface of a cylinder rotating in an annulus at high axial and rotational Reynolds number". In: *International Heat Transfer Conference, Brighton* (1994), p. 13.18. DOI: https://doi.org/10.1615/IHTC10.990.

[37] Motor Design Ltd Dr David Staton. *Improving Motor Efficiency and Motor Miniaturisation The Role of Thermal Simulation.* http://richard.grisel.free.fr/ICEM2012/TUTORIALS/TUT3.pdf. 2012.

[38] A. Lotfi, D.Marcasa, Z. Horvath. "Modeling the Thermal Behaviour of Permanent Magnet Synchronout Motors". In: *International Journal of Engineering and Management Sciences (IJEMS)* Vol. 4 (2019). DOI: 10.21791/IJEMS.2019.1.58..

[39] H.Y. Sohn. *Fluid-Solid Reactions. 2nd edition.* 2020.

[40] Lumen physics. *Thermal Expansion of Solids and Liquids — Physics*. https://courses.lumenlearning.com/physics/chapter/13-2-thermal-expansion-of-solids-and-liquids/. (Accessed on 02/17/2021).

[41] A. Boglietti et al. "A simplified thermal model for variable speed self cooled industrial induction motor". In: *Conference Record of the 2002 IEEE Industry Applications Conference. 37th IAS Annual Meeting (Cat. No.02CH37344)*. Vol. 2. 2002, 723–730 vol.2. DOI: 10.1109/IAS.2002.1042640.

[42] A. Boglietti et al. "Evolution and Modern Approaches for Thermal Analysis of Electrical Machines". In: *IEEE Transactions on Industrial Electronics* 56.3 (2009).

[43] Incropera / DeWitt / Bergman / Lavine. *Fundamentals of Heat and Mass Transfer, 6th edition*. 2007.

[44] Göteborg Sweden 1999 J. Lindström-Report No. 11 R ISSN: 1401-6176 by the Department of Electric Power Engineering Chalmers University of Technology. *Paper D: Thermal Model of a Permanent-Magnet Motor for a Hybrid Elecric Vehicle*. 1999.

[45] Aldo Boglietti. Andrea Cavagnino. Mario Lazzari. and Michele Pastorelli. *A Simplified Thermal Model for Variable-Speed Self-Cooled Industrial Induction Motor*. https://ieeexplore.ieee.org/stamp/stamp.jsp?arnumber=1215422.

[46] Emetor. *Emetor - Glossary - Stacking factor*. https://www.emetor.com/glossary/stacking-factor/. (Accessed on 03/23/2021).

[47] China steel corporation India. *Electrical Steel Coil Product Manual*. https://www.csc.com.tw/csc_e/pd/doc/CSCI_ES_Catalog.pdf. (Accessed on 03/23/2021).

[48] JFE Steel Corporation. *ELECTRICAL STEEL SHEETS*. https://www.jfe-steel.co.jp/en/products/electrical/catalog/f1e-001.pdf. (Accessed on 03/23/2021).

[49] Gunnar Kylander, Submitted to the School of Electrical and Computer Engineering Chalmers University of Technology in partial fulfilment of the requirements for the degree of Doctor of Philosophy. *Thermal modelling of small cage induction motors*. http://webfiles.portal.chalmers.se/et/PhD/KylanderGunnarPhD.pdf.

[50] Jinxin Fan et al. "Thermal Analysis of Permanent Magnet Motor for the Electric Vehicle Application Considering Driving Duty Cycle". In: *Magnetics, IEEE Transactions on* 46 (July 2010), pp. 2493 –2496. DOI: 10.1109/TMAG.2010.2042043.

[51] P. Liang et al. "Equivalent stator slot model of temperature field for high torque-density permanent magnet synchronous in-wheel motor". In: *2014 17th International Conference on Electrical Machines and Systems (ICEMS)*. 2014, pp. 3457–3462. DOI: 10.1109/ICEMS.2014.7014088.

[52] A. Boglietti, A. Cavagnino, and D. Staton. "Determination of Critical Parameters in Electrical Machine Thermal Models". In: *IEEE Transactions on Industry Applications* 44.4 (2008), pp. 1150–1159. DOI: 10.1109/TIA.2008.926233.

[53] F. Hoffmann, B. Jux, and M. Doppelbauer. "Thermal Modeling of the Stator Slot in Electrical Machines Using an Extended Layer Approach". In: *IECON 2019 - 45th Annual*

Conference of the IEEE Industrial Electronics Society. Vol. 1. 2019, pp. 1405–1410. DOI: 10.1109/IECON.2019.8927002.

[54] S. Nategh. "PhD Thesis: Thermal Analysis and Management of High-Performance Electrical Machines". In: 2013.

[55] Motor Design Ltd David Staton. *Thermal analysis of electric motors & Generators*. Delivered as PDF from the course ELK 22 at NTNU. 2007.

[56] Amal Zeaiter. "Thermal Modeling and Cooling of Electric Motors : Application to the Propulsion of Hybrid Aircraft". Submitted as a PhD thesis. PhD thesis. Oct. 2020.

[57] S. K. Chowdhury and P. K. Baski. "A simple lumped parameter thermal model for electrical machine of TEFC design". In: *2010 Joint International Conference on Power Electronics, Drives and Energy Systems 2010 Power India*. 2010, pp. 1–7. DOI: 10.1109/PEDES.2010.5712385.

[58] Deborah Chung. "Applied Materials Science : Applications of Engineering Materials in Structural, Electronics, Thermal, and Other Industries / D.D.L. Chung". In: (Jan. 2001). DOI: 10.1201/9781420040975.

[59] A.F. Mills. *Heat Transfer*. Englewood Cliffs,NJ:Pretice Hall, 1999.

[60] V. Gnielski. "New equations for heat and mass transfer in turbulent pipe and channel flow, Int. Chemical Engineering, 16". In: (1976), pp. 359–368.

[61] Y. Gai et al. "Numerical and Experimental Calculation of CHTC in an Oil-Based Shaft Cooling System for a High-Speed High-Power PMSM". In: *IEEE Transactions on Industrial Electronics* 67.6 (2020), pp. 4371–4380. DOI: 10.1109/TIE.2019.2922938.

[62] Y. Bertin et al. "Thermal behavior of an electrical motor through a reduced model". In: *IEEE Transactions on Energy Conversion* 15.2 (2000), pp. 129–134. DOI: 10.1109/60.866989.

[63] Y. Gai et al. "Cooling of Automotive Traction Motors: Schemes, Examples, and Computation Methods". In: *IEEE Transactions on Industrial Electronics* 66.3 (2019), pp. 1681–1692. DOI: 10.1109/TIE.2018.2835397.

[64] Y. Gai et al. "Shaft cooling and the influence on the electromagnetic performance of traction motors". In: *2017 IEEE International Electric Machines and Drives Conference (IEMDC)*. 2017, pp. 1–6. DOI: 10.1109/IEMDC.2017.8002307.

[65] Y. Gai et al. "On the Measurement and Modeling of the Heat Transfer Coefficient of a Hollow-Shaft Rotary Cooling System for a Traction Motor". In: *IEEE Transactions on Industry Applications* 54.6 (2018), pp. 5978–5987. DOI: 10.1109/TIA.2018.2860558.

[66] Y. Gai et al. "Power Losses and Thermal Analysis of a Hollow-Shaft Rotor Cooling System". In: *2019 22nd International Conference on Electrical Machines and Systems (ICEMS)*. 2019, pp. 1–6. DOI: 10.1109/ICEMS.2019.8922026.

[67] A. M. EL-Refaie et al. "Advanced High-Power-Density Interior Permanent Magnet Motor for Traction Applications". In: *IEEE Transactions on Industry Applications* 50.5 (2014), pp. 3235–3248. DOI: 10.1109/TIA.2014.2305804.

[68] S. Seghir-Ouali et al. “Convective heat transfer inside a rotating cylinder with an axial air flow”. In: *International Journal of Thermal Sciences* 45.12 (2006), pp. 1166–1178. ISSN: 1290-0729. DOI: https://doi.org/10.1016/j.ijthermalsci.2006.01.017. URL: https://www.sciencedirect.com/science/article/pii/S1290072906000408.

[69] E. Kuffel, W. Zaengl, J. Kuffel,. *High Voltage Engineering Fundamentals*. 2000.

[70] Engineers Edge. *Viscosity of Air, Dynamic and Kinematic — Engineers Edge — www.engineersedge.com*. https://www.engineersedge.com/physics/viscosity_of_air_dynamic_and_kinematic_14483.htm.

[71] D. Kowal et al. “The Effect of the Electrical Steel Properties on the Temperature Distribution in Direct-Drive PM Synchronous Generators for 5 MW Wind Turbines”. In: *IEEE Transactions on Magnetics* 49.10 (2013), pp. 5371–5377. DOI: 10.1109/TMAG.2013.2260553.

[72] Bunting E-Magnets. *Characteristics of Neodymium NdFeB Magnets — Bunting - eMagnets*. https://e-magnetsuk.com/introduction-to-neodymium-magnets/characteristics-of-ndfeb-magnets/. (Accessed on 03/30/2021).

[73] Chhaperia. *Muscovite Mica Tapes,Mica Tapes 950 Deg C,Fires M,CM 25 G—Chhaperia Group*. https://www.micagroup.net/en/mica-tapes/resin-rich-mica-tape1. (Accessed on 10/23/2020).

[74] M. Popescu et al. “Modern Heat Extraction Systems for Power Traction Machines—A Review”. In: *IEEE Transactions on Industry Applications* 52.3 (2016), pp. 2167–2175. DOI: 10.1109/TIA.2016.2518132.

Appendix A

Literature extras

A suggestion of the relation between the equivalent thermal conductivity of the slot and the fill factor of the stator slot form [49]. The relation was plotted in [49] and the graph is displayed as figure A.0.1.

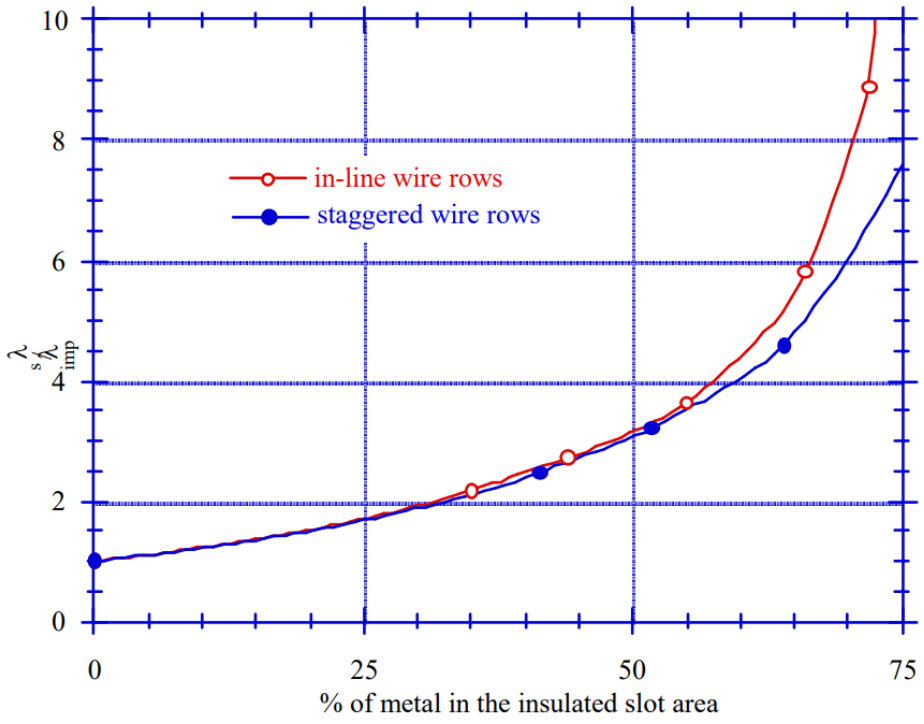

Figure A.0.1: *Relation between the equivalent thermal conductivity of the slot and the fill factor. Figure copied from [49]*

In [69], the breakdown voltage of air at $20°C$ is plotted as a function of the pressure spacing product. The figure is shown as figure A.0.2 and used to compare the Paschens law equation with this Paschens curve in section 3.7. [69]

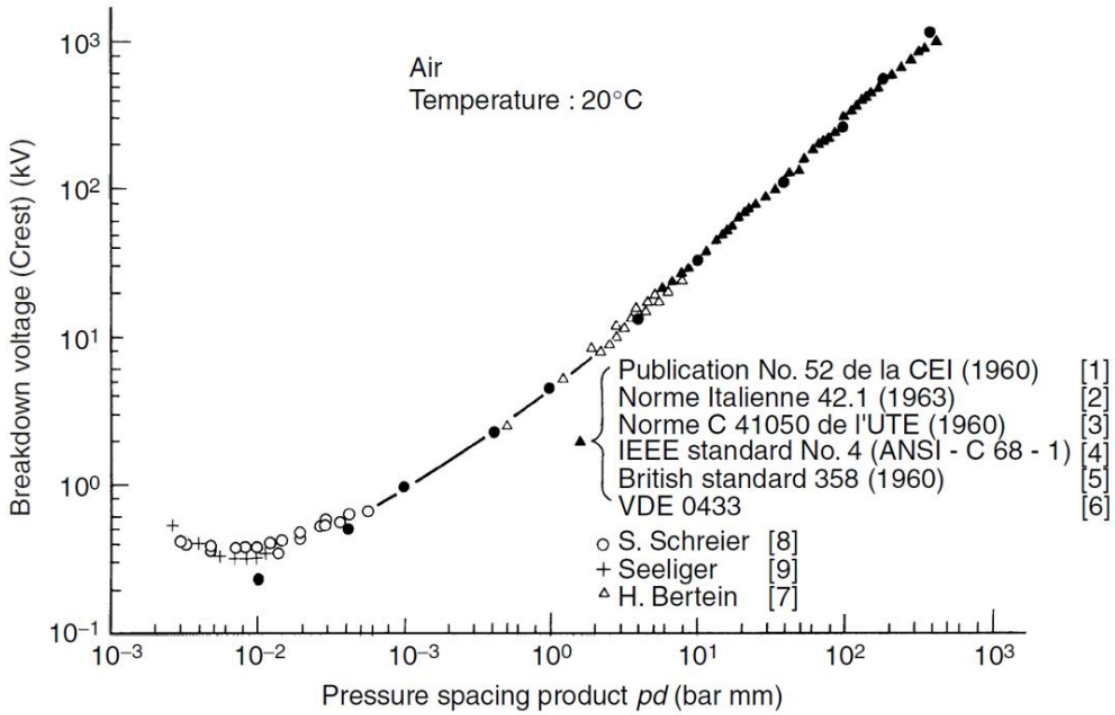

Figure A.0.2: *Paschens curve for air at $20°C$. Plot taken from [69].*

Figure A.0.3 illustrates the use of round cooling ducts in both the stator and in the rotor. The figure is taken from [33] and used as an example in this thesis.

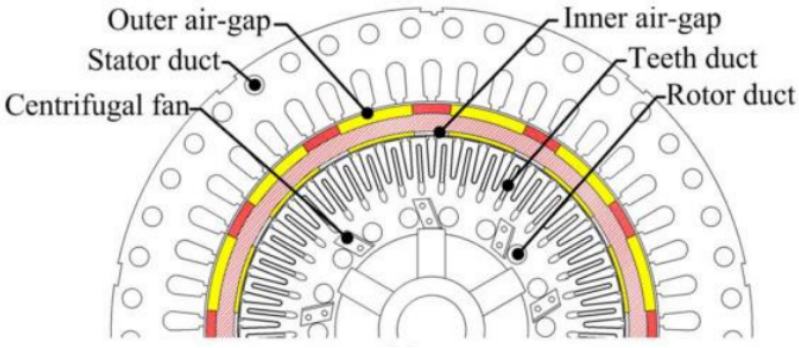

Figure A.0.3: *Figure illustrating the use of round cooling ducts. Here, round ducts are used both in the stator and in the rotor. Figure is taken from [33].*

Equation A.0.1 represents how a thermal resistance due to conduction can be calculated. Where l is the length, A is the area and k is the conduction coefficient of the material. [1, 7]

$$R = \frac{l}{A \cdot k} \tag{A.0.1}$$

Equation A.0.2 shows how a thermal resistance due to convection can be calculated. Where h is the convective heat transfer coefficient. [1, 43]

$$R = \frac{1}{h \cdot A} \tag{A.0.2}$$

Appendix B

Reference machine

This appendix was originally made in the preceding specialization course[1] and have been added as a direct copy.

In every thermal model, machine geometry is needed to calculate the thermal resistances. Because of this, a reference machine is needed if meaningful results are desirable. Solveig Samseth Strand is one of the students who have worked on the ModHVDC project in previous years and has designed two versions of the ModHVDC generator. In her master's thesis, cited as [3], one geared version and one direct drive version of the ModHVDC generator was designed. As a reference machine, it has been decided to use the direct drive machine designed by Solveig. In this appendix the geometry, electrical parameters, losses and material properties for this reference machine is presented.

Geometry & electrical parameters of the ModHVDC

Table B.0.1 shows the geometry of the machine in terms of parameter, value, symbol and source. Most values have been taken from Solveig, but some have been calculated, assumed or interpreted from other sources.

Table B.0.1: *Geometry & electrical parameters of a direct drive modHVDC generator.*

Parameter	Value	Symbol	Source
Frame thickness	100 [mm]	d_{fr}	Assumed
Outer insulation layer height	5.00 [mm]	d_{ins_o}	Solveig Strand Samseth [3]
Outer stator diameter	7478 [mm]	D_o	Solveig Strand Samseth [3]
Stator yoke height	99.0 [mm]	d_{sy}	Calculated, equation B.0.2
Stator slot depth/teeth height	118 [mm]	d_{ss}	Solveig Strand Samseth [3]
Stator slot width	56.7 [mm]	b_{ss}	Solveig Strand Samseth [3]
Stator tooth width	58.4 [mm]	b_{ss}	Solveig Strand Samseth [3]
Stator slot insulation thickness	1.33 [mm]	b_{is}	Solveig Strand Samseth [3]
Stator slot fill factor	0.763	F_{ss}	Solveig Strand Samseth [3]
Winding width	54.04 [mm]	b_{cu}	Calculated, equation B.0.3
Winding height	115.34 [mm]	d_{cu}	Calculated, equation B.0.4
Stator teeth width	58 [mm]	b_{st}	Solveig Strand Samseth [3]
Inner insulation layer height	5.00 [mm]	d_{ins_i}	Solveig Strand Samseth [3]
Inner stator Diameter	7044.0 [mm]	D_i	Calculated, equation B.0.1
Air gap length	10 [mm]	d_{ag}	Solveig Strand Samseth [3]
Magnet thickness	30 [mm]	d_{mag}	Solveig Strand Samseth [3]
Magnet angle	126°	α_m	Solveig Strand Samseth [3]
Magnet relative length	0.7	l_{mag_r}	Solveig Strand Samseth [3]
Magnet circumference length	96.7 [mm]	ω_m	Solveig Strand Samseth [3]
Rotor core diameter	6954 [mm]	D_{rc}	Solveig Strand Samseth [3]
Shaft diameter	6754 [mm]	D_{sh}	Solveig Strand Samseth [3]
Machine length	1500 [mm]	l_{ma}	Solveig Strand Samseth [3]
Number of poles	160	N_{pol}	Solveig Strand Samseth [3]
Number of stator slots	192	Q_s	Solveig Strand Samseth [3]
Number of segments	16	N_{seg}	Solveig Strand Samseth [3]
Design line-to-line voltage	74 [kV]	V_{ll}	Solveig Strand Samseth [3]
Design DC voltage	100 [kV]	V_{DC}	Solveig Strand Samseth [3]
Safety factor for slot insulation	1.5	K_s	Solveig Strand Samseth [3]

Figure B.0.1 illustrates the geometry parameters of the ModHVDC machine. The figure includes most of the geometry parameters used for the calculation of the thermal model in later sections. The figure is made to let the reader have an overview of the parameters stated in table B.0.1. Keep in mind that the machine is cylindrical and not square as the figure might suggest. The sizes are not to scale.

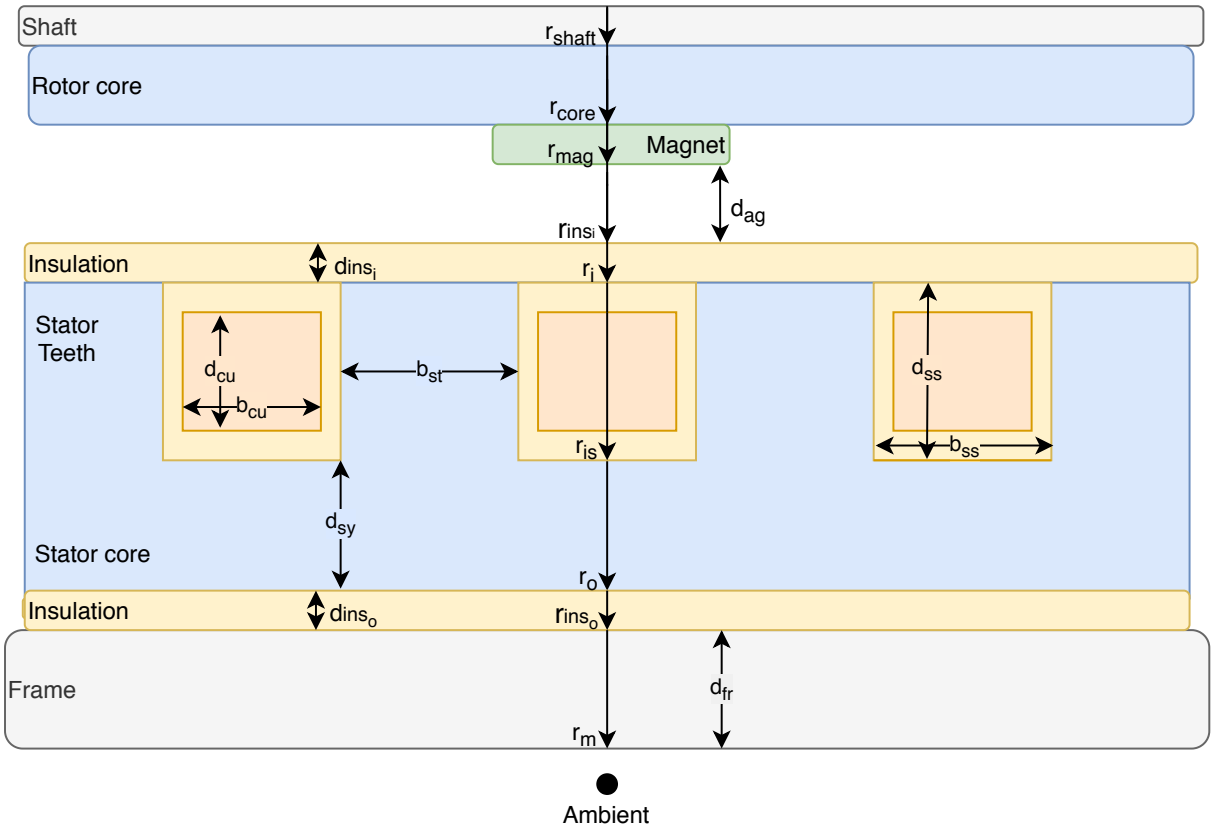

Figure B.0.1: *Illustration of geometry parameters of the ModHVDC machine. Keep in mind that the machine is cylindrical and not square as the figure might suggest.*

From this figure and the given values in table B.0.1, some key parameters are calculated. The inner stator diameter is calculated as shown in equation B.0.1. From the result, the stator yoke height is calculated from equation B.0.2. Knowing the stator slot insulation thickness and the thickness of the slot itself, the corresponding winding thickness is calculated as shown in equation B.0.3. Following the same logic, the winding height is calculated as shown in equation B.0.4. All parameters in figure B.0.1 not yet specified, have been calculated. Table B.0.4 attached in appendix B shows the results.

$$D_i = D_{rc} + 2 \cdot d_{mag} + 2 \cdot d_{ag} + 2 \cdot d_{ins_i} \tag{B.0.1}$$

$$d_{sy} = \frac{D_o}{2} - \frac{D_i + 2 \cdot d_{ss}}{2} \tag{B.0.2}$$

$$b_{cu} = b_{ss} - b_{is} \cdot 2 \tag{B.0.3}$$

$$d_{cu} = d_{ss} - b_{is} \cdot 2 \tag{B.0.4}$$

Losses in reference machine

The total losses of the reference machine has been calculated by Solveig in [3]. Table B.0.2 shows the copper losses in the windings in addition to the eddy-current losses and hysteresis losses for the stator. These losses are further used to calculate the loss values that are implemented in the 2D thermal model. However, Solveig does not give any numbers for the losses in the magnets.

Table B.0.2: *Losses in the machine windings and stator. Values obtained from [3].*

Parameter	Losses [W]
Copper losses, P_{cu}	435 500
Total core losses, P_c	55 537
Magnet losses, P_{mag}	-

Materials used in the machine

The material properties of the machine is important to define, before a thermal analysis can be done. Table B.0.3 displays the materials used for the different parts of the machine. In addition, the frame is assumed to be made of aluminum and all insulation made of mica-glass backed tape. The relevant material properties for the materials can be found in appendix B. These properties are taken from the material library available in COMSOL multiphysics, as this software is used to make a FEM model.

Table B.0.3: *Material used for the different parts of the reference machine. [3]*

Part	Material used
Rotor core	Steel (M250-5A)
Permanent magnets	NdFeB
Air gap	Air
Stator	Steel (M250-5A)
Windings	Copper
Segment insulation	Mica-glass backed tape
Slot insulation	Mica-glass backed tape

Table B.0.4 shows the calculated radius throughout the ModHVDC machine.

Table B.0.4: *Calculated radius of the reference machine. Calculations are done from previous calculated or known geometric values. (see section B) The parameters are displayed in figure B.0.1.*

Parameter	Value	Symbol	Calculation
Shaft radius	3377 [mm]	r_{shaft}	$D_{sh}/2$
Rotor outer core radius	3477 [mm]	r_{core}	$D_{rc}/2$
Magnet outer radius	3507 [mm]	r_{mag}	$r_{core} + d_{mag}$
Inner insulation radius	3517 [mm]	r_{ins_i}	$r_{mag} + d_{ag}$
Inner stator radius	3522 [mm]	r_i	$D_i/2$
Inner slot radius	3640 [mm]	r_{is}	$r_i + d_{ss}$
Outer stator radius	3739.00 [mm]	r_o	$D_o/2$
Outer insulation radius	3744 [mm]	r_{ins_o}	$r_o + d_i ns_o$
Outer machine radius	3844 [mm]	r_m	$r_{ins_o} + d_{fr}$

Material properties in the Reference machine

Table B.0.5 shows the selected properties for air at atmospheric pressure for different temperatures. The values have been taken from [70]. Table B.0.6 through table B.0.10 presents the relevant material properties of the Permanent magnet (NdFeB), electrical steel, copper, aluminium and Mica-glass backed tape, respectively. In addition, the density of air between $15 - 30°C$ is about $\rho_{air} = 1.2kg/m^3$.[70]

Table B.0.5: *Properties of air at atmospheric pressure for different temperatures. Table gathered from [70].*

Temperature [°C]	Specific heat [J/kg·K]	Dynamic viscosity, μ [kg/m·s]	Kinematic viscosity, v [m^2/s]	Prandtl number	Thermal conductivity [W/m·K]
20	1007	$1.825 \cdot 10^{-5}$	$1.516 \cdot 10^{-5}$	0.7309	0.02514
30	1007	$1.8724 \cdot 10^{-5}$	$1.608 \cdot 10^{-5}$	0.7282	0.02588
40	1007	$1.916 \cdot 10^{-5}$	$1.702 \cdot 10^{-5}$	0.7255	0.02662
50	1007	$1.963 \cdot 10^{-5}$	$1.798 \cdot 10^{-5}$	0.7228	0.02735
60	1007	$2.008 \cdot 10^{-5}$	$1.896 \cdot 10^{-5}$	0.7202	0.02808
80	1008	$2.096 \cdot 10^{-5}$	$2.097 \cdot 10^{-5}$	0.7154	0.02953

Table B.0.6: *Material properties for Permanent magnets (NdFeB) [3, 71, 72].*

Parameter	Value
Electrical conductivity	$6.25 \cdot 10^5$
Maximum Temperature	$80°C$
Thermal conductivity	7.7 W/mK
Specific heat capacity	500 J/kgK

Table B.0.7: *Material properties of Iron. Values are taken from the material library available in COMSOL.*

Parameter	Value
Thermal conductivity	76.2 W/mK
Heat capacity	440 J/kgK
Electrical conductivity	$1.12 \cdot 10^7$ S/m
Density	7870 kg/m^3

Table B.0.8: *Material properties of Copper. Values are taken from the material library available in COMSOL. Maximum temperature is taken from [3].*

Parameter	Value
Thermal conductivity	400 W/mK
Heat capacity	385 J/kgK
Maximum temperature	$150°C$
Electrical conductivity	$5.998 \cdot 10^7$ S/m
Density	8960 kg/m^3

Table B.0.9: *Material properties of Aluminum.Values are taken from the material library available in COMSOL.*

Parameter	Value
Thermal conductivity	238 W/mK
Heat capacity	900 J/kgK
Density	2700 kg/m^3

Table B.0.10: *Material properties of Mica-glass backed tape [73].*

Parameter	Value
Thermal conductivity	0.20-0.30 W/mK

Appendix C

Material properties extended

In this appendix, additional material properties are displayed. These material properties are used in for example cooling methods in the thesis and are referred to when necessary.

Table C.0.1: *Material properties of water. Values are given as an average between 0°C and 40 °C. Values are taken from [74].*

Parameter	Value
Thermal conductivity	0.56 W/mK
Density	1000 kg/m^3
Kinematic viscosity	$1.78{\cdot}10^{-6}$ m^2/s
Specific heat	$4.217{\cdot}10^3$ J/kgK

Table C.0.2: *Material properties of Silicone KF96 oil. The values are given as an average between 0°C and 40 °C. Values are taken from [74].*

Parameter	Value
Thermal conductivity	0.15 W/mK
Density	1000 kg/m^3
Kinematic viscosity	$8{\cdot}10^{-5}$ m^2/s
Specific heat	$1.75{\cdot}10^3$ J/kgK

An other important factor may be the Prandtl number. The prandtl number can be calculated as shown by equation C.0.1. In the equation μ is the dynamic viscosity, ν the kinematic viscosity, ρ the density, k the thermal conductivity and c_p the specific heat. [61]

$$P_r = \frac{\mu \cdot c_p}{k} = \frac{\rho \cdot \nu \cdot c_p}{k} \tag{C.0.1}$$

Appendix D

Modelling extras

In this appendix, additional information or figures describing the models made in this thesis can be found. All figures are referred to when necessary.

Figure D.0.1 illustrates a combined hollow shaft and a rectangular duct in the stator cooling method implemented in the base FEM thermal model.

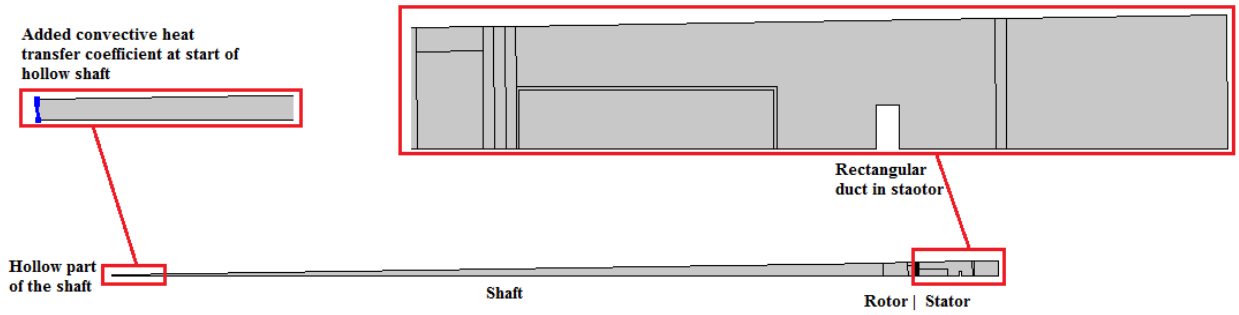

Figure D.0.1: *Illustration of how a hollow shaft and a rectangular duct is implemented in the base FEM model.*

Figure D.0.2 shows the resulting equivalent circuit for a cooling situation where hollow shaft cooling and rectangular duct cooling in the stator is implemented. In addition, the constant temperature in the air gap is removed.

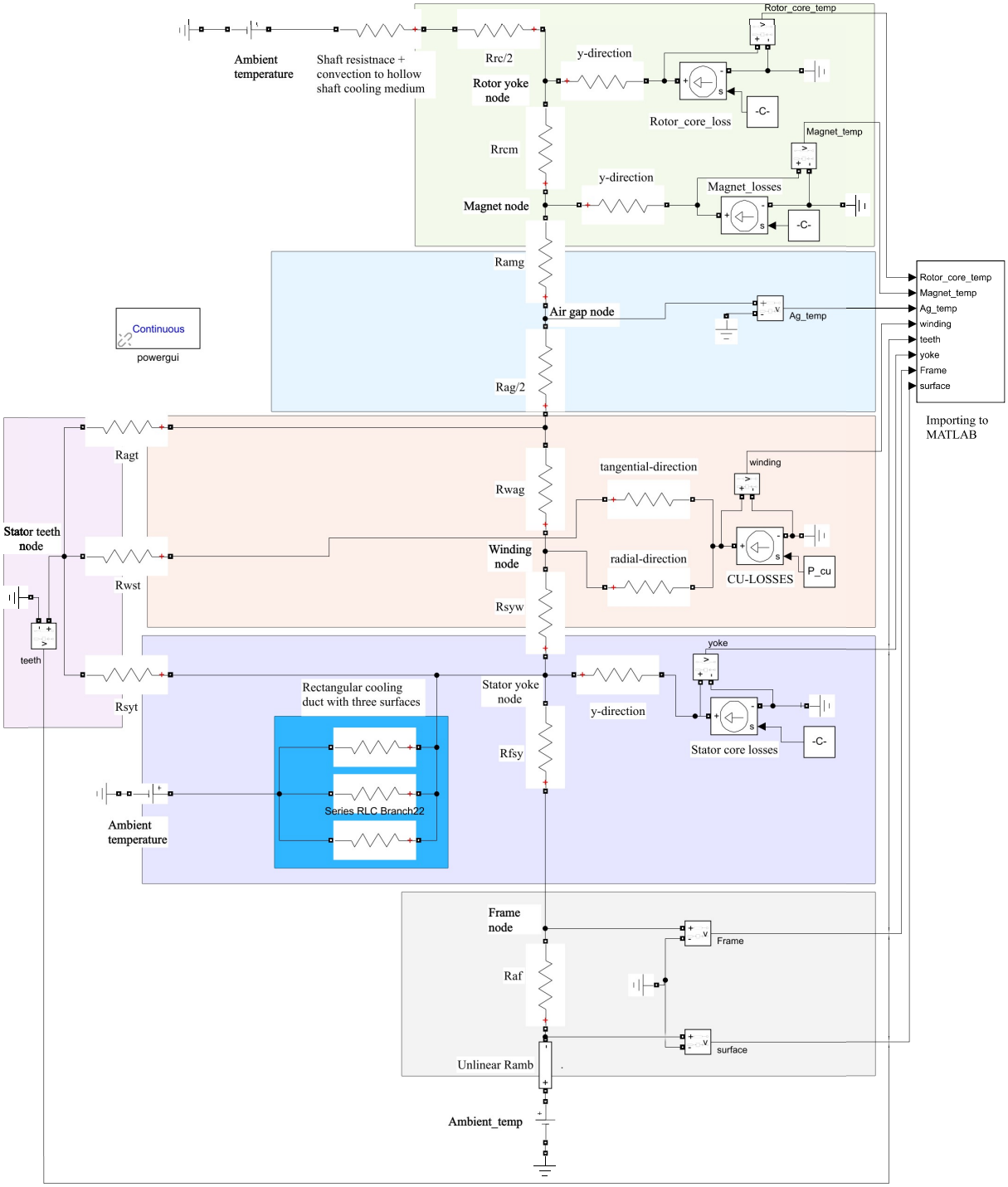

Figure D.0.2: *Resulting equivalent circuit for a cooling situation where hollow shaft cooling and rectangular duct cooling in the stator is implemented. In addition, the constant temperature in the air gap is removed.*

Figure D.0.3 displays the thermal equivalent circuit when forced air in the air gap and rectangular duct cooling is implemented.

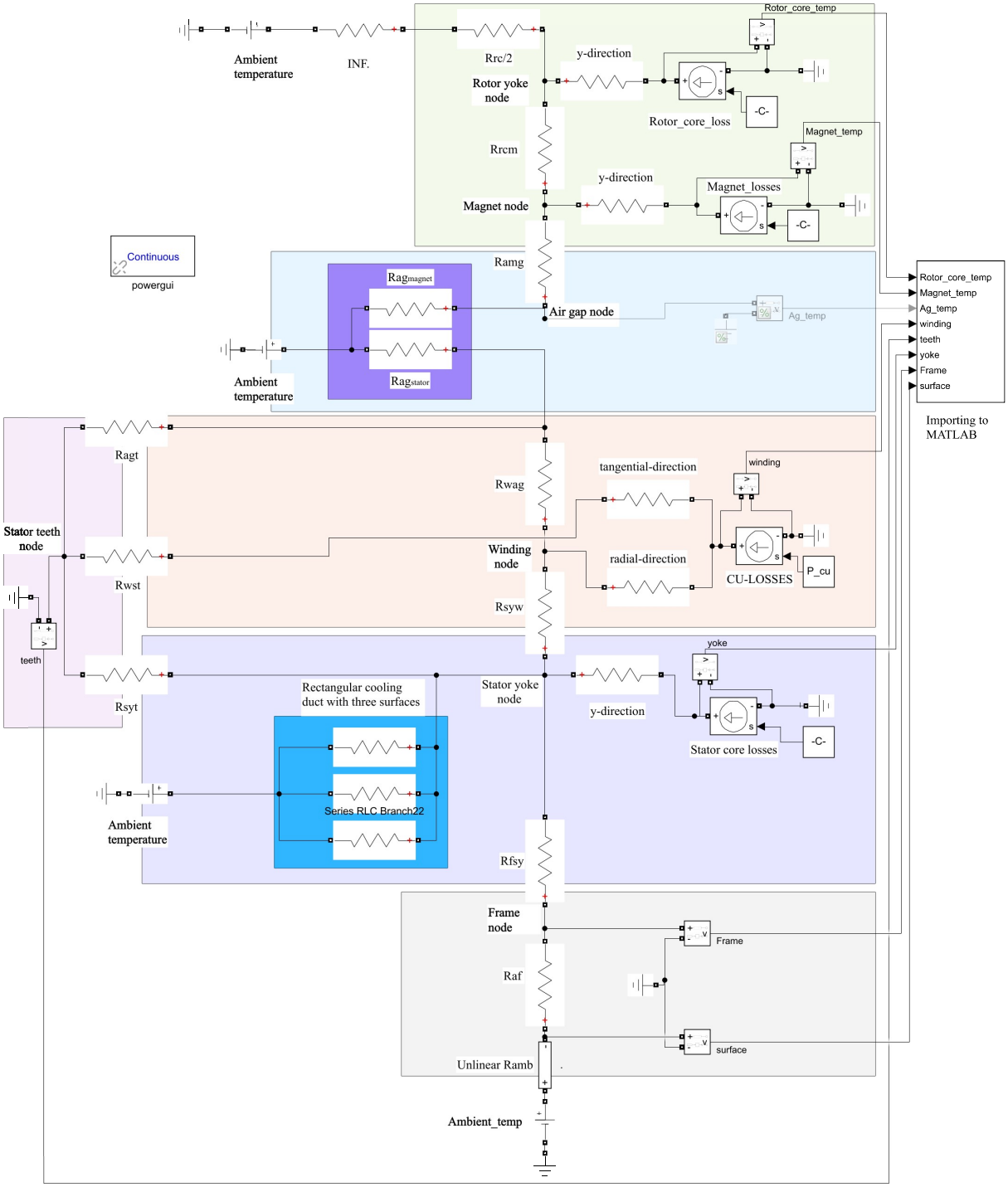

Figure D.0.3: *The resulting equivalent circuit for the combined cooling method of forced air gap cooling and rectangular duct cooling in stator.*

Figure D.0.4 illustrates the resulting thermal equivalent circuit when a rectangular duct in the stator and a concentric duct between the stator surface and the frame is implemented. For this specific cooling situation, air is used as the cooling fluid.

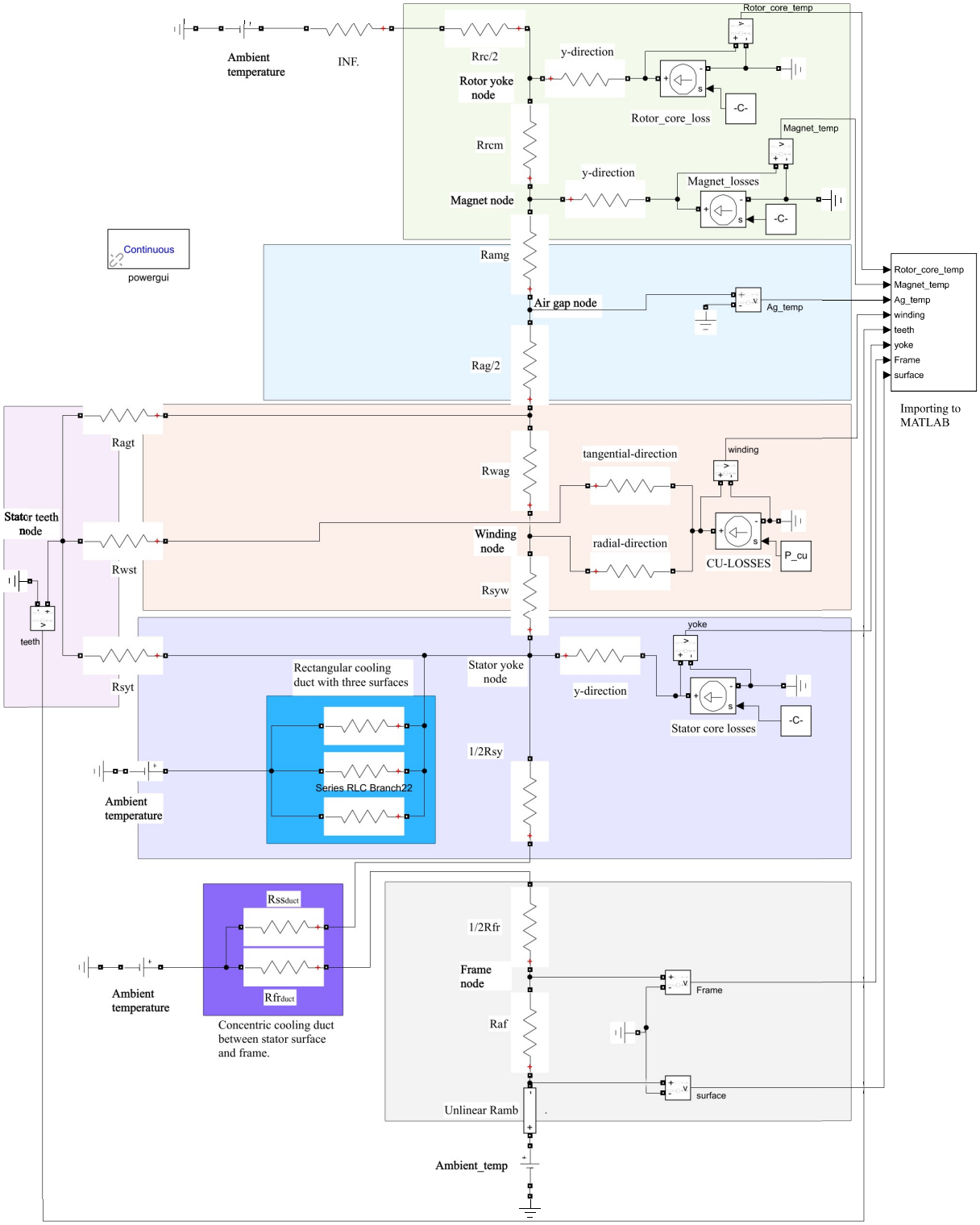

Figure D.0.4: *Equivalent circuit for a cooling combination of rectangular duct in stator and a concentric duct between stator surface and frame.*

Figure D.0.5 shows the resulting thermal equivalent circuit for a cooling combination of forced air in the air gap and a air cooled concentric duct between the stator surface and frame.

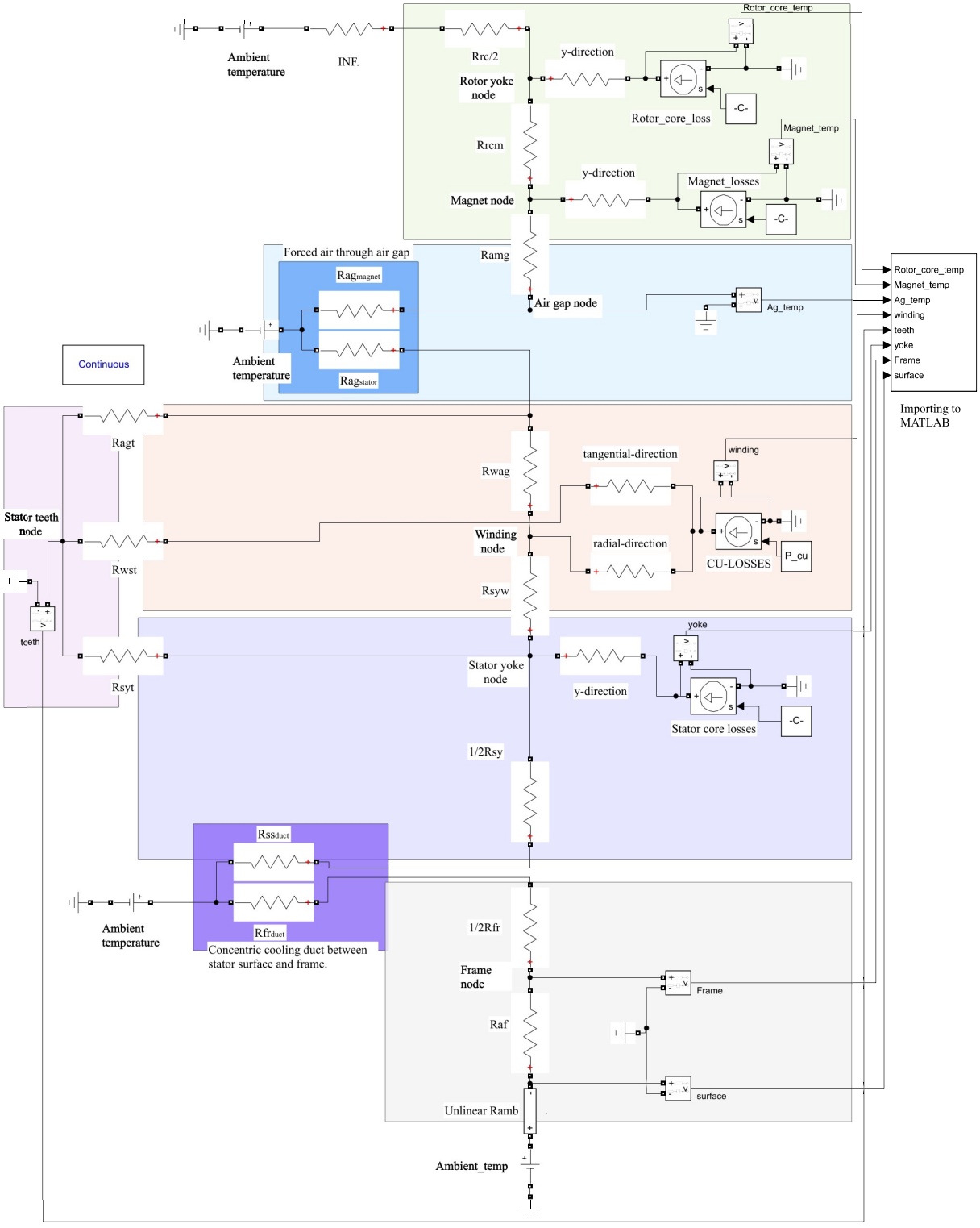

Figure D.0.5: *Equivalent circuit for a cooling combination of air cooled air gap and air cooled concentric duct at stator surface.*

Appendix E

MATLAB-scripts

This appendix is made to attache the different MATLAB scripts that have been used for calculations throughout the thesis.

Convection coefficients in the rotor-stator air gap

The MATLAB-script used to calculate and illustrate the convection coefficients in the rotor stator air gap is shown below.

```
clear all
clc
close all
%Radiuses in meters:
r_insi=3517/1000;
r_mag=3507/1000;
L=1.5; %length of machine


%% Constants for air in air gap + nominal speed of modHVDC machine

rho=1.2; %density of air between 15-25 degrees.
my=1.825*10^-5; %Dynamic viscosity of air at 20 degrees
k_air=0.0251; %Thermal conductivity of air at 20 degree
v_i=1.516*10^-5;% kinematic viscosity at 20 degrees.
% Machine rotational speed
w=10*2*pi/60; %Nominal rotational speed in rad/s (from 10 rpm)

delta=0.01; %air gap length

%%Geometric functions
eta=r_mag/r_insi %radial Cylindrical gap aspect ratio
Gamma=L/(r_insi-r_mag) %axial cylindrical gap aspect ratio
e=r_insi-r_mag; % gap thickness (same as d_ag).
ratio=e/r_mag
```

```
D_h=e; %hydraulic diameter
s=e;
%dimentionless numbers:

T_a=(rho^2*w^2*r_mag*delta^3)/(my^2) %calculating Taylor number
T_a_a=(rho*w*r_mag^0.5*s^1.5)/my % from both source
T_a_a_a=(w^2*r_mag*(D_h)^3)/(v_i^2) % from rotation source
P_r=0.73; %Prandtl number of air between 20-40 degrees
%% Only axial air flow:
for v=1:20
R_e(v)=(rho*v*D_h)/my; %Reynolds number based on the axial speed of air "v".

N_u_axial_only_1(v)=0.023*P_r^(1/3)*R_e(v)^0.8;
f_c(v)=1/((1.82*log10(R_e(v))-1.64)^2);
N_u_axial_only_2(v)=(f_c(v)/8*(R_e(v)-1000)*P_r)/(1+12.7*sqrt(f_c(v)/8)*(P_r
    ^(2/3)-1));
N_u_axial_only_avg(v)=(N_u_axial_only_1(v)+N_u_axial_only_2(v))/2;
h_c_axial_only_avg(v)=N_u_axial_only_avg(v)*(k_air/D_h);

end
figure
plot(1:v,h_c_axial_only_avg)
grid
legend('Convection coefficient as a function of axial airflow velocity','
    Interpreter','latex','Location','northwest')
xlabel('Axial air velocity [m/s]','Interpreter','latex')
ylabel('Convection coefficient [$W/m^2/^{\circ}C$]','Interpreter','latex')
%% Only rotation
%Based on Gamma, eta, ratio and T_a, the correlation that fits the best is
%bjoklund and kays. OR useing AOKI that does not need these geometric
%relations.

%Bjorklund and kays:
for O=1:10
w=O*2*pi/60; %calculating rad/s from rpm (O)
T_a(O)=(rho^2*w^2*r_mag*delta^3)/my^2;

N_u_rot_only_1(O)=0.35*T_a(O)^0.25;
h_c_rot_only(O)=N_u_rot_only_1(O)*(k_air/D_h);
end

%Aoki:
for O=1:10
w=O*2*pi/60; %calculating rad/s from rpm (O)
T_a_3(O)=(rho^2*w^2*r_mag*delta^3)/my^2;

N_u_rot_only_3(O)=0.44*T_a_3(O)^0.25*P_r^(0.3);
h_c_rot_only_3(O)=N_u_rot_only_3(O)*(k_air/D_h);
end
```

```
73
74 %Bekker and kaye:
75 for O=1:10
76 w=O*2*pi/60; %calculating rad/s from rpm (O)
77 T_a_4(O)=(rho^2*w^2*r_mag*delta^3)/my^2;
78
79 if T_a_4(O)<1700
80     N_u_rot_only_4(O)=2;
81 elseif T_a_4(O)<10^4
82     N_u_rot_only_4(O)=0.128*T_a_4(O)^0.367;
83 elseif T_a_4(O)>10^4
84     N_u_rot_only_4(O)=0.409*T_a_4(O)^0.241;
85 end
86
87 h_c_rot_only_4(O)=N_u_rot_only_4(O)*(k_air/D_h);
88 end
89
90 % THE METHOD SHOWN BY EQUATION 2.1.10.
91 for O=1:10
92 w(O)=O*2*pi*r_mag/60; % velocity from RPM to m/s.
93 R_e_2(O)=rho*w(O)*e/my;
94 T_a_2(O)=R_e_2(O)*sqrt(D_h/r_mag);
95
96 if T_a_2(O)<41
97     N_u_rot_only_2(O)=2;
98 elseif T_a_2(O)<100
99     N_u_rot_only_2(O)=0.212*T_a_2(O)^0.63*P_r^0.27;
100 elseif T_a>100
101     N_u_rot_only_2(O)=0.386*T_a_2(O)^0.5*P_r^0.27;
102 end
103
104 h_c_rot_only_2(O)=N_u_rot_only_2(O)*(k_air/D_h);
105
106 end
107 h_c_rot_only_avg=(h_c_rot_only_3+h_c_rot_only+h_c_rot_only_4)/3;
108 figure
109 hold on
110 grid
111 plot(1:10,h_c_rot_only,'LineWidth',1.3)
112 plot(1:10,h_c_rot_only_3,'LineWidth',1.3)
113 plot(1:10,h_c_rot_only_4,'LineWidth',1.3)
114 plot(1:10,h_c_rot_only_avg,'LineWidth',1.3)
115 legend('Bjorklund and Kays','Aoki et al.','Becker and Kaye','Average','
    Interpreter','latex','Location','northwest')
116 xlabel('Rotor speed [RPM] ','Interpreter','latex')
117 ylabel('Convection coefficient [$W/m^2/^{\circ}C$]','Interpreter','latex')
118 hold off
119
120 %% Gazley et al:
```

```
for v=1:15
O=10; %rpm
w=O*2*pi/60;% rad/s from rpm
v_axial=v;
V_e(v)=sqrt(((w*r_mag)/(2))^2+v_axial^2);
R_e_c(v)=(rho*D_h*V_e(v))/my;
N_u_both_3(v)=0.03*R_e_c(v)^0.8;
h_c_both_3(v)=N_u_both_3(v)*(k_air/D_h);
end
figure
plot(1:length(V_e),h_c_both_3,'LineWidth',1.3)
grid
legend('Convection coefficient using Gazley et al. correlation','Interpreter','
    latex','Location','northwest')
xlabel('Axial air flow velocity [m/s]','Interpreter','latex')
ylabel('Convection coefficient [$W/m^2/^{\circ}C$]','Interpreter','latex')
xticks([0 2.5 5 7.5 10 12.5 15])
hold off
```

Analytical calculations for the Simulink models

In this section of the appendix, the MATLAB-script used to do all the analytical calculations for the thermal equivalent circuit is presented. If the script is to be used by other students or researchers, it is important to read all the comments within the script. The comments give instruction to comment out or comment in different lines, depending on cooling solutions etc. The MATLAB-script is built on from the preceding specialization course[1] and some of the equations, definitions and calculations are therefore the same. The new contribution is all the convective heat transfer calculations, implementation of cooling solutions, equivalent thermal conductivity in slot, all the rotor calculations and all contact resistance calculations. Some of the equations for calculation of the thermal resistances have also been changed, according to the explanations in the thesis.

```
clear all
clc
%% Geometry and machine parameters
%Machine heights in meters:
d_fr=100/1000; %assumed
d_inso= 5/1000;
d_insi=5/1000;
d_sy= 99/1000;
d_cu=115.34/1000;
d_ss=118/1000;
d_ag=10/1000;
d_mag=30/1000;
l_m=1500/1000;
%Machine widths in meters:
```

```
15 b_ss= 56.7/1000;
16 b_is=1.33/1000;
17 b_cu= 54.04/1000;
18 b_st=58.4/1000;
19 %Radiuses in meters:
20 r_shaft=3377/1000;
21 r_core=3477/1000;
22 r_mag=3507/1000;
23 r_insi=3517/1000;
24 r_i=3522/1000;
25 r_is=3640/1000;
26 r_o= 3739/1000;
27 r_inso = 3744/1000;
28 r_m= 3844/1000;
29 D_outer=7.578;
30
31 % Angle as function of radius with constant arc length:
32 s=(b_ss/2+b_st/2); % section tangential length
33 theta_s=s/r_is;
34
35 %Electrical parameters:
36 N_pol=160; % Number of poles
37 Q_s=192;   % Number of stator slots
38 F_ss=0.763; % stator slot fill factor
39
40 %Needed areas:
41 A_core=pi*r_o^2-pi*r_is^2+b_st*d_ss*Q_s+pi*r_core^2-pi*r_shaft^2; %Total core
       area
42 A_stator=pi*r_o^2-pi*r_is^2+b_st*d_ss*Q_s; %Total stator core area
43 A_stator_section=pi*r_o^2*(theta_s/2*pi)-pi*r_is^2*(theta_s/2*pi)+(b_st*d_ss)
       /2; %Area of Stator yoke + teeth for section
44 A_rotor_section=pi*r_core^2*(theta_s/2*pi)-pi*r_shaft^2*(theta_s/2*pi);
45 A_cu_slot=(d_cu*b_cu); % area of copper in ONE slot
46 A_slot=(d_ss*2+b_ss*2)*l_m; %area of slot (perimiter*length)
47
48 %% Losses:
49 %See chapter 3 for an explination.
50 P_c_tot=55537;
51 P_c_prvol=P_c_tot/(A_core*l_m);
52 P_c_segment=P_c_prvol*A_stator_section/A_core; % Used in COMSOL
53 P_c_segment_2d=P_c_segment*A_stator_section; %  Used in eq.circuit
54 P_c_rotor=P_c_prvol*A_rotor_section/A_core; % Used in COMSOL
55 P_c_rotor_2d=P_c_rotor*A_rotor_section; %  Used in eq.circuit
56 P_cu=380.05; %Copper losses for half a slot.
57
58 %% Needed heat transfer coefficients and other thermal parameters
59 k_fr=238; %From COMSOL material lib.
60 k_f=0.95;% Stacking factor of 5mm thick lamination sheets.
61 k_ins= 0.25; % Mica-glass backed tape assumed for insulation material
```

```
k_sy=76.2; % From COMSOL material lib.
k_st=k_sy; % Same material as stator yoke
k_air_slot= 0.03; %From Gunnar Kylander.
k_cu=400; %From COMSOL material lib.
k_air_40=0.02662; %Thermal conductivity air at 40 degree
P_r_40=0.7255; %Prandtl number for air at 40 deg.
n=1; %counter
T_ambient=30+273.15; %Ambient temperature
T_s=T_ambient+10; %initial temperature for surface
%% Thermal resistances
%Ambient and frame

R_fr= (log(r_m/r_inso))/(2*pi*k_fr)*(2*pi/theta_s); %frame
h_amb(n)=1.475*abs((T_s-T_ambient))^(0.33); %Nonlinear convection coefficient
    frame-ambient

%stator yoke
R_sy=(log(r_o/r_is))/(2*pi*k_sy*k_f)*(2*pi/theta_s);

%insulation stator yoke-> frame for only insulating material
R_inso=((log(r_inso/r_o))/(2*pi*k_ins))*(2*pi/theta_s);

%stator teeth
R_st=(log((r_is)/(r_i))/(2*pi*k_st*k_f*((b_st*d_ss)/(b_ss*d_ss+b_st*d_ss))))
    *(2*pi/theta_s); %Radial dir
R_st2=b_st/(k_st*d_ss); %tangential dir

%Slot/windings
w_r=d_ss-(1.33/1000)*2; %Width radial
w_t=b_ss-(1.33/1000)*2; %Width tangential
N_t=6; %Tangential turns
N_r=24; %Radial turns
t_iso=0.13/1000; %Insulation thickness

t_cur=(w_r-(t_iso*(N_r*2))); %Radial copper thickness
t_cut=(w_t-(t_iso*(N_t*2))); %Tangential copper thickness
R_xo=((t_iso*(N_t*2)))/(t_cur*(k_ins)); %tangential resistance
R_yo=((t_iso*(N_r*2)))/(t_cut*k_ins); %radial resistance

%Equivalent thermal conductivity in slot (USED FOR COMSOL):
k_t_dot=(k_ins*w_t)/(t_iso*2*N_t);
k_t_dott=t_cur/w_r*k_t_dot;
k_r_dot=(k_ins*w_r)/(t_iso*2*N_r);
k_r_dott=t_cut/w_t*k_r_dot;

%slot liner insulation resistance
R_ix=((b_is)/(d_ss*k_ins)); %without air in slots
R_iy=((b_is)/(b_ss/2*k_ins)); %without air in slots

```

```
109 %Insulation layer between stator and air gap:
110 R_insi=log(r_i/r_insi)/(2*pi*k_ins)*(2*pi/theta_s);
111
112 %% Rotor:
113 theta_snet=(126/360)*(2*pi); %magnet angle in rad.
114 N_pol=160; %number of poles in the ref.machine
115 k_magnet=7.7; %Thermal conductivity of NdFeB magnets
116 k_core=k_sy; %Thermal conducticity of rotor core (same material as stator yoke)
117 P_magnet_2d=126.5; % Magnet_losses
118 m_l=96.7*10^-3;% Magnet circumference length
119 p_mag=0.8;%  percentage of magnet mangle inside the modelled section
120 R_mag=log(r_mag/r_core)/(N_pol*theta_snet*k_magnet)*(N_pol*theta_snet/(theta_s*
        p_mag));%Thermal resistance of magnets in radial direction
121 R_rotor_core=(log(r_core/r_shaft)/(2*pi*k_core))*(2*pi/theta_s); %Thermal
        resistance of rotor core in radial dir.
122
123 %Thermal contact resistance between magnet and rotor core
124 G=5000; %Equivalent thermal conductance
125 R_c=1/G; %Contact resistance between magnet and rotor core.
126 % Thermal resistance of the air gap, assuming airflow due to rotation only and
        10 RPM of the machine.
127 h_ag=10.8; %see chapter 3.1.2 Where this coefficient is calculated.
128 R_ag=(log((r_mag+d_ag)/r_mag)/(2*pi*h_ag))*(2*pi/(theta_s)); %Resistance of air
         gap assumed to be purely conductive. See section 3.1.
129
130 %% IMPLEMENTING HOLLOW SHAFT COOLING: Remember to connect cooling solution in
        Simulink.
131 k_shaft=k_fr; %Assuming shaft as aluminum.
132 R_shaft=(log((r_shaft)/0.25)/(2*pi*k_shaft))*(2*pi/(theta_s)); %Resistance of
        shaft. Inner radius =0.25m
133
134 h_shaft_cooling=123.7; % with water
135 R_hollow_shaft_cooling=(2*pi/(theta_s))*1/(2*pi*(0.25)*h_shaft_cooling);
136 %% IMPLEMENTING RECTANGULAR COOLING DUCT IN STATOR: Remember to connect cooling
         solution in Simulink.
137
138 h_rect_water_cooling=1800; %For water cooling solution
139 h_rect_air_cooling=50; % For air cooling solution
140
141 %FOR WATER COOLING SOLUTION:
142 R_rect_cooling=1/(h_rect_water_cooling*0.02);
143 R_rect_cooling_2=1/(h_rect_water_cooling*0.01);
144 % FOR AIR COOLING SOLUTION:
145 R_rect_cooling=1/(h_rect_air_cooling*0.02);
146 R_rect_cooling_2=1/(h_rect_air_cooling*0.01);
147  %Remember to comment in/out the solution that is being simulated.
148
149 %% IMPLEMENTING AIR COOLING IN AIR GAP: Remember to connect cooling solution in
        Simulink.
```

```
150 h_ag=88; % with water
151 R_ag_stator=(2*pi/(theta_s))*1/(2*pi*(r_mag+d_ag/2)*h_ag);
152 R_ag_magnet=(2*pi/(theta_s*0.8))*1/(2*pi*(r_mag)*h_ag);
153
154 %% IMPLEMENTING CONCENTRIC DUCT BETWEEN FRAME AND STATOR:
155 %ENABLE FOR WAVED STATOR SURFACE DUCT COOLING, REMEMBER TO REMOVE R_inso
156 %and add R_yoke_duct in SIMULINK CIRCUIT.
157 s_new=(4*sqrt((10/1000)^2+(s/4)^2));
158 h_con_duct=50;
159 R_ss_duct=(2*pi/(theta_s))*1/(2*pi*(r_o)*h_con_duct);
160 R_fr_duct=(2*pi/(theta_s))*1/(2*pi*(r_o+0.02)*h_con_duct);
161 R_ss_duct=(2*pi/(theta_s))*1/(2*pi*(r_inso)*h_con_duct)*s/s_new; %use for %
        stator surface cooling with two waves.
162
163
164 %% Calculating thermal equivalent resistances
165 R_af=1/2*R_fr; %Resistance between frame node and ambient
166 R_fsy=1/2*R_fr+1/2*R_sy+R_inso; %Resistance between frame node and stator yoke
        node COMMENT IN/OUT R_inso DEPENDING ON COOLING SITUATION.
167 R_syt=1/2*R_sy+1/2*R_st; %Resistance between stator yoke node and teeth node
168 R_wst=R_st2/2+R_ix+R_xo/2; % Resistance between windings and stator teeth
169 R_syw=R_yo/2+R_iy+R_sy/2; %Resistance between stator yoke and windings
170 R_wag=R_insi*(s/(b_ss/2))+R_iy+R_yo/2; %Resistance between windings and air gap
        node
171 R_agt=R_insi*(s/(b_st/2))+1/2*R_st; %Resistance between stator teeth and air
        gap node
172 R_amg=R_mag/2+R_ag/2; %COMMENT IN/OUT R_ag DEPENDING ON COOLING SITUIATION.
173 R_rcm=R_mag/2+(R_rotor_core/2)+R_c; % Resistance between rotor core node and
        magnet node.
174
175 %% TEMPERATURE
176 T_ambient=30+273.15; %Kelvin
177 T_airgap=40+273.15; %Kelvin
178
179 %% Resulting temperatures from Simulink model:
180 sim('thermal_simulink_simple_ferdig_ny_1.slx');
181 T_w=ans.simout.Data(1,1); %Temperature in windnigs
182 T_t=ans.simout.Data(1,3); % temp in teeth
183 T_f=ans.simout.Data(1,2); % Temp in frame
184 T_y=ans.simout.Data(1,4); % Temp in yoke
185 T_s=ans.simout.Data(1,5); %Temp at frame surface
186 T_m=ans.simout.Data(1,6); %Temp in rotor magnet
187 T_rc=ans.simout.Data(1,7); %Temp in rotor core
188 T_ag=ans.simout.Data(1,8); %Temp in air gap
189 % temps in degrees:
190 T_w_c=T_w-273.15;
191 T_t_c=T_t-273.15;
192 T_f_c=T_f-273.15;
193 T_y_c=T_y-273.15;
```

```
194 T_s_c=T_s-273.15;
195 T_m_c=T_m-273.15;
196 T_rc_c=T_rc-273.15;
197 T_ag_c=T_ag-273.15;
198 %%Resulting R_amb (LAST VALUE):
199 R_amb=ans.simout1.Data(1,1);
```

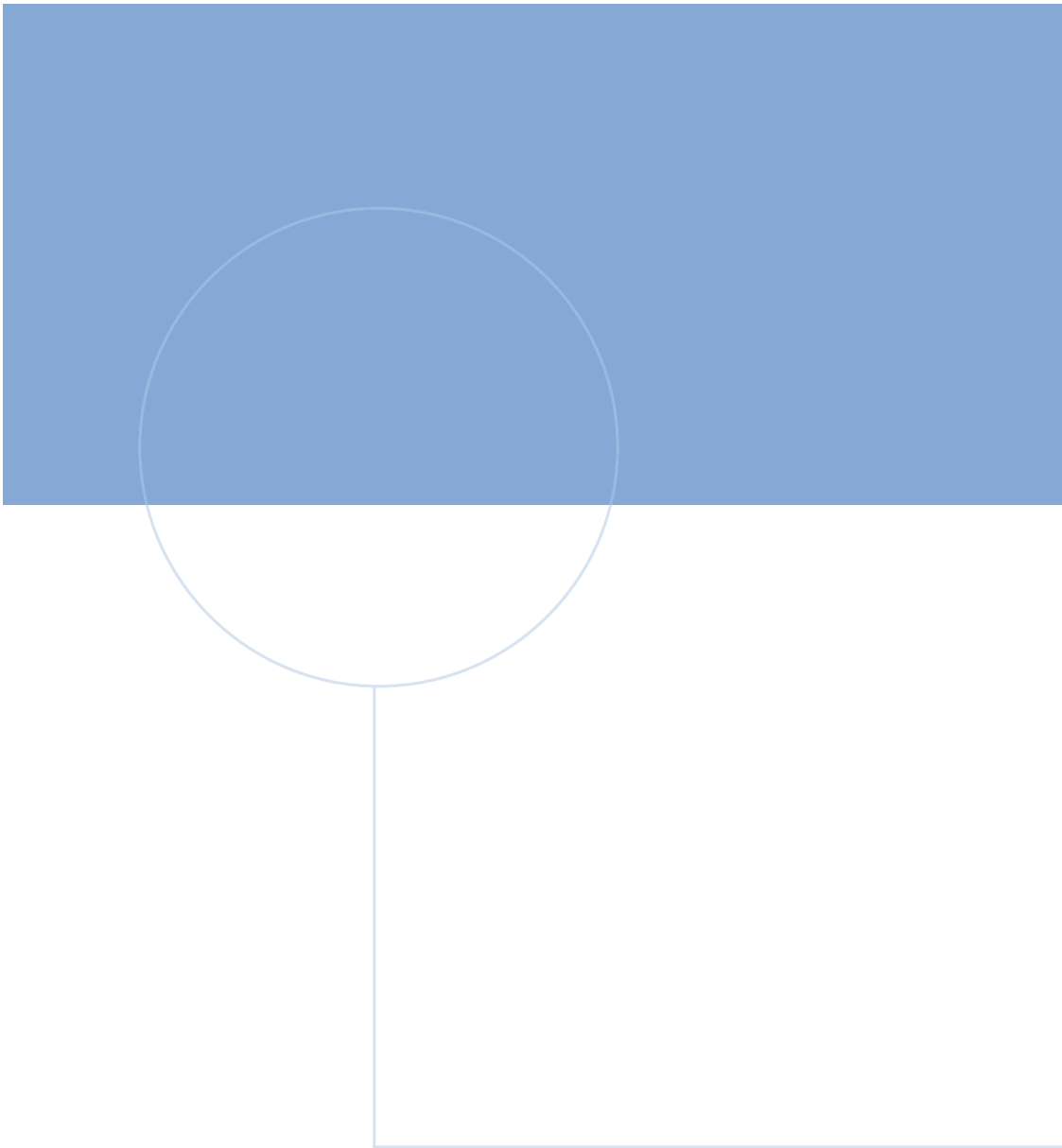

NTNU

Norwegian University of
Science and Technology